Pomeron loop effects in high density and high energy QCD

Wenchang Xiang
Department of Physics
University of Bielefeld

Thesis submitted for the Degree of Doctor of Philosophy in the
University of Bielefeld
· June 2009 ·

Nuclei as heavy as bulls
Through collision
Generate new states of matter
— Keran Li

Contents

Chapter 1

Introduction

Much progress has been made over the last three decades in understanding high energy evolution in quantum chromodynamics (QCD) in the vicinity of the unitarity limit. The first major step towards a description of high energy evolution in QCD is the Balitsky-Fadin-Kuraev-Lipatov (BFKL) [1] equation which was proposed in the leading logarithmic approximation in the mid seventies. The BFKL equation is a linear evolution equation, therefore the solution to the BFKL equation gives a power like energy dependence for the total cross section ($\sigma^{tot} \sim s^{\delta}$). The power like energy dependence is a shortcoming of the BFKL equation, as it causes the total cross section to violate the unitarity bound at very high energy [2].

A crucial progress in the description of high energy evolution in QCD is the color dipole picture which was proposed by Al Mueller in the mid nineties [3, 4]. The dipole model provides an elegant construction of the BFKL wave function of an energetic hadron in the large N_c limit, where gluons are replaced by quark-antiquark pairs and gluon radiation is replaced by dipole splitting. In the dipole model the BFKL evolution becomes much simpler.

Based on Mueller's dipole model, Kovchegov derived an equation to deal with deep inelastic scattering (DIS) of a virtual photon on a large nucleus at or near the unitarity limit, which includes all multiple Pomeron exchanges in the leading logarithmic approximation [5]. In the conventional Feynman diagram language the Kovchegov equation resums the so-called "fan" diagrams in the leading logarithmic approximation. In addition to the linear BFKL term, the Kovchegov equation has a *non-linear* term which comes from the resummation of multiple Pomeron exchanges, thus making the solution to the Kovchegov equation saturate the unitarity limit.

Moreover, the Kovchegov equation can be reduced to the linear BFKL evolution equation in the weak scattering regime in which the *non-linear* effect is not important and can be neglected.

Further progress has been made at the end of nineties and the beginning of 21st century in small x physics. An alternative description of the evolution equation was provided by the Jalilian-Marian, Iancu, McLerran, Werget, Leonidov and Kovner (JIMWLK) formalism [6], in which the evolution is achieved by boosting the target, and the non-linear effects correspond to the saturation effects in the target wave function. The JIMWLK equation describes the evolution of the probability to find a given configuration of color fields in the wave function of the target with increasing rapidity. It is equivalent to the Balitsky hierarchy of equations [7], where the evolution is implemented by boosting the projectile. In the mean field approximation, the Balitsky equations reduce to the Kovchegov equation, and usually we call this mean field equation as Balitsky-Kovchegov (BK) equation [7, 5]. One of the main results following from the BK equation is the *geometric scaling* behavior of T matrix, $T(r,x) = T(r^2 Q_s^2(x))$, namely the scattering amplitude is a function of a single variable, $r^2 Q_s^2(x)$, instead of depending on r and x separately.

Over the last five years, there has been a tremendous theoretical progress in understanding the high energy QCD evolution beyond the mean field approximation, i.e. beyond the BK equation. Salam has shown that the particle number fluctuations are important in the evolution of wave function of a hadron from dilute regime to a high density regime [8]. And also the authors of Ref. [9] found that the fluctuations slow down the scattering amplitude near the unitarity limit as compared to the solution to the Balitsky-Kovchgov equation [7, 5]. The groundbreaking work beyond the mean field approximation, from the systematic theory point of view, has been established in [10] by extending the Kovchegov equation by taking into account the *discreteness* of gluon numbers. It has been found that the *discreteness* of gluon numbers brings in a large correction for the rapidity dependence of the saturation momentum and makes the scattering amplitude violate the *geometric scaling*. This work has triggered further developments in small x physics. Later on a relation between high energy QCD evolution and reaction diffusion processes in statistical physics has been set up [11], which shows that the results obtained in [10] are similar to those emerging in the reaction diffusion processes in statistical physics. The outcomes in [11] clarify even further that the *discreteness* of gluon numbers and the

gluon number fluctuations are very important in the low parton density regime and, are the new elements in the course of the evolution.

Soon after the first breakthroughs in understanding the high energy QCD evolution beyond the mean field approximation, it was realized in Refs.[12, 13, 14] that both the BK and the JIMWLK equations do not properly describe the evolution of a wave function of a hadron in the low parton density regime where the *fluctuations in gluon numbers* become important, as they include only the Pomeron splittings (BK) and Pomeron mergings (JIMWLK) but not Pomeron mergings (BK) and Pomeron splittings (JIMWLK) respectively (depending upon the perspective from which one views the evolution), therefore they miss the Pomeron loops in the course of the evolution. The Kovchegov or JIMWLK equations have been extended by Pomeron loops and new equations have emerged, the so-called Pomeron loop equations [12, 13, 14]. One of the main hallmarks of the Pomeron loop equations is the so-called *diffusive scaling* behavior of the scattering amplitude T, namely T is a function of a single variable $\ln(1/r^2Q_s^2(x))/\sqrt{DY}$, where D is the diffusion coefficient.

During the last two years, another source of large corrections to the BK equation has been studied, the next to leading order corrections (running coupling effects). This study was triggered by the reason that the BK equation may not give the correct quantitative description of the data since it corresponds to a leading order approximation. The evolution equations which include running coupling effects have been derived by Balitsky and Kovchegov-Weigert in [15, 16]. They found that the running coupling corrections are included in the BK kernel by replacing the fixed coupling α_s in it with a "triumvirate" of the running couplings. A numerical study of the running coupling evolution was carried out in [17], which shows that the running coupling effects lead to a considerable increase in the anomalous dimension and slow down of the evolution with rapidity.

My work is motivated by the recent progress in the high energy QCD evolution beyond the mean field approximation, i.e. beyond the BK equation. We have studied the consequences of gluon number fluctuations on different observables, like the inclusive and diffractive cross section in DIS [18]. Further we have studied how the Froissart bound emerges once the gluon number fluctuations are included which are important at very high energies.

It has been shown that the description of both inclusive and diffractive DIS data is improved once gluon number fluctuations are included. By fitting the HERA data,

including the gluon number fluctuations, we have obtained the values of the saturation exponent and the diffusion coefficient, which turn out to be reasonable and agree with values obtained from numerical simulations of toy models which also take into account fluctuations. These outcomes seem to indicate the evidence of geometric scaling violations and a possible implication of the gluon number fluctuations in the DIS data.

In order to make sure that the description of the HERA data is really improvement once the gluon number fluctuations are included, we have used the already known parameters from fitting the inclusive DIS data to compute the χ^2 in the diffractive DIS case. We have obtained the $\chi^2 = 1.031$ after including the gluon number fluctuations and the $\chi^2 = 1.282$ before including the gluon number fluctuations, which obviously illustrates the better description of the HERA data after including fluctuations.

The gluon number fluctuations are important at very high energies, therefore we have calculated the Froissart bound including the gluon number fluctuations. We see a clear effect of the fluctuations in the energy dependence of the black disk radius. We have also calculated the value of the slope parameter B and compared it with the experimental data to check whether the gluon number fluctuations are present in the HERA data. The result shows a quite good agreement with the experimental data.

Another area of my research was the study of evolution equation including the running of the coupling [19]. We have analytically solved the running coupling Balitsky and Kovchegov-Weigert evolution equations in the saturation regime. We have found that these equations are exactly the same in the saturation regime, which is an interesting result and means that the evolution equations with running coupling corrections are independent of the choice of the transverse coordinate of the subtraction point in the saturation regime. And we also have found that the analytic form for the S matrix at high energy including the running coupling corrections is different as compared to the fixed coupling case: The running coupling slows down the evolution of the scattering amplitude with rapidity. The effect of the rare fluctuations on top of the running coupling is computed in Chapter 5, showing that rare fluctuations are less important in the running coupling case as compared to the fixed coupling case.

This thesis is organized as follows: In Chapter 2 we introduce the evolution equations. The phenomenological consequences of gluon number fluctuations are studied in Chapter 3. In Chapter 4, we study how the Froissart bound emerges once gluon number fluctuations are taken into account. Finally in Chapter 5, we study the

high energy scattering in the saturation regime including running coupling and rare fluctuation effects.

Chapter 2

Small x physics

2.1 Mean field approximation

The evolution equation obtained in the mean field approximation is the BK equation. The BK equation [7, 5] gives the evolution with rapidity $Y = \ln(1/x)$ of the scattering amplitude $S(x_\perp, y_\perp, Y)$ of a $q\bar{q}$ dipole with a target which may be another dipole, a hadron or a nucleus. The BK equation is a simple equation to deal with the onset of unitarity and to study parton saturation phenomena at high energies. The analytic solution to the fixed coupling BK equation for the S-matrix deep in the saturation regime has been derived by Levin and Tuchin [20]. This solution agrees with the one derived by solving the BK equation in the small S limit [21]. In this section we will give a simple derivation of the BK equation and its solution in the saturation regime.

2.1.1 The BK equation

In the high-energy scattering of a quark-antiquark dipole on a target, it is convenient to view the scattering process in a frame where the dipole is moving along the negative z-axis and the target is moving along the positive z-axis. Further we assume that almost all of the rapidity of the scattering, Y, is taken by the target. We denote the scattering amplitude of a dipole, consisting of a quark at transverse coordinate $x_\perp$ and an antiquark at transverse coordinate $y_\perp$, scattering on a target by $S(x_\perp, y_\perp, Y)$. Now suppose we increase Y by a small amount dY. We wish to know how $S(x_\perp, y_\perp, Y)$ changes with the small amount dY. If the rapidity of the dipole is increased while that of the target is kept fixed, then the dipole has a probability to emit a gluon due to the change dY. We now calculate the probability for producing this quark-

antiquark-gluon state. In the large N_c limit the quark-antiquark-gluon state can be viewed as a system of two dipoles – one of the dipoles consists of the initial quark and the antiquark part of the gluon while the other dipole is given by the quark part of the gluon and the initial antiquark. Using the dipole model the probability for producing the quark-antiquark-gluon state from the initial quark-antiquark state is [23, 10]

$$dP = \frac{\alpha N_c}{2\pi^2} d^2 z_\perp dY \frac{(x_\perp - y_\perp)^2}{(x_\perp - z_\perp)^2 (z_\perp - y_\perp)^2}, \tag{1}$$

where $z_\perp$ is the transverse coordinate of the emitted gluon. The change in the S-

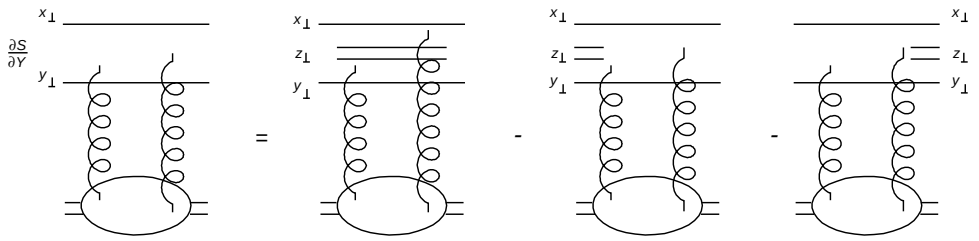

Figure 2.1: Diagrams corresponding to terms in the evolution equation (2).

matrix, dS, for a dipole-hadron scattering is given by multiplying the probability dP with the S-matrix

$$\begin{aligned} \frac{\partial}{\partial Y} S(x_\perp - y_\perp, Y) &= \frac{\alpha N_c}{2\pi^2} \int d^2 z_\perp \frac{(x_\perp - y_\perp)^2}{(x_\perp - z_\perp)^2 (z_\perp - y_\perp)^2} \\ &\quad \times \left[S^{(2)}(x_\perp - z_\perp, z_\perp - y_\perp, Y) - S(x_\perp - y_\perp, Y) \right] , \end{aligned} \tag{2}$$

where $S^{(2)}(x_\perp - z_\perp, z_\perp - y_\perp, Y)$ stands for a simultaneous scattering of the two produced dipoles on the target (see the first diagram on r.h.s of Fig. 2.1). The last term in (2) describes the scattering of a single dipole on the target because the gluon is not in the wave function of the dipole at the time of the scattering (see the last two diagrams in Fig. 2.1).

It is hard to directly use Eq. (2) to study problems of parton evolution and parton saturation phenomena at high density and high energy QCD, since $S^{(2)}$ is not known. Using the mean field approximation for the gluonic fields in the target

$$S^{(2)}(x_\perp - z_\perp, z_\perp - y_\perp, Y) = S(x_\perp - z_\perp, Y) S(z_\perp - y_\perp, Y) , \tag{3}$$

one gets the Kovchegov equation [5]

$$\frac{\partial}{\partial Y}S(x_\perp - y_\perp, Y) = \frac{\alpha N_c}{2\pi^2}\int d^2 z_\perp \frac{(x_\perp - y_\perp)^2}{(x_\perp - z_\perp)^2(z_\perp - y_\perp)^2} \times [S(x_\perp - z_\perp, Y)S(z_\perp - y_\perp, Y) - S(x_\perp - y_\perp, Y)] \ . \quad (4)$$

With $T(x_\perp - y_\perp, Y) = 1 - S(x_\perp - y_\perp, Y)$, another useful version of the Kovchegov equation is obtained

$$\frac{\partial}{\partial Y}T(x_\perp - y_\perp, Y) = \frac{\alpha N_c}{2\pi^2}\int d^2 z_\perp \frac{(x_\perp - y_\perp)^2}{(x_\perp - z_\perp)^2(z_\perp - y_\perp)^2} [T(x_\perp - z_\perp, Y) + T(z_\perp - y_\perp, Y) - T(x_\perp - y_\perp, Y) - T(x_\perp - z_\perp, Y)T(z_\perp - y_\perp, Y)] \ . \quad (5)$$

Eq. (5) has the following probabilistic interpretation: when evolved in rapidity, the initial quark-antiquark dipole of size $x_\perp - y_\perp$ decays into two dipoles of size $x_\perp - z_\perp$ and $z_\perp - y_\perp$ with the decay probability $(\alpha N_c/2\pi^2)(x_\perp - y_\perp)^2/((x_\perp - z_\perp)^2(z_\perp - y_\perp)^2)$ which is usually called as BFKL kernel. These two dipoles then interact with the target. The non-linear term takes into account a simultaneous interaction of two produced dipoles with the target. On the right-hand side of Eq. (5), the first three terms (the third one is virtual) describe the scattering of single dipole with the target, the non-linear term prevents the amplitude from growing boundlessly with rapidity and ensures the unitarity of the scattering amplitude. For a small dipole, $x_\perp - y_\perp \ll 1/Q_S(Y)$, $T_Y(x_\perp - y_\perp)$ is small as well, $T_Y(x_\perp - y_\perp) \ll 1$, the non-linear term $T(x_\perp - z_\perp, Y)T(z_\perp - y_\perp, Y)$ can be dropped, and the linear equation remaining is the dipole version [23] of the BFKL equation [1].

2.1.2 Solution to the BK equation in the saturation regime

In the high-energy regime where unitarity corrections become important or $S(x_\perp - y_\perp, Y)$ is small, Eq. (4) is easier to use since the quadratic term $S(x_\perp - z_\perp, Y)S(z_\perp - y_\perp, Y)$ can be neglected, in which case one only needs to keep the second term on the r.h.s of (4), giving

$$\frac{\partial}{\partial Y}S(x_\perp - y_\perp, Y) = -\frac{\alpha N_c}{2\pi^2}\int d^2 z_\perp \frac{(x_\perp - y_\perp)^2}{(x_\perp - z_\perp)^2(z_\perp - y_\perp)^2} S(x_\perp - y_\perp, Y) \ . \quad (6)$$

In the above equation, we have assumed that S is small which holds only when the dipole size is large compared to $1/Q_s$. Therefore the lower bound of integration in

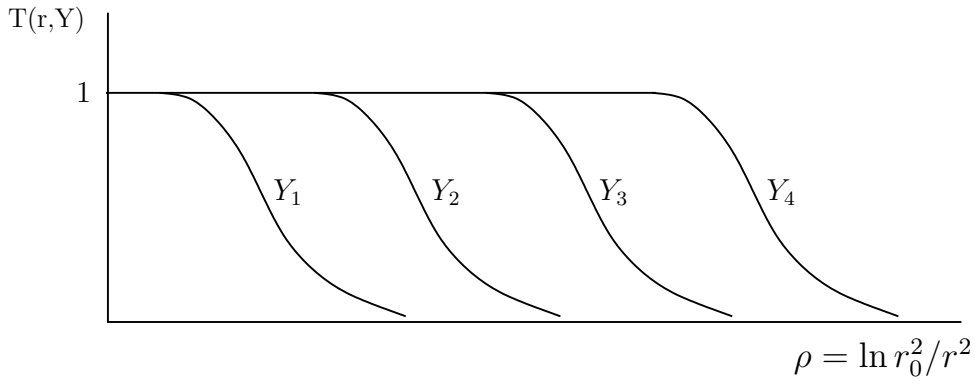

Figure 2.2: The "traveling wave" behavior of the solution to the BK-equation.[Figure taken from [22].]

(6) should be restricted to the regimes $(x_\perp - y_\perp)^2 \gg 1/Q_s^2$ and $(x_\perp - z_\perp)^2 \gg 1/Q_s^2$, $(z_\perp - y_\perp)^2 \gg 1/Q_s^2$. In the logarithmic regime of integration one gets

$$\frac{\partial}{\partial Y} S(x_\perp - y_\perp, Y) = -2\frac{\alpha N_c}{2\pi^2}\pi \int_{1/Q_S^2}^{(x_\perp - y_\perp)^2} d(z_\perp - y_\perp)^2 \frac{1}{(z_\perp - y_\perp)^2} S(x_\perp - y_\perp, Y) \ . \quad (7)$$

Note that the factor 2 in the above equation comes from the symmetry of the two regions dominating the integral, either from $1/Q_s \ll |x_\perp - z_\perp| \ll |x_\perp - y_\perp|$, $|y_\perp - z_\perp| \sim |x_\perp - y_\perp|$ or $1/Q_s \ll |y_\perp - z_\perp| \ll |x_\perp - y_\perp|$, $|x_\perp - z_\perp| \sim |x_\perp - y_\perp|$. Now it is easy to get the solution to Eq. (7)

$$S(x_\perp - y_\perp, Y) = \exp\left[-\frac{c}{2}\left(\frac{\alpha N_c}{\pi}\right)^2 (Y - Y_0)^2\right] S(x_\perp - y_\perp, Y_0), \quad (8)$$

where we have used [10, 24, 18]

$$Q_s^2(Y) = \exp\left[c\frac{\alpha N_c}{\pi}(Y - Y_0)\right] Q_s^2(Y_0) \quad (9)$$

and

$$Q_s^2(Y_0)(x_\perp - y_\perp)^2 = 1. \quad (10)$$

Eq. (8) gives the standard result given in the literature [21].

One of the hallmarks of the BK-equation is the geometric scaling behavior of the T matrix in a large kinematical window [25, 24, 26]

$$T(r_\perp, Y) = T(r_\perp^2\, Q_s^2(Y)) \ , \quad (11)$$

with the saturation scale $Q_s(Y)$ which is defined as $T(r \simeq 1/Q_s, Y)$ to be a constant of order 1. Eq. (11) shows that T is a function of a single variable $r_\perp^2\, Q_s^2(Y)$ instead

of depending on $r_\perp$ and Y separately. This behavior indicates a similar geometric scaling for the DIS cross section, $\sigma^{\gamma^* p}(Y, Q^2) = \sigma^{\gamma^* p}(Q^2/Q_s^2(Y))$, which is supported by the HERA data [27].

Another hallmark extracted from the BK-equation is the dependence of the saturation momentum on rapidity [24, 26],

$$Q_s^2(Y) = Q_0^2 \exp\left[\frac{2\alpha_s N_c}{\pi}\frac{\chi(\lambda_0)}{1-\lambda_0}Y\right] , \tag{12}$$

with $\lambda_0 = 0.372$, and $\chi(\lambda)$ is the BFKL kernel.

The shape of the solution to the BK-equation, T, is preserved in the transition regime from strong (T of order 1) to weak (T of order α_s^2) scattering with increasing Y, "traveling wave" behavior as shown in Fig.2.2. As rapidity increases, the saturation region at $r \gg 1/Q_s(Y)$ widens up, more and more smaller dipoles are included, due to the growth of the saturation scale. However, we will see in the next sections that the gluon number fluctuations change the situation a lot.

2.2 Beyond the mean field approximation

2.2.1 Beyond the BK equation

The Balitsky-Kovchegov equation [7, 5] resums, in the leading logarithmic approximation, all diagrams which include the effects of multiple BFKL Pomeron exchanges, with Pomeron ladders together with Pomeron splitting vertices being included in the dipole wave function. In the traditional Feynman diagram language, the BK equation resums the so-called "fan" diagrams in the leading logarithmic approximation, see Fig. 2.3. However, another kind of diagrams, the Pomeron loop diagrams (see Fig. 2.4), are not included in the Kovchegov equation, since the BK equation only takes into account the Pomeron splittings but misses the Pomeron mergings. Therefore, the BK equation misses the Pomeron loops. It was shown that the Pomeron loop effects play an important role in the evolution of the scattering amplitude towards the unitarity limit [10, 11, 12, 13]. We will discuss these effects in the next pages.

When one takes into account the Pomeron loop effects in the high energy QCD

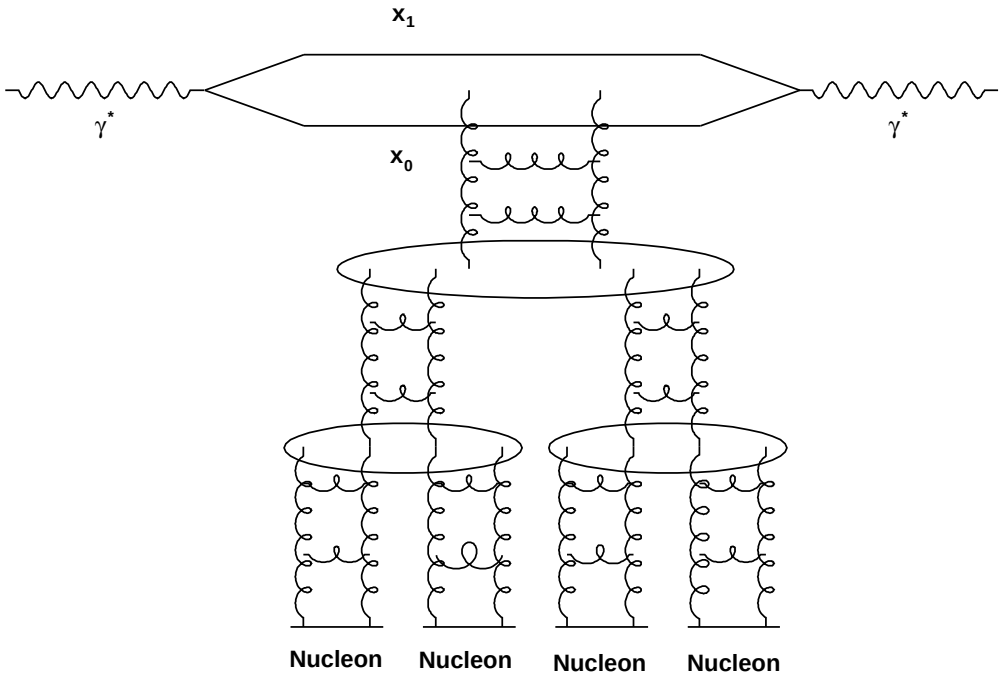

Figure 2.3: Diagram which is included multiple pomeron exchanges [5].

evolution, the Pomeron loop equations can be written as [14]

$$
\begin{aligned}
\frac{\partial\langle T(x_\perp,y_\perp)\rangle_Y}{\partial Y} &= \frac{\bar{\alpha}_s}{2\pi}\int d^2z_\perp\{\mathcal{M}_{x_\perp y_\perp z_\perp}\otimes\langle T(x_\perp,y_\perp)\rangle_Y \\
&\quad -\mathcal{M}(x_\perp,y_\perp,z_\perp)\times\langle T^{(2)}(x_\perp,z_\perp;z_\perp,y)\rangle_Y\} \\
\frac{\partial\langle T^{(2)}(x_{\perp 1},y_{\perp 1};x_{\perp 2},y_{\perp 2})\rangle_Y}{\partial Y} &= \frac{\bar{\alpha}_s}{2\pi}\int d^2z_\perp\,\{[\mathcal{M}_{x_{\perp 1},y_{\perp 1},z_\perp} \\
&\quad \otimes\langle T^{(2)}(x_{\perp 1},y_{\perp 1};x_{\perp 2},y_{\perp 2})\rangle_Y \\
&\quad -\mathcal{M}(x_{\perp 1},y_{\perp 1},z_\perp) \\
&\quad \times\langle T^{(3)}(x_{\perp 1},z_\perp;z_\perp,y_{\perp 1};x_{\perp 2},y_{\perp 2})\rangle_Y] \\
&\quad +[1\leftrightarrow 2]\} + \left.\frac{\partial\langle T^{(2)}(x_{\perp 1},y_{\perp 1};x_{\perp 2},y_{\perp 2})\rangle_Y}{\partial Y}\right|_{fluct} \\
&\vdots
\end{aligned}
\tag{13}
$$

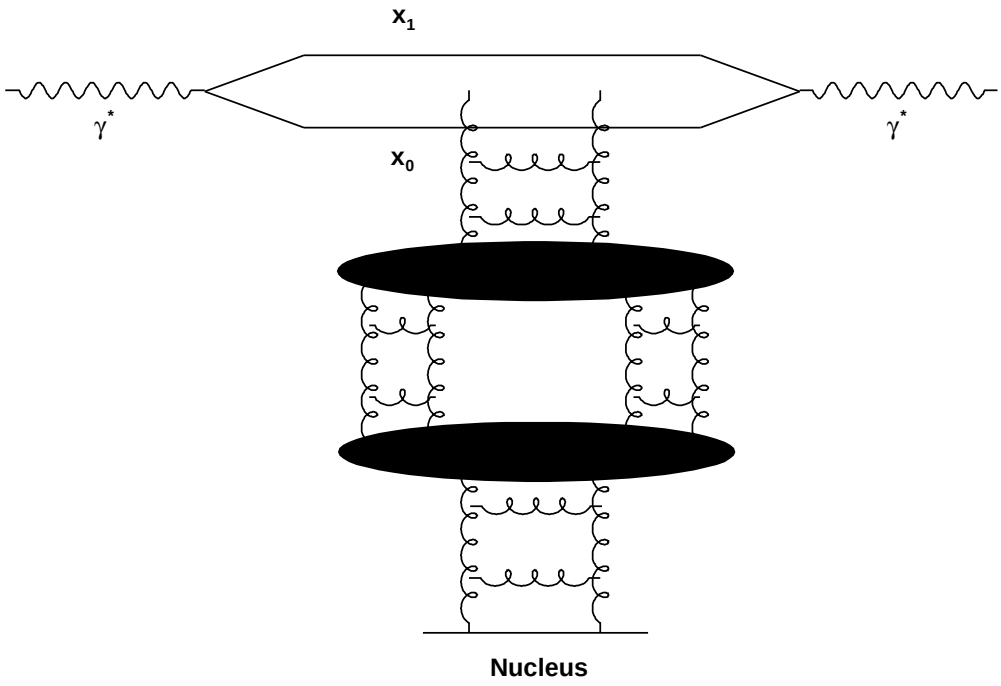

Figure 2.4: A Pomeron loop diagram [5].

with

$$\left.\frac{\partial\langle T^{(2)}(x_{\perp 1},y_{\perp 1};x_{\perp 2},y_{\perp 2})\rangle_Y}{\partial Y}\right|_{fluct} = \left(\frac{\alpha_s}{2\pi}\right)^2\frac{\bar{\alpha}_s}{2\pi}\int d^2u_\perp d^2v_\perp d^2z_\perp \mathcal{M}(u_\perp,v_\perp,z_\perp) \times\mathcal{A}_{dd}(x_{\perp 1},y_{\perp 1}|u_\perp,z_\perp)\mathcal{A}_{dd}(x_{\perp 2},y_{\perp 2}|z_\perp,v_\perp) \times\nabla^2_{u_\perp}\nabla^2_{v_\perp}\langle T(u_\perp,v_\perp)\rangle_Y \quad (14)$$

where the dipole kernel is

$$\mathcal{M}(x_\perp,y_\perp,z_\perp) = \frac{(x_\perp-y_\perp)^2}{(x_\perp-z_\perp)^2(z_\perp-y_\perp)^2} \quad (15)$$

and

$$\mathcal{M}_{x_\perp,y_\perp,z_\perp}\otimes f(x_\perp,y_\perp) \equiv \mathcal{M}(x_\perp,y_\perp,z_\perp)\left[-f(x_\perp,y_\perp)+f(x_\perp,z_\perp)+f(z_\perp,y_\perp)\right], \quad (16)$$

and $\mathcal{A}_{dd}$ is the amplitude for dipole-dipole scattering and for large N_c

$$\mathcal{A}_{dd}(x_\perp,y_\perp|u_\perp,v_\perp) = \frac{\alpha_s^2}{8}\left[\ln\frac{(x_\perp-v_\perp)^2(y_\perp-u_\perp)^2}{(x_\perp-u_\perp)^2(y_\perp-v_\perp)^2}\right]^2. \quad (17)$$

Here $x_\perp$, $y_\perp$, $z_\perp$, $u_\perp$ and $v_\perp$ are the transverse coordinates of the dipoles.

The complete evolution equation Eq. (13) for the scattering amplitude deserves comments:

- In the mean field approximation, $\langle TT\rangle = \langle T\rangle\langle T\rangle$, the first equation in (13) reduces to the BK equation which describes the evolution of the scattering amplitude of a single dipole off a target, see Fig. 2.5. Note that the last diagram in Fig. 2.5 expresses the two dipoles simultaneously scattering off the target. In the mean field approximation, the scattering of the two dipoles on the target is independent, namely the correlation between the two dipoles are neglected.

- Beyond the mean field approximation, the correlations between dipoles scattering off the target are taken into account. The evolution equations in Eq. (13) include Pomeron splittings, Pomeron mergings, and therefore in the course of the evolution, also *Pomeron loops*. As an example [1], the evolution equation for $\langle T^{(2)}\rangle_Y$ in Eq. (13) is represented by the linear term $\langle T^{(2)}\rangle$ (see the corresponding Feynman diagram Fig. 2.6(b)), the non-linear term which is exhibited in Fig. 2.6(c), and the term which is proportional to $\alpha_s^2\langle T\rangle$ (see Fig. 2.7). The first two terms are already present in the corresponding Balitsky-JIMWLK hierarchy equations. The last one is a new term which takes into account the effect of fluctuations and is missed in the BK equation. It is very important in the low parton density region, since in this region ($T \sim \alpha_s^2$) the Pomeron merging term is of the same order as the BFKL terms, $\mathcal{O}(\alpha_s^4)$, while the Pomeron splitting terms are suppressed by a factor $\mathcal{O}(\alpha_s^2)$.

- The last comment is on the validity regime of the Pomeron merging terms, see Fig. 2.7. The Pomeron merging terms are assumed to be important only in the low parton density region. In the region close to the unitarity limit, $T \sim 1$, we do not expect that the Pomeron mergings can properly describe the physics in this region, since their derivation is based on the two gluon exchange approximation in the Mueller's color dipole model [22].

I would like to note that the Pomeron loop equations can equivalently be written

[1] The other evolution equations for $\langle T^{(N)}\rangle_Y (N > 2)$ in Eq. (13) are similar as $\langle T^{(2)}\rangle_Y$.

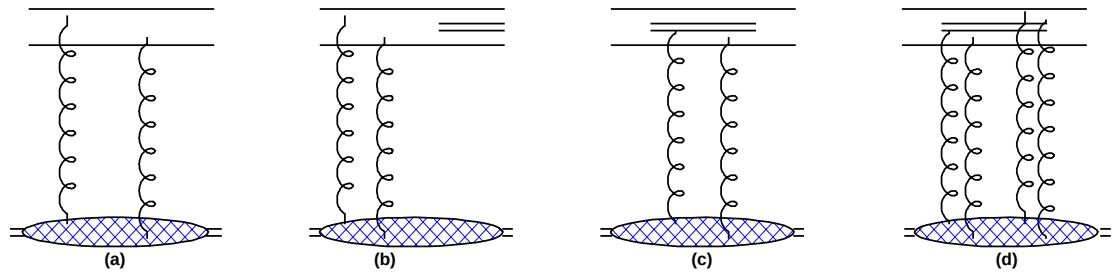

Figure 2.5: A single dipole scattering with a target from the perspective of projectile evolution.

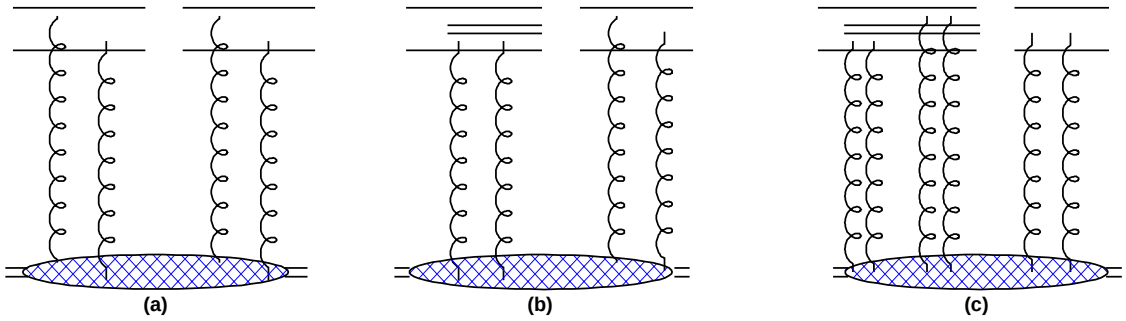

Figure 2.6: A dipole pair scattering with a target from the perspective of projectile evolution.

as a single stochastic equation of Langevin type [14],

$$\frac{\partial T_Y(x_\perp,y_\perp)}{\partial Y} = \frac{\bar{\alpha}_s}{2\pi}\int d^2z_\perp\,[\mathcal{M}_{x_\perp,y_\perp,z_\perp}\otimes T_Y(x_\perp,y_\perp) - \mathcal{M}(x_\perp,y_\perp,z_\perp)T_Y(x_\perp,z_\perp) \times T_Y(z_\perp,y_\perp)] + \left.\frac{\partial T_Y(x_\perp,y_\perp)}{\partial Y}\right|_{fluct} \quad (18)$$

with the noise term

$$\left.\frac{\partial T_Y(x_\perp,y_\perp)}{\partial Y}\right|_{fluct} = \frac{\alpha_s}{2\pi}\sqrt{\frac{\bar{\alpha}_s}{2\pi}}\int d^2u_\perp d^2v_\perp d^2z_\perp \mathcal{A}_{dd}(x_\perp,y_\perp|u_\perp,z_\perp)\frac{|u_\perp-v_\perp|}{(u_\perp-z_\perp)^2} \times\sqrt{\nabla^2_{u_\perp}\nabla^2_{v_\perp}T_Y(u_\perp,v_\perp)}\nu(u_\perp,v_\perp,z_\perp,Y), \quad (19)$$

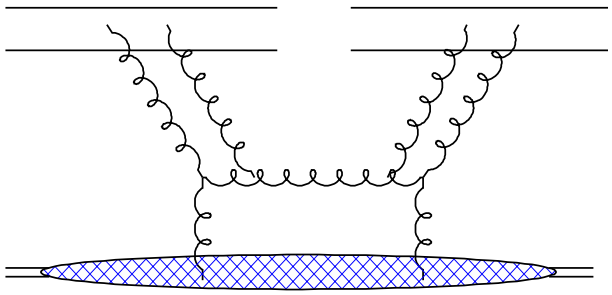

Figure 2.7: The missing diagram of both Balitsky-JIMWLK and Kovchegov equations.

where the noise satisfies

$$\begin{aligned}\langle \nu(u_{\perp 1}, v_{\perp 1}, z_{\perp 1}, Y)\nu(u_{\perp 2}, v_{\perp 2}, z_{\perp 2}, Y')\rangle &= \delta^{(2)}(u_{\perp 1} - v_{\perp 2})\delta^{(2)}(v_{\perp 1} - u_{\perp 2}) \\ &\quad \times\delta^{(2)}(z_{\perp 1} - z_{\perp 2})\delta(Y - Y'). \qquad (20)\end{aligned}$$

The noise term clarifies that the Pomeron loop equations take into account gluon number fluctuations.

2.2.2 Statistical physics - high density QCD correspondence

Consider the scattering of a dipole of variable size r (the projectile) off a dipole of size r_1 (the target). We go to the rest frame of the probe so that the target carries all the available rapidity Y. We denote $T(r_1, r, Y)$ as the scattering amplitude of the probe off a given partonic realization $|\omega\rangle$ of the target. It is a random variable, whose probability distribution is related to the stochastic ensemble of dipole configurations endowed with a probability distribution which evolves with Y according to a master equation [12]. Thus, the high energy evolution can be viewed as a process which is inspired by dynamics of a reaction-diffusion process in statistical physics. The physical dipole-dipole scattering amplitude $\bar{T}(r_1, r, Y)$ is the statistical average over all possible dipole realization of the target at rapidity Y,

$$\bar{T} = \langle T((\rho - \rho_s(Y))\rangle = \int d\rho_s \; T(\rho - \rho_s(Y)) \; P(\rho_s(Y) - \langle \rho_s(Y)\rangle) \quad , \qquad (21)$$

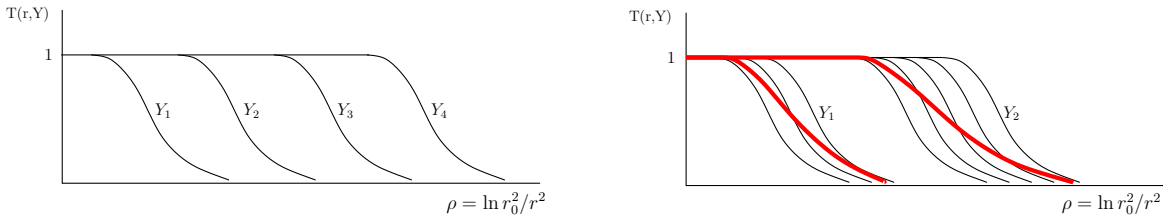

Figure 2.8: Left-hand side: The "traveling wave" behavior of the scattering amplitude at four different rapidities. Right-hand side: The thin lines represent T-matrix at two different rapidities for different realizations. The thick lines denote the average over the realization, $\langle T\rangle$, at the two rapidities, respectively. The shape of $\langle T\rangle$ becomes flatter as rapidity increases.[Figures taken from [22].]

where the distribution of $\rho_s(Y)$ is, to a very good approximation, a Gaussian [28]:

$$P(\rho_s) \simeq \frac{1}{\sqrt{\pi\sigma^2}} \exp\left[-\frac{(\rho_s - \langle\rho_s\rangle)^2}{\sigma^2}\right] . \tag{22}$$

and $\rho = \ln(r_0^2 Q^2)$, $\rho_s = \ln(r_0^2 Q_s^2)$.

An illustration is shown in Fig.2.8, the left-hand side plot is the traveling wave behavior of the solution to the BK equation at different rapidities, and the right-hand side plot is the averaged amplitude at two different rapidities after including gluon number fluctuation effects.

The gluon number fluctuations in the dilute regime result in fluctuations of the saturation scale from event to event, with the variance σ of the saturation scale

$$\sigma^2 = \langle\rho_s^2\rangle - \langle\rho_s\rangle^2 \propto \frac{\alpha_s Y}{(\Delta\rho)^3} \tag{23}$$

from numerical simulations of statistical models. $\rho_s = \ln(r_0^2 Q_s^2(Y))$ is the position of the front. To calculate the physical amplitude, we average the event-by-event scattering amplitude over all possible gluon number realizations [12, 18]. The operation leads to a replacement of the geometric scaling resulting from the BK equation by a new scaling, the diffusive scaling, namely, $\langle T(r,Y)\rangle$ is a function of a single variable

$$\langle T(r,Y)\rangle = f\left(\frac{\ln(r^2 Q_s^2(Y))}{\sqrt{\alpha_s Y/(\Delta\rho)^3}}\right) . \tag{24}$$

The result in Eq.(24) changes the shape of the scattering amplitude with increasing rapidity, which is illustrated in Fig. 2.8 (right-hand side) by the decreasing slope of

the thick line with growing rapidity, in contrast to the solution to the BK-equation in Eq.(11).

Let us consider the scattering amplitude of a dipole scattering off a highly evolved hadron in the geometric and diffusive scaling region. To explain the relevant physics in these two regions, let us look at the phase diagram of the hadron in the high energy limit shown in Fig. 2.9, in which the coordinate $Y = \ln(1/x)$ is the rapidity of the hadron, ρ is the logarithm of the transverse momentum of the gluons inside the hadron, and $\langle \rho_s \rangle$ is the averaged saturation line. To the left of the saturation line, $\rho < \langle \rho_s \rangle$, is the saturation region with large size gluons at high density, of order $1/\alpha_s$, or $T \sim 1$, in which the non-linear effect becomes important. For $\rho \gg \langle \rho_s \rangle$, the gluon density is low, in which neither saturation nor fluctuation effects are important, the scattering amplitude shows color transparency. There are two different regions within the transition region (see shadowing region in Fig. 2.9) which are separated by the rapidity scale Y_{DS}, the geometric scaling regime and diffusive scaling regime, where the dynamics of the QCD evolution is different. For $Y \ll Y_{DS}$, the dispersion is small $\sigma^2 \ll 1$, the effects of fluctuations can be neglected and the evolution of the hadron is described to a good approximation by the BK equation. While for $Y \gg Y_{DS}$, where $\sigma^2 \gg 1$, the fluctuations become important and the geometric scaling regime is replaced by the diffusive scaling.

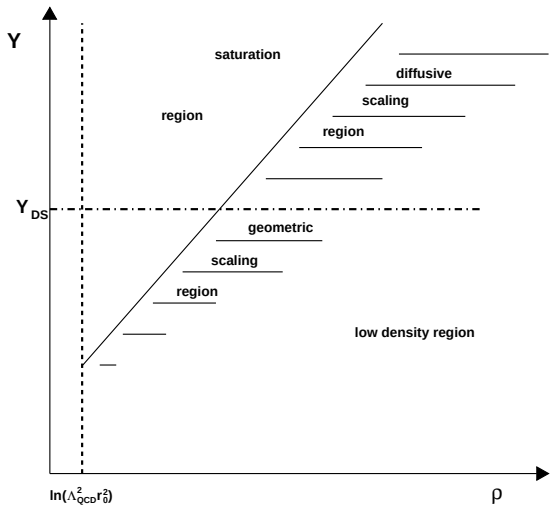

Figure 2.9: The phase diagram of the wave function of a highly evolved hadron [22].

2.3 Running coupling corrections

The BK equation only considers the resummation of leading logarithmic (LL) $\alpha_s \ln(1/x_{Bj})$ corrections with a fixed coupling constant α_s. The running coupling corrections due to fermion (quark) bubble diagrams, which would bring in a factor of $\alpha_s N_f$, modify the evolution equation, which is not leading logarithms anymore. Once including $\alpha_s N_f$ corrections, the obtained contributions have to be divided into two parts, the running coupling part and the "subtraction" part. The first part has a form as the leading order BK kernel but with the running coupling replacing the fixed coupling and the second part brings in new structures into the evolution equation.

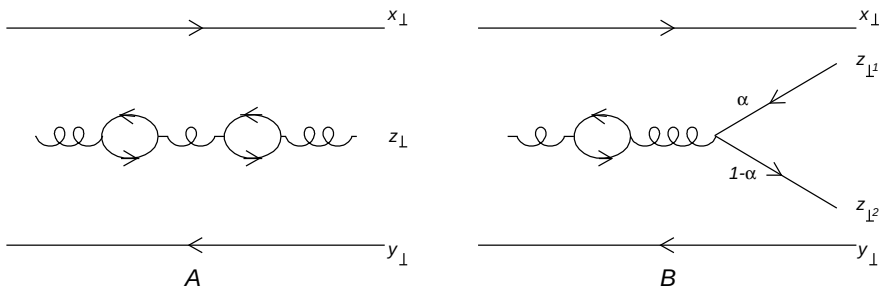

Figure 2.10: The higher order diagrams contribution to BK evolution.

The evolution equation including higher order corrections reads [17]

$$\frac{\partial S(x_\perp - y_\perp, Y)}{\partial Y} = \mathcal{R}[S] - \mathcal{S}[S] \ . \tag{25}$$

The first term in r.h.s of (25), $\mathcal{R}$, which is referred to as the 'running coupling' contribution resums all power of $\alpha_s N_f$ corrections to the evolution. The $\mathcal{R}$ has a form as the leading order one but with modified kernel which includes all effects of the running coupling

$$\begin{aligned} \mathcal{R}\left[S(x_\perp - y_\perp, Y)\right] \ &= \ \int d^2 z_\perp \, \tilde{K}(x_\perp, y_\perp, z_\perp) \left[S(x_\perp - z_\perp, Y)\, S(z_\perp - y_\perp, Y)\right. \\ &\quad \left. - S(x_\perp - y_\perp, Y)\right] \ . \end{aligned} \tag{26}$$

The BK kernel is modified because the propagator of the emitted gluon in the original parent dipole is now dressed with quark loops in contrast to leading order or fixed coupling one. This modifies the emission probability of the gluon but doesn't change the leading order interaction terms (see Fig. 2.10A).

Using $T(x_\perp - y_\perp, Y) = 1 - S(x_\perp - y_\perp, Y)$, another useful version of (26) is:

$$\begin{aligned}\mathcal{R}\left[T(x_\perp - y_\perp, Y)\right] &= \int d^2 z_\perp \, \tilde{K}(x_\perp, y_\perp, z_\perp) \left[T(x_\perp - z_\perp, Y) + T(z_\perp - y_\perp, Y)\right. \\ &\left. - T(x_\perp - y_\perp, Y) - T(x_\perp - z_\perp, Y) T(z_\perp - y_\perp, Y)\right] \end{aligned} \tag{27}$$

with the modified kernel $\tilde{K}(x_\perp, y_\perp, z_\perp)$ which has two kinds of expressions since two different separation schemes of running coupling and subtraction have been used in [15, 16](see [17] for more discussions on separation schemes). Balitsky took the transverse coordinate of either the quark at $z_{\perp 1}$ or the antiquark at $z_{\perp 2}$ to be the subtraction point. He got the kernel of the running coupling contribution as [15]

$$\tilde{K}^{\rm Bal}(\mathbf{r}, \mathbf{r}_1, \mathbf{r}_2) = \frac{N_c \, \alpha_s(r^2)}{2\pi^2} \left[\frac{r^2}{r_1^2 \, r_2^2} + \frac{1}{r_1^2}\left(\frac{\alpha_s(r_1^2)}{\alpha_s(r_2^2)} - 1\right) + \frac{1}{r_2^2}\left(\frac{\alpha_s(r_2^2)}{\alpha_s(r_1^2)} - 1\right)\right] . \tag{28}$$

Here we introduce the notation $\mathbf{r} = x_\perp - y_\perp$, $\mathbf{r}_1 = x_\perp - z_\perp$ and $\mathbf{r}_2 = z_\perp - y_\perp$ for the sizes of parent and of the new daughter dipoles produced by the evolution. On the other hand, in the subtraction scheme proposed by Kovchegov-Weigert the subtraction point is fixed at the transverse coordinate of the gluon at $z_\perp = \eta z_{\perp 1} + (1-\eta) z_{\perp 2}$ in which η is the longitudinal momentum fraction of the gluon carried by the quark. They got the modified kernel of the running coupling contribution [16]:

$$\tilde{K}^{\rm KW}(\mathbf{r}, \mathbf{r}_1, \mathbf{r}_2) = \frac{N_c}{2\pi^2} \left[\alpha_s(r_1^2) \frac{1}{r_1^2} - 2 \, \frac{\alpha_s(r_1^2) \, \alpha_s(r_2^2)}{\alpha_s(R^2)} \, \frac{\mathbf{r}_1 \cdot \mathbf{r}_2}{r_1^2 \, r_2^2} + \alpha_s(r_2^2) \frac{1}{r_2^2}\right] \tag{29}$$

with

$$R^2(\mathbf{r}, \mathbf{r}_1, \mathbf{r}_2) = r_1 \, r_2 \left(\frac{r_2}{r_1}\right)^{\frac{r_1^2 + r_2^2}{r_1^2 - r_2^2} - 2 \frac{r_1^2 \, r_2^2}{\mathbf{r}_1 \cdot \mathbf{r}_2} \frac{1}{r_1^2 - r_2^2}} . \tag{30}$$

The second term in r.h.s of (25), $\mathcal{S}$, which is referred to as the 'subtraction' contribution, is given by

$$\begin{aligned}\mathcal{S}[S] &= \alpha_\mu^2 \int d^2 z_{\perp 1} \, d^2 z_{\perp 2} \, K_{①}(x_\perp, y_\perp; z_{\perp 1}, z_{\perp 2}) \, \left[S(x_\perp - w_\perp, Y) \, S(w_\perp - y_\perp, Y)\right. \\ &\left. - S(x_\perp - z_{\perp 1}, Y) \, S(z_{\perp 2} - y_\perp, Y)\right] \end{aligned} \tag{31}$$

with α_μ the bare coupling. The interaction structures are modified in the above equation since the quark-antiquark pair is added to the evolved wave function (see Fig. 2.10B). The $\mathcal{K}_{①}(x_{\perp m}, x_{\perp n}; z_{\perp 1}, z_{\perp 2})$ is a resummed JIMWLK kernel which can be found in [17]

$$K_{①}(x_\perp, y_\perp; z_{\perp 1}, z_{\perp 2}) \, = \, C_F \sum_{m,n=0}^{1} (-1)^{m+n} \, \mathcal{K}_{①}(x_{\perp m}, x_{\perp n}; z_{\perp 1}, z_{\perp 2}). \tag{32}$$

In terms of Balitsky's subtraction scheme, one substitutes $w_\perp = z_{\perp 1}$ or $w_\perp = z_{\perp 2}$ in Eq. (31) and gets the subtraction term

$$\begin{aligned}\mathcal{S}^{Bal}[S] &= \alpha_\mu^2 \int d^2 z_{\perp 1}\, d^2 z_{\perp 2}\, K_{①}(x_\perp, y_\perp; z_{\perp 1}, z_{\perp 2})\, [S(x_\perp - z_{\perp 1}, Y)\, S(z_{\perp 1} - y_\perp, Y) \\ &\quad - S(x_\perp - z_{\perp 1}, Y)\, S(z_{\perp 2} - y_\perp, Y)]\,. \end{aligned} \tag{33}$$

According to Kovchegov-Weigert's subtraction scheme, one substitutes $w_\perp = z_\perp = \eta z_{\perp 1} + (1-\eta) z_{\perp 2}$ in Eq. (31) and gets

$$\begin{aligned}\mathcal{S}^{KW}[S] &= \alpha_\mu^2 \int d^2 z_{\perp 1}\, d^2 z_{\perp 2}\, K_{①}(x_\perp, y_\perp; z_{\perp 1}, z_{\perp 2})\, [S(x_\perp - z_\perp, Y)\, S(z_\perp - y_\perp, Y) \\ &\quad - S(x_\perp - z_{\perp 1}, Y)\, S(z_{\perp 2} - y_\perp, Y)]\,. \end{aligned} \tag{34}$$

Chapter 3

Phenomenological consequences of gluon number fluctuations

In this Chapter, we study the effect of gluon number fluctuations (Pomeron loops) on inclusive and diffractive deep inelastic scattering (DIS) in the fixed coupling case.

3.1 Gluon number fluctuations in inclusive deep inelastic scattering

The mean-field dynamics of the high-energy dipole-proton scattering is described by the BK-equation [7, 5]. Phenomenological ansätze for the dipole-proton scattering amplitude $T(r,x)$ (where r is the transverse dipole size and x the Bjorken-variable) inspired by the BK-equation have led to quite successful descriptions of the HERA data. The T-matrix following from the BK-equation shows within a restricted kinematical window, which increases with collision energy, the geometric scaling behavior [29, 25, 26], $T(r,x) = T(r^2\,Q_s^2(x))$, where $Q_s(x)$ is the saturation scale, which seems well supported by the HERA data [27]. The correction to the solution outside the restricted window, the "BK-diffusion term", violates the geometric scaling [29, 25, 26] and depends on the variable $\ln(1/r^2\,Q_s^2(x))/\sqrt{D_{\mathrm{BK}}Y}$. Iancu, Itakura and Munier (IIM) [30] have shown that the "BK-diffusion term", giving a substantial amount of geometric scaling violations, is needed in order to accurately describe the experimental HERA data. The exponent λ of the saturation scale, $Q_s^2(x) \simeq (x_0/x)^\lambda$, is known at NLO [31], $\lambda \simeq 0.3$, and agrees with the values extracted from fits to HERA data.

Recently, there has been a tremendous theoretical progress in understanding the high-energy QCD evolution beyond the mean field approximation, i.e. beyond the BK-equation. It has been understood how to include discreteness and fluctuations of gluon numbers (Pomeron loops) in small-x evolution [10, 11, 12, 14, 13, 32]. After including these elements, the evolution becomes stochastic and one has to distinguish between the event-by-event amplitude $T(r,x)$, which corresponds to an individual gluon number realization, and the physical amplitude $\langle T(r,Y)\rangle$, which one obtains by averaging over all individual realizations [11]. At very high energy, the discreteness effect *decreases* the exponent λ as compared to BK-value and the gluon number fluctuations, i.e., the averaging over all events to calculate the physical amplitude, replaces the geometric scaling resulting from the BK-equation (in the "wave front" region) by a new scaling [10, 11], the *diffusive scaling*, namely, $\langle T(r,Y)\rangle$ is a function of a single variable $\ln(1/r^2\,Q_s^2(x))/\sqrt{D\,Y}$, where D is the diffusion coefficient. The value of D determines the rapidity above which gluon number fluctuations become important, $Y \geq Y_D = 1/D$, which is the case when the fluctuation of the saturation scales of the individual events becomes large, in formulas, when the dispersion $\sigma^2 = 2(\langle\rho_s^2(Y)\rangle - \langle\rho_s(Y)\rangle^2) = D\,Y \gg 1$, where $\rho_s(Y) = \ln(Q_s^2(Y)/Q_0^2)$. At high energy, such that $\sigma^2 \gg 1$, it has been shown that fluctuations do strongly modify measurable quantities [33, 34]. (A more detailed presentation of the recent theoretical progress is given in Refs.[35] while the most recent studies on Pomeron loops based on toy models can be found in Refs. [36, 37, 38, 39, 40, 41, 43, 44, 45].)

In this section we elaborate, in a quite approximative way, whether the HERA data [46] do indicate any possible implication of gluon number fluctuations. The coupling is kept fixed throughout this work. We proceed in the following way: We use for the event-by-event amplitude several models, the GBW model [47], the IIM model [30] and a model which is close to the theoretical findings for T at very large energy (see Eq. (7)). For the averaging over all events we use the high-energy QCD/statistical physics correspondence [11], i.e., a Gaussian for the distribution of $\rho_s(Y) = \ln(Q_s^2(Y)/Q_0^2)$. Moreover, assuming that the DIS cross section shows diffusive scaling in the HERA energy range, we have used the "quality factor" method of Ref. [48] to get an estimation for the value of λ, in a model-independent way. The procedure we use in this work is always based on approximations and, therefore, can at best give hints on a possible implication of gluon number fluctuations in the HERA data.

After including fluctuations in the way described above, we obtain from the analysis of the HERA data values for the exponent λ and the diffusion coefficient D which are quite independent of the ansätze for the event-by-event amplitude. Also the model-independent approach gives a similar value for λ. We find $\lambda \simeq 0.2$ which is smaller than the value from the BK-inspired models (no fluctuations), $\lambda \simeq 0.3$, and the decrease is in agreement with theoretical expectations. For the diffusion coefficient we find a sizeable value, $D \simeq 0.35$. Surprisingly, this value is very close to the values found for D in numerical simulation of the $(1 + 1)$ dimensional model [39] and of evolution equations in QCD [49] (approximations to Pomeron loop equations [13, 12, 14, 32]) in the fixed coupling case. The sizeable value of D may indicate a possible involvement of fluctuations in the HERA data since $Y \geq Y_D = 1/D$ for rapidities at HERA.

We observe that after including fluctuations the description of the HERA data is improved for all models we have used for the event-by-event amplitude. In the case of the GBW model, which exhibits pure geometric scaling, after the inclusion of fluctuations, which lead to a violation of geometric scaling, a much better description is obtained, namely, $\chi^2/\text{d.o.f} = 1.74$ without and $\chi^2/\text{d.o.f} = 1.14$ with fluctuations. The situation seems to be similar with all event-by-event amplitudes which show geometric scaling. In the case of the IIM model, which contains already the geometric scaling violating BK-diffusion term, the inclusion of fluctuations also improves, however less than in the GBW case, the description of the HERA data; $\chi^2/\text{d.o.f} = 0.983$ before and $\chi^2/\text{d.o.f} = 0.807$ after including fluctuations.[1] The outcomes seem to tell us that violations of geometric scaling are required for an accurate description of the HERA data. The improvement of the description of the HERA data together with the very reasonable values for the parameters discussed above seem to indicate that gluon number fluctuations may be the reason for geometric scaling violations in the HERA data. However, we wish to emphasize here that the BK-diffusion term gives similar geometric scaling violations as fluctuations and may as well be the reason for the geometric scaling violations in the HERA data.

This work is organized as follows: In Sec. 3.1.1, we show the results for the T-matrix for dipole-proton scattering and for the energy dependence of the saturation scale which are obtained in the mean field approximations, i.e., from the BK-equation. The results for the same quantities beyond the mean field approximation, or the effects

[1] The χ^2 is defined such that the smallest χ^2 gives the best description to the HERA data.

of discreteness and fluctuations in gluon numbers on these quantities, are summarized in Sec. 3.1.2. Finally, we give numerical results and discuss a possible implication of the physics beyond the mean field approximation in the HERA data.

3.1.1 Event-by-event scattering amplitude

- Mean field approximation

  In the mean field approximation, the Y-dependence of the T-matrix for a dipole of transverse size r scattering off a proton is given by the BK-equation. In the fixed coupling case, the solution to the BK-equation in the saturation region, where $T \simeq 1$, is [20](see Section 2.1.2 for more discussions on the solution to the BK-equation in the saturation region)

$$T(r,Y) = 1 - C_0 \ \exp\left[-C_1(\rho - \rho_s(Y))^2\right] \quad \text{for} \quad \rho - \rho_s(Y) \ll 1 \ , \tag{1}$$

  while for the front of the T-matrix, where $T \ll 1$ (but not too small), one finds [24, 26]

$$T(r,Y) = C_2 \ \left[\rho - \rho_s(Y) + C_3\right] \ \exp\left[-\lambda_s(\rho - \rho_s(Y)) - \frac{(\rho - \rho_s(Y))^2}{2\bar{\alpha}\chi''(\lambda_s)Y}\right] \tag{2}$$
$$\text{for} \quad 1 \ll \rho - \rho_s(Y) \ll 2\chi''(\lambda_s)\bar{\alpha}_s Y \ ,$$

  where have used $\bar{\alpha}_s = \alpha_s N_c/\pi$, $\rho = \ln(1/r^2\, Q_0^2)$ and $\rho_s(Y) = \ln(Q_s^2(Y)/Q_0^2)$ with $Q_s(Y)$ the saturation scale. In above equations, the constants C_0, C_2, C_3 are of $\mathcal{O}(1)$, $C_1 = -C_F(1-\lambda_0)/N_c 2\chi(\lambda_s)$ (C_F is the casimir factor in the fundamental representation), $\lambda_s = 0.6275$, and $\chi(\lambda) = 2\psi(1) - \psi(\lambda) - \psi(1-\lambda)$ is the eigenvalue of the BFKl kernel. For the rapidity dependence of the saturation scale, which separates the saturated ($r \gg 1/Q_s(Y)$) from the dilute ($r \ll 1/Q_s(Y)$) regime, one obtains from the BK equation [24, 26]

$$Q_s^2(Y) = Q_0^2 \ \frac{\exp[\bar{\alpha}\chi'(\lambda_s)Y]}{[\bar{\alpha}Y]^{\frac{3}{2(1-\lambda_0)}}} \ . \tag{3}$$

  Note that within the even more restricted window, $\rho - \rho_s(Y) \ll \sqrt{2\chi''(\lambda_s)\bar{\alpha}_s Y}$, where the diffusion term in the exponent in Eq.(2) can be neglected, the T-matrix shows the geometric scaling behavior, i.e., it depends only on the difference $\rho - \rho_s(Y)$ instead of depending on r and Y separately. At very small r, so

that $\rho - \rho_s(Y) \gg 2\chi''(\lambda_s)\bar{\alpha}_s Y$, the T-matrix exhibits color transparency, i.e., it shows a faster decrease with ρ as compared to Eq.(2); $T \sim \exp[-\rho]$.

Iancu, Itakura and Munier [30] have used the following ansätze for the T-matrix,

$$T^{\rm IIM}(r,Y) = \begin{cases} 1 - \exp\left[-a \ln^2(b\, r\, Q_s(x))\right] & , \quad r\, Q_s(x) > 2 \\ \\ N_0 \left(\frac{r\, Q_s(x)}{2}\right)^{2\left(\lambda_s + \frac{\ln(2/r\, Q_s(x))}{\kappa\, \lambda\, Y}\right)} & , \quad r\, Q_s(x) < 2 \ , \end{cases} \tag{4}$$

which obviously includes the features of the solution to the BK equation, to compare the theory in the mean field approximation with the DIS data. They have used for the saturation momentum the leading Y-dependence of Eq.(3), $Q_s^2(x) = (x_0/x)^\lambda$, however, with λ and x_0 being fixed by fitting the DIS data. The constant $\kappa = \chi''(\lambda_s)/\chi'(\lambda_s) \approx 9.9$ is a LO result coming from the BK-equation, N_0 is a constant around 0.5 and a and b are determined by matching the two pieces in Eq.(4) at $r\, Q_s = 2$.

The "BK-diffusion term" in the IIM-ansatz (4),

$$\left(\frac{r\, Q_s(x)}{2}\right)^{2\frac{\ln(2/r\, Q_s(x))}{\kappa\, \lambda\, Y}} = \exp\left[-\frac{\ln^2(4/r^2\, Q_s^2(x))}{2\, \kappa\, \lambda\, Y}\right] \ , \tag{5}$$

which is the quadratic term in the exponent of Eq.(2), does explicitly violate the geometric scaling behavior. We wish to emphasize here that, as also shown in [30], this violation seems required in order to get an accurate description of the DIS data. Without it, even allowing λ_s to be an additional fitting parameter, one can not get a better description of the DIS data. For further details on the importance of the diffusion term see Ref. [30].

In this work, we wish to elaborate whether the violation of the geometric scaling may come from gluon number fluctuations (Pomeron loops) and not from the BK-equation. As we will see in the next sections, the fluctuations do indeed give a similar violation of the geometric scaling and also lead to a better description of the DIS data as compared to the case where the T-matrix shows a geometric scaling behavior.

- Discreteness of gluon number

  In a single scattering process, the mean field approximation breaks down when the occupancy of gluons inside the evolved proton is low so that the discreteness

of the gluon number needs to be taken into account; the number of gluons cannot less than one since it has to be discrete. When including the discreteness effect, as compared to the results from the BK-equation, the energy dependence of the saturation momentum changes to [10, 11]

$$Q_s^2(Y) = Q_0^2 \ \exp\left[\bar{\alpha}_s \chi'(\lambda_s) Y \left(1 - \frac{\pi^2 \chi''(\lambda_s)}{2(\Delta\rho)^2 \chi(\lambda_s)}\right)\right] \tag{6}$$

and the piecewise, approximate, shape of the T-matrix at fixed coupling and very high energy reads [10, 11]

$$T(r,Y) = \begin{cases} 1 & \text{for} \quad \rho - \rho_s(Y) \ll 0 \\ N_1 \left[\rho - \rho_s(Y)\right] e^{\lambda_s [\rho - \rho_s(Y)]} & \text{for} \quad 0 < \rho - \rho_s(Y) < \Delta\rho \\ N_2 \, e^{-[\rho - \rho_s(Y)]} & \text{for} \quad \rho - \rho_s(Y) \gg \Delta\rho \end{cases} \tag{7}$$

where N_1 and N_2 are irrelevant constants and the front width is $\Delta\rho \simeq (1/\lambda_s)\ln(1/\alpha_s^2)$. The front width cannot be larger than $\Delta\rho$ which is the distance when the amplitude decreases from its maximal value $T \approx 1$ down to the value $T = \mathcal{O}(\alpha_s^2)$ where the discreteness of gluon numbers becomes important. The width is formed via diffusion, $\rho - \rho_s(Y) \propto \sqrt{\alpha_s Y}$, and it requires the rapidity $Y_F \simeq (\Delta\rho)^2/(2\chi''(\lambda_s)\bar{\alpha}_s)$ until it is completed. The event-by-event amplitude given in Eq.(7), which is formed at $Y > Y_F$, shows, approximately, geometric scaling: $T(r,Y) \approx T(\rho - \rho_s(Y))$.

The main differences as compared to the mean-field results are: The exponent of the saturation scale in the event-by-event amplitude, cf. Eq.(6) and Eq. (3), is decreased due to the discreteness of gluon numbers. Further the width of the front of the event-by-event amplitude is fixed, $\Delta\rho$, instead of increasing with rapidity as in Eq.(3).

3.1.2 Physical scattering amplitude

To go beyond the mean field approximation one has to include the effect of discreteness and fluctuations of gluon numbers [10, 11]. After including fluctuations one has to distinguish between the even-by-event amplitude and the averaged (physical) amplitude. They can be explained by considering the evolution of a proton from $y = 0$ up to $y = Y$ which is probed by a dipole of size r, giving the amplitude $\bar{T}(r,Y)$.

The evolution of the proton is stochastic and leads to random gluon number realizations inside the proton at Y, corresponding to different events in an experiment. The physical amplitude, $\bar{T}(r,Y)$, is then given by averaging over all possible gluon number realizations/events, $\bar{T}(r,Y) = \langle T(r,Y)\rangle$, where $T(r,Y)$ is the amplitude for the dipole r scattering off a particular realization of the evolved proton at Y. In the following we discuss the averaged amplitude $\bar{T}(r,Y)$.

Based on the relation between high-energy QCD evolution and reaction-diffusion processes in statistical physics [11], the fluctuations in gluon numbers are taken into account by averaging over all event-by-event amplitudes,

$$\langle T((\rho - \rho_s(Y))\rangle = \int d\rho_s \; T(\rho - \rho_s(Y)) \; P(\rho_s(Y) - \langle \rho_s(Y)\rangle) \quad , \tag{8}$$

where the distribution of $\rho_s(Y)$ is, to a very good approximation, a Gaussian [28]:

$$P(\rho_s) \simeq \frac{1}{\sqrt{\pi\sigma^2}} \exp\left[-\frac{(\rho_s - \langle\rho_s\rangle)^2}{\sigma^2}\right] \; . \tag{9}$$

The expectation value of the front position, $\langle\rho_s(Y)\rangle$, increases with rapidity as $\langle\rho_s(Y)\rangle = \ln(Q_s^2(Y)/Q_0^2)$ at high energy [11], with $Q_s(Y)$ given in Eq. (6). The dispersion of the front at high energy increases linearly with rapidity,

$$\sigma^2 = 2\left[\langle\rho_s^2\rangle - \langle\rho_s\rangle^2\right] = D\,Y \tag{10}$$

where D is the diffusion coefficient, whose value is known only for $\alpha \to 0$ (asymptotic energy) [10, 50]. Since the values of D and the exponent λ of the saturation scale, $Q_s^2(x) = 1\,\mathrm{GeV}^2\,(x_0/x)^\lambda$, see Eq. (6), are not known for finite energies, e.g. at HERA energy, in what follows we will treat them as free parameters.

At very high energy, such that $\sigma^2 \gg 1$, the dispersion of the fronts due to the gluon number fluctuations from event to event has large consequences on $\langle T(r,Y)\rangle$: the geometric scaling of the single events $T(\rho - \rho_s(Y))$, cf. Eq.(7), is replaced by a new form of scaling, known as diffusive scaling, namely, $\langle T(r,Y)\rangle$ is a function of $(\rho - \langle\rho_s(Y)\rangle)/\sqrt{DY}$,

$$\langle T(r,Y)\rangle = \bar{T}(r,Y) = \bar{T}\left(\frac{\rho - \langle\rho_s(Y)\rangle}{\sqrt{DY}}\right) \; . \tag{11}$$

The diffusive scaling is expected to set in at $Y > Y_D = 1/D$, which follows from the requirement $\sigma^2 \gg 1$.

The goal of this section is to study whether the diffusive scaling behavior of the dipole-proton scattering amplitude in Eq. (11), which is caused by gluon number

fluctuations, may be present in the HERA data. As we will see in the next section, the fluctuations do improve the description of the HERA data, indicating that the violation of geometric scaling seems important for an accurate description of the data. We will discuss whether the violation preferred by the DIS data is due to the gluon number fluctuations, which lead to the diffusive scaling $(\rho - \rho_s(Y))/\sqrt{DY}$, or due to the BK diffusion term, cf. Eq.(5), which corrects the geometric scaling in a similar way, namely, via $(\rho - \rho_s(Y))/\sqrt{2\,\bar{\alpha}_s\,\chi''\,Y}$.

3.1.3 Numerical results

Our fit includes the ZEUS data for the F_2 structure function,

$$F_2(x,Q^2) = \frac{Q^2}{4\pi^2\alpha_{em}}\,(\sigma_T(x,Q^2) + \sigma_L(x,Q^2)),$$
$$\sigma_{T,L}(x,Q^2) = \int dz\,d^2r\;|\psi_{T,L}(z,r,Q^2)|^2\;\sigma_{dip}(x,r) \tag{12}$$

in the kinematical range $x \leq 10^{-2}$ and $0.045\,\mathrm{GeV}^2 < Q^2 < 50\,\mathrm{GeV}^2$ (see also [30] for more discussions on the range). The upper limit on Q^2 has been chosen large enough to include a large amount of "perturbative" data points, but low enough in order to justify the use of the BFKL dynamics, rather than DGLAP evolution. We use in our fit the same photon wave functions $\psi_{T,L}$ as in Ref.[47], which are computable in QED

$$\begin{aligned}
|\psi_T^{(f)}(r,z;Q^2)|^2 &= e_f^2\frac{\alpha_e N_c}{2\pi^2}\{[z^2+(1-z)^2]\bar{Q}_f^2K_1^2(r\bar{Q}_f^2) + m_f^2K_0^2(r\bar{Q}_f)\},\\
|\psi_L^{(f)}(r,z;Q^2)|^2 &= e_f^2\frac{\alpha_e N_c}{2\pi^2}4Q^2z^2(1-z)^2K_0^2(r\bar{Q}_f^2)
\end{aligned} \tag{13}$$

where the e_f and m_f are the charge and mass of the quark with flavor f and $\bar{Q}_f^2 = z(1-z)Q^2 + m_f^2$, and three light quarks with equal mass, $m_{u,d,s} = 140\,\mathrm{MeV}$ and two heavy quarks with mass,$m_c = 1.5\,\mathrm{GeV}$ and $m_b = 4.5\,\mathrm{GeV}$, respectively. The Bjorken x is modified by $x(1+4m_f^2/Q^2)$ in the contribution of heavy quarks. Note that the contribution of the charm and bottom quark to (13) directly give the charm and bottom structure function. We have considered only the ZEUS data because there is a mismatch between the H1 and ZEUS with regard to the data normalization and since only ZEUS has data also in the low Q^2 region, i.e., in the saturation region. To fix the parameters we minimize $\chi^2 = \sum_i(\mathrm{model}(i,p_1,...,p_n) - F_2(i))^2/(\mathrm{error}(i))^2$, where the sum goes over the data points, $p_1,...,p_n$ denote the parameters to be found, $F_2(i)$ the experimental results for the F_2 structure function, and for the error of F_2, i.e., $(\mathrm{error}(i))^2$, we use the systematic error squared plus the statistical error squared.

The interesting ingredient for us in Eq. (12) is the dipole-proton cross section, $\sigma_{dip} = 2\pi R^2 \langle T(r,x)\rangle$, with $2\pi R^2$ being the outcome of the integration over the impact parameter. We will use different ansätze for the event-by-event amplitude, $T(r,x)$, and the physical amplitude, $\langle T(r,x)\rangle$, is obtained according to the rules outlined in section 3.1.2. (We wish to note that the ansätze for $T(r,x)$, which are derived/motivated based on perturbative QCD, are used to describe also the low virtuality data, $Q^2 \leq 1\,\mathrm{GeV}^2$, in the fit to the HERA data. In this region non-perturbative physics [51] is involved which is only approximately given by our ansätze.) In σ_{dip} we will use the event-by-event amplitude and the physical amplitude in order to study the effects of gluon number fluctuations. In the case of $T(r,x)$ there are three free parameters which will be fixed by fitting the HERA data: R ("radius of the proton") and x_0 and λ coming via the saturation momentum $Q_s^2(x) = 1\,\mathrm{GeV}^2\,(x_0/x)^\lambda$. In the case of the averaged (physical) amplitude, $\langle T(r,x)\rangle$, there is another free parameter, the diffusion coefficient D.

1. Fit to the HERA data with only light quarks

In this part, we fit the HERA inclusive DIS data with only the light quarks contribution to the proton structure function. Both light quarks and heavy quarks contribution to the proton structure function will be discussed in the next subsection. We use for the event-by-event amplitude several models, the GBW model, the IIM model and a model which is close to the theoretical findings for T at very large energy.

Now let us look at all the models:

- Golec-Biernat, Wüsthoff (GBW) model [47]:

  The GBW model

  $$T^{GBW}(r,x) = 1 - \exp\left[-\frac{r^2\,Q_s^2(x)}{4}\right] , \tag{14}$$

  is one of the most simple models which shows geometric scaling, $T(r,x) = T(r^2\,Q_s^2(x))$, and leads to a quite successful description of the HERA data, as can be seen from Figs. 3.1, 3.2 and the χ^2 (error) in Table 3.1 (denoted by GBW). It is nice to see that the value of the saturation exponent, $\lambda \simeq 0.285$, which is found by fitting the HERA data with the GBW model, comes out close to the theoretical NLO results for λ [31].

  Now, using the GBW model as an event-by-event amplitude, we include the effect of gluon number fluctuations by averaging over all events via Eq. (8). The

model/parameters	χ^2	χ^2/d.o.f	x_0 ($\times 10^{-4}$)	λ	R(fm)	D
T^{GBW} (light quarks only)	266.22	1.74	4.11	0.285	0.594	0
$\langle T^{\mathrm{GBW}} \rangle$ (light quarks only)	173.39	1.14	0.0546	0.225	0.712	0.397

Table 3.1: GBW model: The parameters of the event-by-event (2 line) and of the physical (3 line) amplitude.

resulting $\langle T^{GBW}(r,x) \rangle$, which breaks the geometric scaling, leads to a relatively much better description of the HERA data, as can be seen from the comparison of the χ^2 values and the two lines in Figs. 3.1, 3.2. The large improvement after including fluctuations seems to indicate that violations of geometric scaling, and probably even gluon number fluctuations, are implicated in the HERA data.

It is important to note that the values of the fitting parameters come out reasonable also after including the gluon number fluctuations. The value of λ becomes smaller after including fluctuations which is in agreement with theoretical expectations, as can be seen from the comparison of Eq. (3) with Eq. (6). Furthermore, the value of the diffusion coefficient D is sizeable, and is surprisingly close to the values which have been found numerically by solving the (1+1) dimensional toy model [39] and the approximate QCD evolution equations [49] (they represent an approximation of the Pomeron loop equations [13, 12, 14, 32]) in the fixed coupling case. Note also that the radius of the proton, R, increases somewhat and x_0 becomes smaller, meaning that $Q_s < 1\,\mathrm{GeV}$ up to $x \simeq 10^{-6}$, due to fluctuations. Also the reasonable values of the parameters, especially the sizeable value of D yielding $Y_D = 1/D \simeq 2.5$, in addition to the better description of the HERA data after including fluctuations, seem to be in favor of an implication of gluon number fluctuations in the HERA data.

- Iancu, Itakura, Munier (IIM) model [30],

The IIM model, which inspires from BK-equation, given in Eq. (4) includes the BK-diffusion term, $\ln(4/r^2\,Q_s^2)/\sqrt{2\,\kappa\,\lambda\,Y}$, which explicitly violates the geometric scaling. It has been shown in [30] that this violation does noticeably improve the description of the HERA data in comparison with the GBW model, as can be seen from the much smaller χ^2 value in the IIM case in Table 3.2 (we always

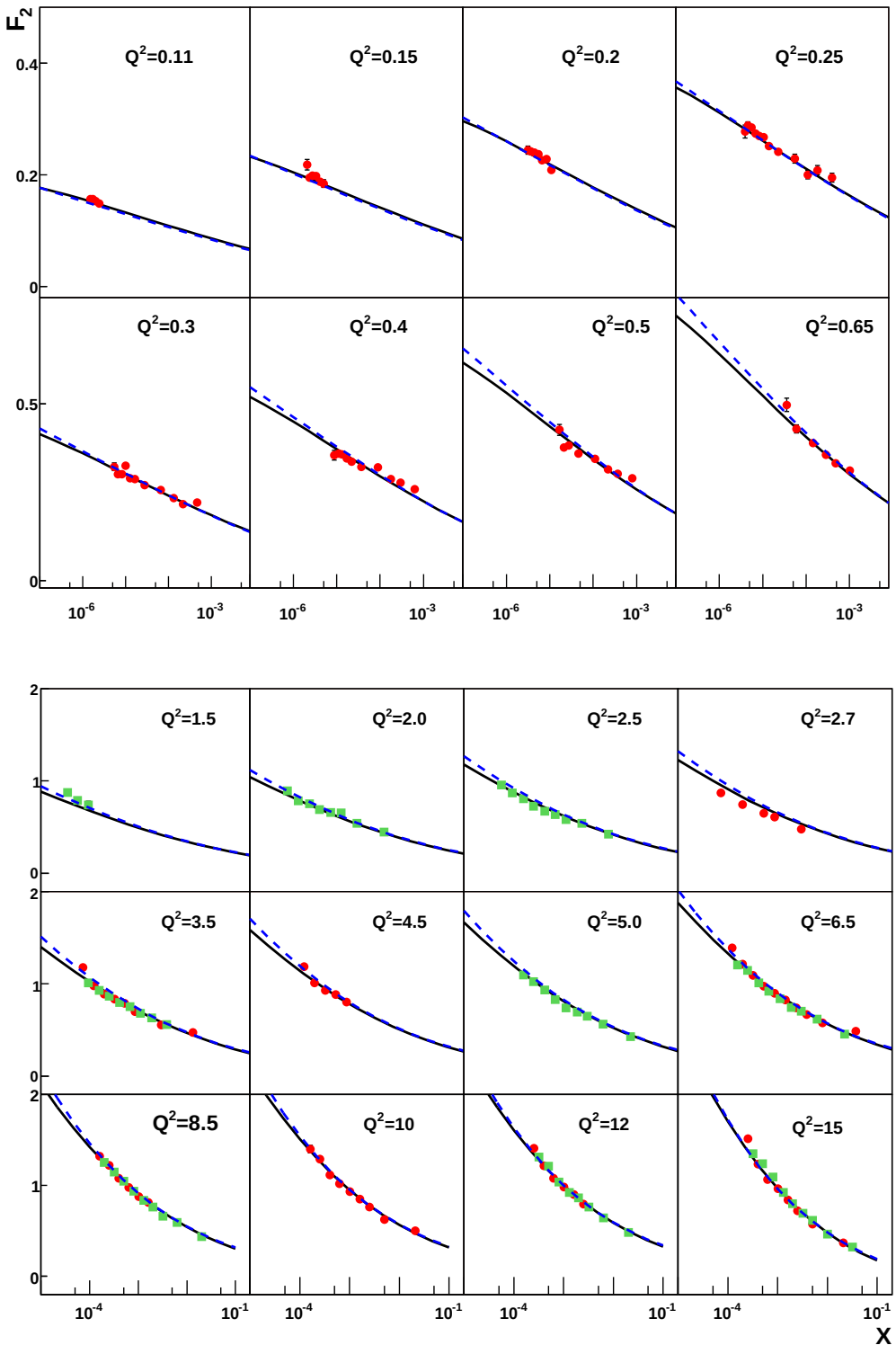

Figure 3.1: The F_2 structure function versus x at different values of Q^2. The solid lines represent the results of the averaged GBW fit and the dashed lines represent the results of the GBW fit to the ZEUS data. The data points at lowest Q^2 values, 0.045, 0.065 and 0.085 GeV^2, are not shown here although they are included in the fits.

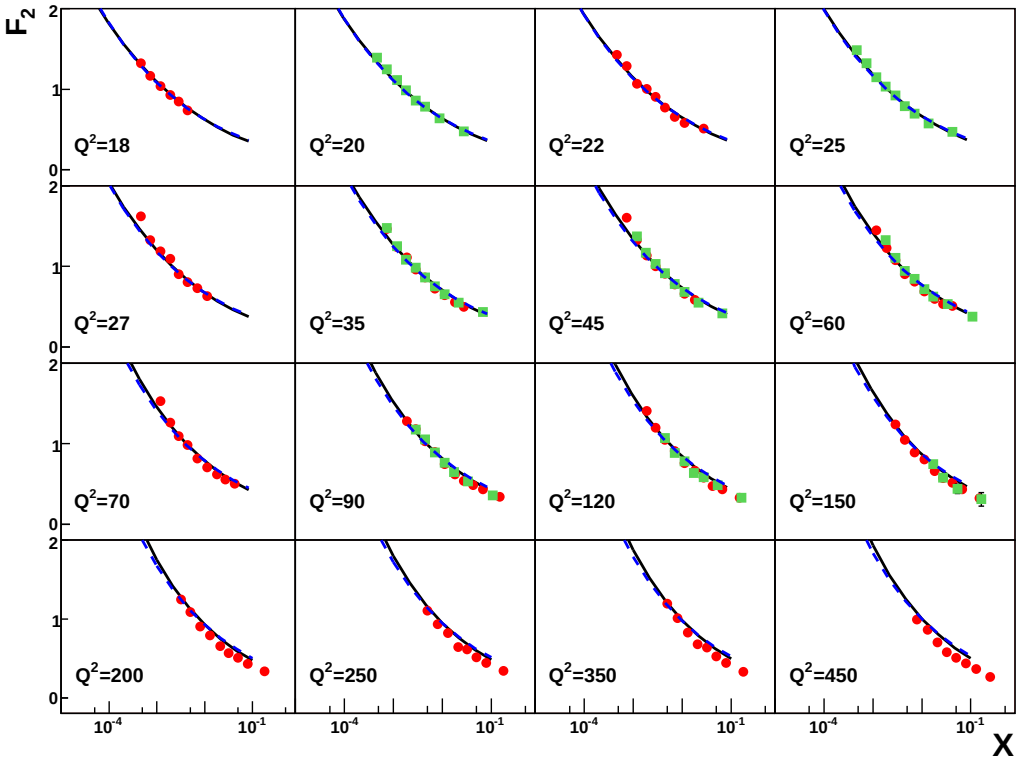

Figure 3.2: The same as in Fig. 3.1, but for larger values of Q^2. Note that we show in this figure our results up the highest Q^2 although our fit is performed including only the data for $Q^2 < 50\,\mathrm{GeV}^2$.

use $N_0 = 0.5$ in the IIM model) and two lines in Figs. 3.3, 3.4. In Ref. [30] has been further shown that without the BK-diffusion term, although allowing for an additional free parameter λ_s (one parameter more than in the GBW model), the χ^2/d.o.f value does not improve and is close to the GBW value.

Note that the GBW model only after including gluon number fluctuations gives a χ^2/d.o.f value which is comparable with the IIM one. This may mean that the violation of the geometric scaling is favored by the HERA data. The violation may come from the gluon number fluctuations or from the BK-diffusion term. To demonstrate that both GBW and IIM model after including gluon number fluctuations can be better description HERA data, Figs. 3.5, 3.6 give the F_2 comparison of these two models with gluon number fluctuations. Both of them give fairly well description to the HERA data for $Q^2 < 50\,\mathrm{GeV}^2$. However, for higher Q^2 both the averaged GBW and IIM model describes the HERA data not

quite well, since our fit is performed including only the data for $Q^2 < 50\,\mathrm{GeV}^2$ and $x \leq 0.01$, in which the use of BFKL dynamics keeps valid.

model/parameters	χ^2	χ^2/d.o.f	x_0 ($\times 10^{-4}$)	λ	R(fm)	D
T^{IIM} (light quarks only)	150.45	0.983	0.5379	0.252	0.709	0
$\langle T^{\mathrm{IIM}} \rangle$ (light quarks only)	122.62	0.807	0.0095	0.198	0.812	0.325

Table 3.2: IIM model: The parameters of the event-by-event (2 line) and of the physical (3 line) amplitude.

In the case of the IIM model, after including fluctuations, we can give an analytic expression for the physical amplitude

$$\begin{aligned}
\langle T^{\mathrm{IIM}}(r,Y)\rangle \;=\; & \frac{N_0}{2\sigma}\Bigg[\sigma\,\mathrm{Erfc}\left(\frac{\ln\frac{4}{r^2Q_s^2}}{\sigma}\right) - \frac{\mathrm{Exp}\left(\frac{-\frac{a}{4\sigma^2}\,\ln^2(b^2\,r^2Q_s^2)}{\frac{1}{\sigma^2}+\frac{a}{4}}\right)}{\sqrt{\frac{1}{\sigma^2}+\frac{a}{4}}} \\
& \times\mathrm{Erfc}\left(\frac{\frac{a\ln(4b^2)}{4}+\frac{1}{\sigma^2}\,\ln(\frac{4}{r^2Q_s^2})}{\sqrt{\frac{1}{\sigma^2}+\frac{a}{4}}}\right) \\
& + \frac{1}{\sqrt{\frac{1}{2\kappa\lambda Y}+\frac{1}{\sigma^2}}}\left(1+\mathrm{Erf}\left(\frac{-\frac{\lambda_s}{2}+\frac{1}{\sigma^2}\,\ln(\frac{4}{r^2Q_s^2})}{\sqrt{\frac{1}{2\kappa\lambda Y}+\frac{1}{\sigma^2}}}\right)\right) \\
& \times\,\mathrm{Exp}\left(-\frac{\left[\frac{\ln^2(\frac{4}{r^2Q_s^2})}{2\kappa\lambda Y\sigma^2}-\frac{\lambda_s^2}{4}+\lambda_s\frac{\ln(\frac{4}{r^2Q_s^2})}{\sigma^4}\right]}{\sqrt{\frac{1}{2\kappa\lambda Y}+\frac{1}{\sigma^2}}}\right)\Bigg]\,, \qquad (15)
\end{aligned}$$

which can be used in phenomenological applications, where Erfc(x) is the complementary error function. Also in the IIM case fluctuations do improve the description of the HERA data, however not much, as can be seen from the comparable χ^2/d.o.f values for T^{IIM} and $\langle T^{\mathrm{IIM}} \rangle$ in Table 3.2. This is so because the IIM model does already contain the geometric scaling violations via the BK-diffusion term, $\ln(4/r^2Q_s^2)/\sqrt{2\kappa\lambda Y}$, and describes accurately the HERA data, before including fluctuations. However, note that the diffusion coefficients in case of fluctuations and the BK-diffusion term are quite different, namely, $D = 0.325$ and $2\,\kappa\,\lambda \simeq 3.9$, respectively.

- Other models and a model-independent approach:

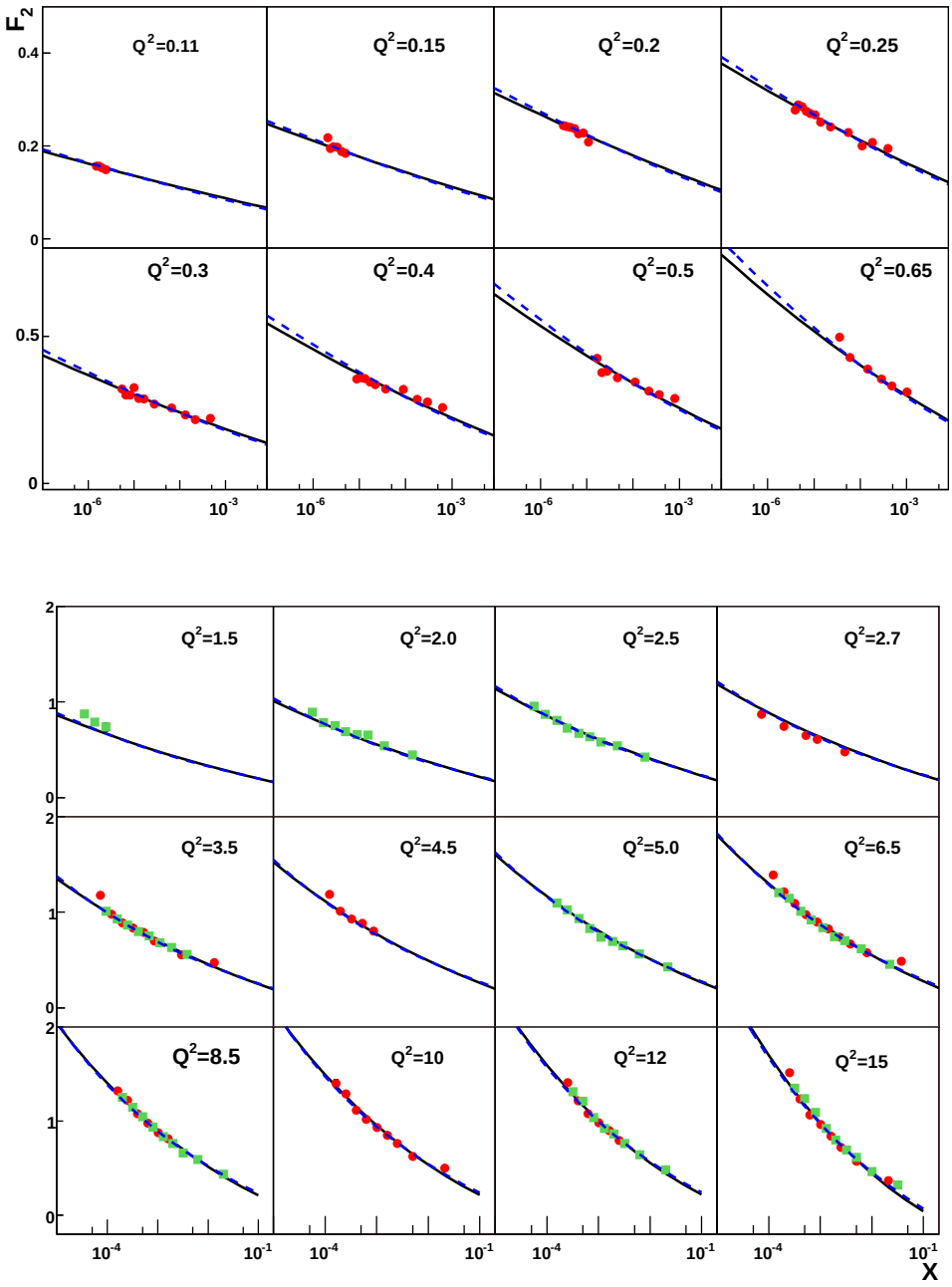

Figure 3.3: The same as in Fig. 3.1, but we use IIM model for the event-by-event scattering amplitude.

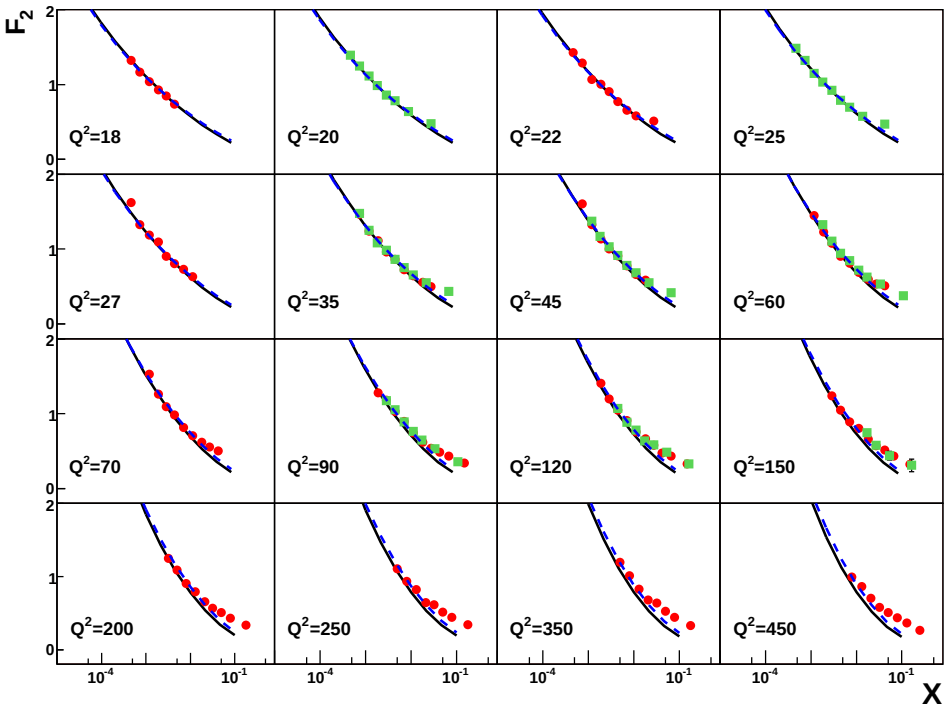

Figure 3.4: The same as in Fig. 3.3, but for larger values of Q^2.

After including fluctuations, the parameters in the GBW and the IIM case are close to each other. Apart from the fact that similar values for D are found in numerical simulations of evolution equations [39, 49] and the decrease of λ due to fluctuations is theoretically expected, at least at high energy, the parameters λ and D also seem to be quite model-independent. Indeed, similar values for λ and D would come out also if one uses a model as suggested by the theoretical findings at high energy as given in Eq. (7), for reasonable values of the proton radius, $R \simeq 0.7 - 0.8\,\mathrm{fm}$. Such a model would be for instance the IIM model with the diffusion variable $\ln(4/r^2\,Q_s^2)/\sqrt{2\,\kappa\,\lambda\,Y}$ replaced by $\ln(4/r^2\,Q_s^2)(1-\lambda_s)/\sqrt{\Delta\rho}$, such that the new model interpolates between the three regions of Eq.(7) and shows the geometric scaling behavior. The constant $\Delta\rho$ is given by Eq.(7). We use in $\Delta\rho$ a small value for α_s, $\alpha_s = 1/15$, which is the value required such that the exponent of Q_s^2 in Eq.(3) agrees with experimental or NLO results, $\lambda \simeq 0.3$. With this input, we find for $R = 0.8\,\mathrm{fm}$, the following results: $\lambda = 0.235$ and $D = 0.58$.

Moreover, the similar value of λ coming out of the different models is also sup-

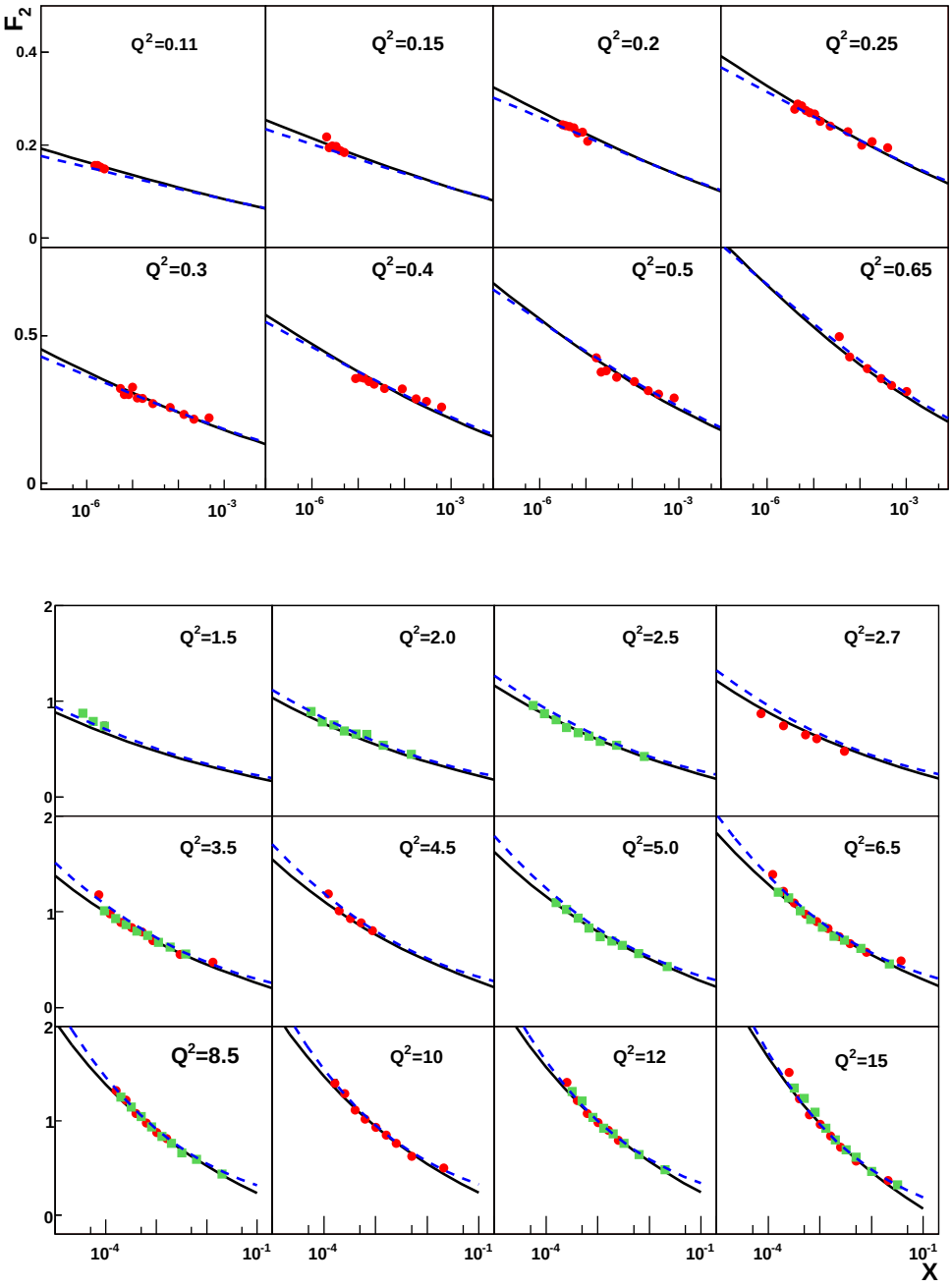

Figure 3.5: The F_2 structure function versus x at different values of Q^2. The solid lines represent the results of the averaged IIM fit and the dashed lines represent the results of the averaged GBW fit to the ZEUS data. The data points at lowest Q^2 values, 0.045, 0.065 and 0.085 GeV^2, are not shown here although they are included in the fits.

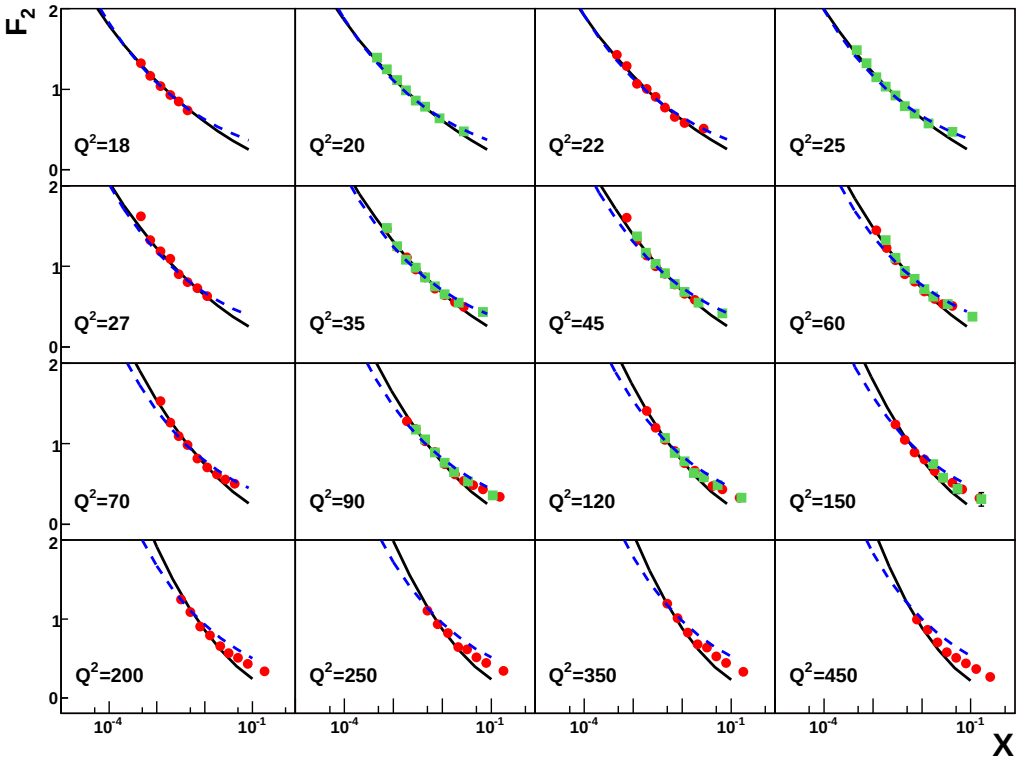

Figure 3.6: The same as in Fig. 3.5, but for larger values of Q^2. Note that we show in this figure our results up the highest Q^2 although our fit is performed including only the data for $Q^2 < 50\,\mathrm{GeV}^2$.

ported by the following model-independent approach: In case fluctuations are important in the range of HERA data, one finds the diffusive scaling behavior [52], i.e., $\sigma^{\gamma^* p}/\sqrt{DY}$ is a function of $\tau = \ln(1/r^2\,Q_s^2)/\sqrt{DY}$. We define a "quality factor" $\mathcal{O}(\lambda, x_0, D)$ as done in [48],

$$\mathcal{O}(\lambda) = \sum_i \frac{(\sigma_i - \sigma_{i-1})^2}{(\tau_i - \tau_{i-1})^2 + \varepsilon^2}, \tag{16}$$

which tests the quality of this diffusive scaling in HERA data. The definition for the quality factor obviously achieves our aim: when the points (τ_i, σ_i) lie on a unique curve the quality factor (QF) will take minimum and when two successive points are close in τ and far in σ, we expect them "not to lie on the same curve" and, indeed, they give a large contribution to the sum in (16), leading to large χ^2. Note that there are some difference as compared with Ref.[48]: in Ref.[48] they used a Gauss fit to find the maximum of the QF which was defined as

$\mathcal{Q}(\lambda) = \mathcal{O}(\lambda)^{-1}$, while we employ minuit to minimize the QF. We proceed in the following way: we reorder the data points (τ_i, σ_i) like this: Let the τ's order from minimum to maximum and record the positions of the σ_i corresponding to τ_i. And then we define $\chi^2 = \sum_i (\sigma_i - \sigma_{i-1})^2/((\tau_i - \tau_{i-1})^2 + \varepsilon^2)$, in which the constant ε^2 is a small number [2] which prevents the sum from becoming infinite when two points have the same value for τ[48]. We use minuit to minimize the χ^2, and find this way that $\lambda = 0.215$, at least for the input-values $0.01 \leq D \leq 0.7$ which we have investigated.

The seemingly model-independent values of the parameters λ and D, their agreement with the numerical values found, and the improvement of the description of the HERA data in all models after including fluctuations, seem to tell us that gluon number fluctuations are relevant in the range of HERA data. However, since in the case of the IIM model the fluctuations do not improve much the description of the HERA data, one may conclude that the BK-equation alone should describe the HERA data and that fluctuations are negligible in the energy range of the HERA data. The intention of this section is to illustrate the possibility that fluctuations may be present in the HERA data.

2. Fit to the HERA data including both light and heavy quarks

Now let us look at the heavy quarks contribution to the proton structure function at small x. It is straightforward to include the heavy quarks mass in the photon wave functions $\psi_{T,L}$. So the main difference from the previous fit is that the contribution to the photon wave functions $\psi_{T,L}$ does not only come from light quarks (u, d, s), but also from heavy quarks (c, b). After including the heavy quarks contribution to the photon wave functions, we perform the fit as in the previous case. Note that we only use the IIM model for the event-by-event scattering amplitude in our fit. For the case of GBW model, similar results as for the as IIM model are found.

The outcomes from fitting the ZEUS data including light and heavy quarks deserve more comments:

- The both fits of IIM model with and without fluctuations seem to be improved with heavy quarks. However the improvement is not much, as can be seen from the comparable χ^2 values for T^{IIM} and $\langle T^{\mathrm{IIM}} \rangle$ in Table 3.3 and Table 3.2. Note

[2] we have taken $\varepsilon = 1/n$ with n being the number of data points

that the values of χ^2 of IIM model with fluctuations are quite similar before and after including heavy quarks. It seems that in the case of gluon number fluctuations the heavy quarks contribution does not play a role in the description of the HERA inclusive DIS data, as can be seen from the comparison χ^2/d.o.f of the physical amplitude in Table 3.2 with χ^2/d.o.f of the physical amplitude in Table 3.3.

- The value of λ becomes smaller after including the heavy quarks and fluctuations which is in agreement with theoretical expectations, as can be seen from the comparison of Eq.(3) with Eq.(6).

- The value of the critical exponent λ_s which obtains from the fit of ZEUS data with heavy quarks larger than LO values used in literature. However, it is in agreement with one from the various renormalization-group-improved NLO BFKL kernels [53].

- The value of the diffusion coefficient D is sizeable, and is surprisingly close to the values which have been found numerically by solving the (1+1) dimensional toy model [39] and the Pomeron loop equations [49] in the fixed coupling case.

model/parameters	χ^2	χ^2/d.o.f	x_0 ($\times 10^{-4}$)	λ	λ_s	R_p(fm)	D
$N^{\rm IIM}$ (light+heavy quarks)	138.06	0.908	0.126	0.217	0.731	0.661	0
$\langle N^{\rm IIM} \rangle$ (light+heavy quarks)	121.28	0.803	0.0017	0.162	0.689	0.836	0.1105

Table 3.3: IIM model: The parameters of the event-by-event (2 line) and of the physical (3 line) amplitude after including the heavy quarks contribution.

The contribution of the charm and bottom quarks to (13) can directly use to compute the charm and bottom structure functions. We compare the results of our parametrization with the HERA measurements [54, 55] of the charm and bottom structure functions. These are naturally obtained from our formalism by only taking the charm or bottom contribution to the photon-proton cross-section in (12). The results from our model are plotted in Fig. 3.7 for charm and bottom structure functions respectively. In both case, we observe a good agreement with the data. Similarly, by taking the contribution only coming from the longitudinal part of the wave function in (12), we can obtain the results for the longitudinal structure function. Our results

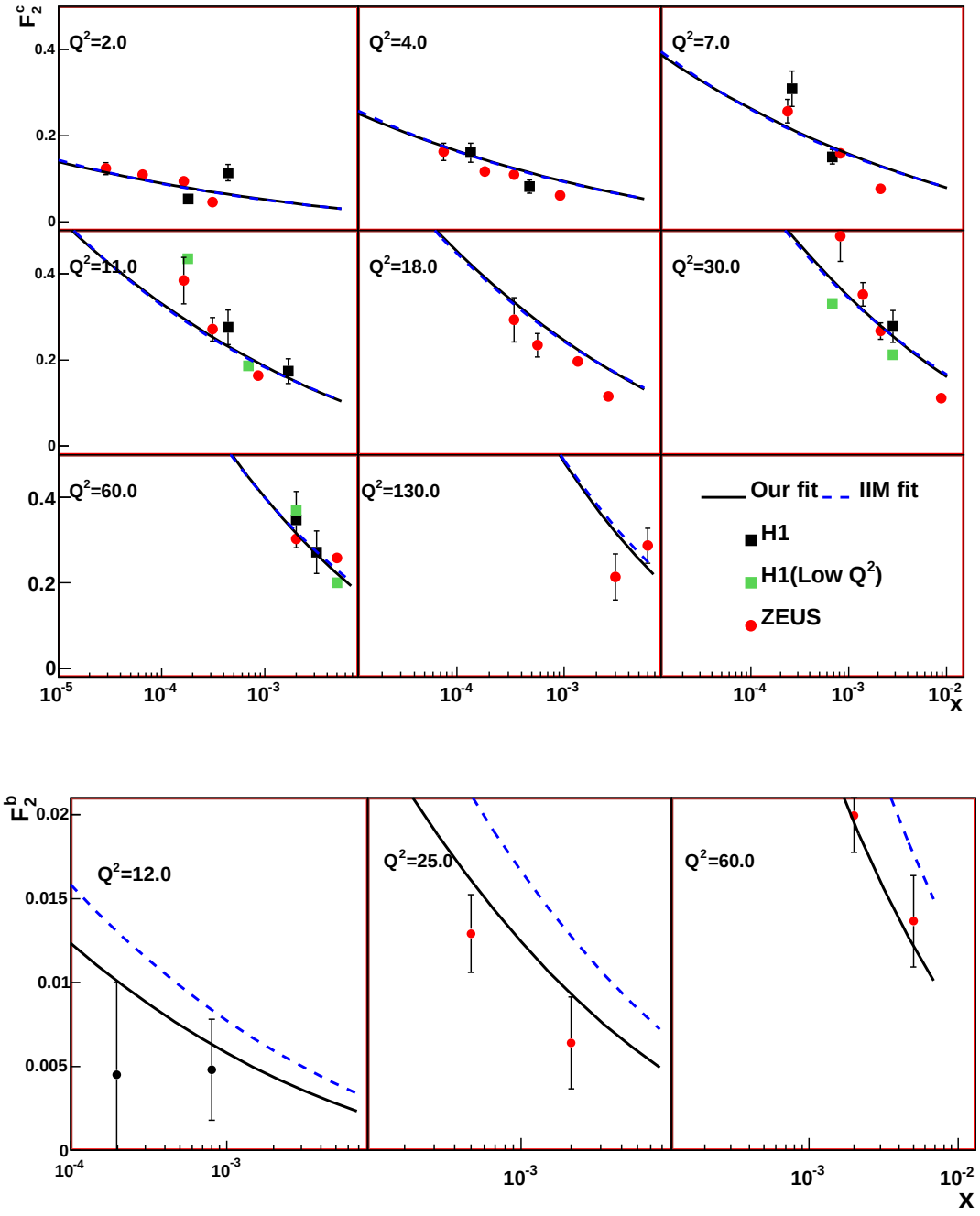

Figure 3.7: The structure function versus x at different values of Q^2. The up and down plane are charm and bottom structure functions, respectively. The solid lines represent the results of averaged IIM fitting experimental data and the dashed lines represent the results of IIM model fitting experimental data [56].

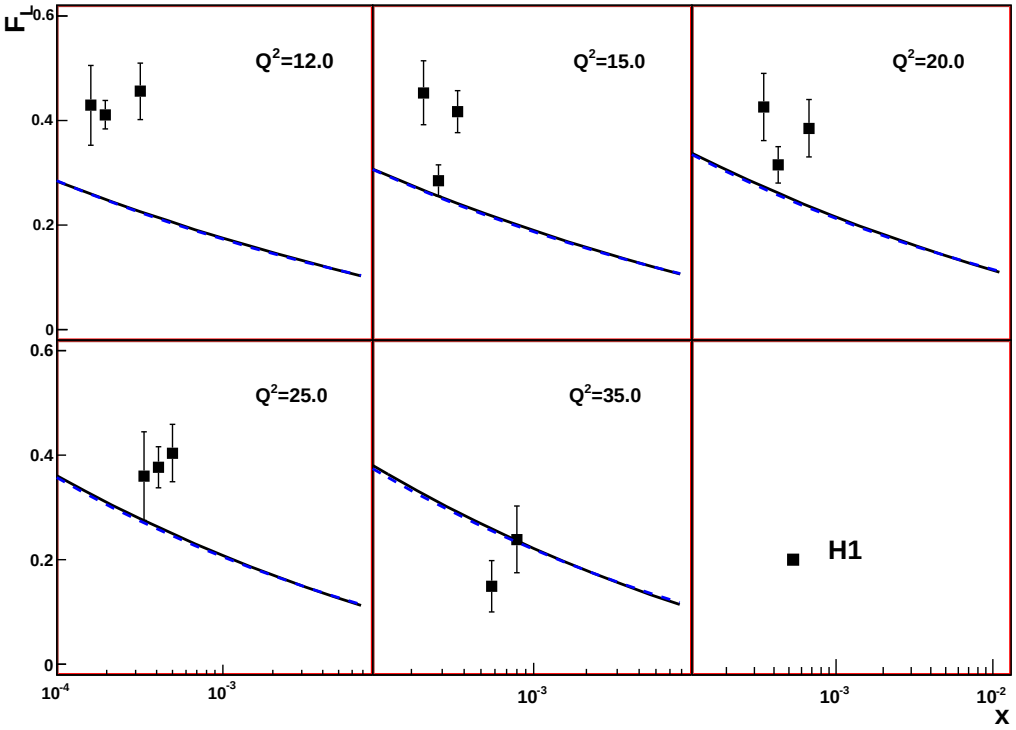

Figure 3.8: The results of our fit for the longitudinal structure functions. The solid lines represent the results of averaged IIM fitting data and the dashed lines represent the results of IIM model fitting experimental data [56].

are shown in Fig. 3.8 together with the H1 measurements [46]. Again, the present parametrization gives a good description of the data.

3.1.4 Discussion

The gluon number fluctuations would become more clear at even higher collision energies as compared to the HERA energy. With growing Y, according to the BK-equation the window for the geometric scaling behavior would increase, and the scaling violating term would become less important. On the other side, the small-x dynamics including gluon number fluctuations leads to a more clear diffusive scaling behavior with increasing Y. The forthcoming LHC may tell us more whether geometric or diffusive scaling is more appropriate for the description of the observables in the LHC energy range.

Throughout this work the coupling is kept fixed. As mentioned above, the $(1+1)$

dimensional model in [39], which accommodates Pomeron loops, gives similar values for D as our analysis for a fixed coupling. However, it has been recently shown that if allowing the coupling to run in this toy model [40] then the effects of gluon number fluctuations can be neglected up to energies far beyond the HERA and LHC energies. We plan to extend our work by the running coupling in order to see whether the HERA data can tell something about the running coupling and whether the prediction of the toy model remains valid also in the QCD case.

3.2 Gluon number fluctuations in diffractive deep inelastic scattering

Diffractive deep inelastic scattering (DIS) has triggered a wide interest since diffractive events were observed at HERA [57, 58]. Generally, such events are expect to be much more sensitive to the saturation regime [59, 60] of QCD than the inclusive ones [47, 61].

It is well known, that diffractive DIS is a process where the proton remains intact after the virtual photon scattering off proton and that there is a rapidity gap between the proton and the rest of final-state particles. There are two distinct processes contributing to the diffractive final state:

1. When the photon fluctuates into a $q\bar{q}$ pair which scatters elastically off the target without any further radiation and the mass M_X of the diffractive final state is of the order of the virtuality of the photon, which corresponds to the region of intermediate or large values of β.

2. When the $q\bar{q}$ pair interacts through higher Fock state fluctuation, i.e. $q\bar{q}g$, and the mass M_X of the diffractive final state is much larger than Q^2, which is related to the regime of small β. This process is often called a diffractive photon dissociation process.

In this section, we extend the previous analysis of diffractive DIS data (see for example [62]), which are done in the mean field approximation, to the case beyond mean field approximation, namely by taking into account the gluon number fluctuations in the high energy QCD evolution [10, 11, 13, 12, 14, 32, 33, 34].

For the event-by-event amplitude we use the Iancu, Itakula and Munier (IIM) model [30] which was inspired by BK-equation and the gluon number fluctuations are taken into account by averaging over all events. The procedure we use in this work is

always based on approximations and, therefore, can at best give hints on a possible implication of gluon number fluctuations in the HERA data.

One can observe that after including fluctuations the description of the diffractive HERA data is improved as compared to the IIM model: $\chi^2/\text{d.o.f} = 1.282$ before and $\chi^2/\text{d.o.f} = 1.031$ after including fluctuations [3]. The improvement of the description of the HERA data seems to indicate that the geometric scaling violations in the HERA data may come from gluon number fluctuations. However, we wish to emphasize here that the BK-diffusion term gives similar geometric scaling violations as fluctuations and only looking on the HERA data we still can not completely discriminate that the observed geometric scaling violations in the HERA data are the outcome of the BK-diffusion term.

This work is organized as follows: The $q\bar{q}$ and $q\bar{q}g$ components contribution to the diffractive structure function are given in Section 3.2.1. In $q\bar{q}g$ component case, we will show the diffractive structure function at large Q^2 and small β limits in the mean field and beyond the mean field approximation, respectively. In Section 3.2.2 we show numerical results and discuss possible implications of gluon number fluctuations in the diffractive HERA data. Finally, we give a conclusion in Section 3.2.3.

3.2.1 Diffractive structure function at high energy

In the diffractive DIS ($\gamma^* p \longrightarrow Xp$), the proton remains intact after the scattering, and there is a rapidity gap between the proton and the rest of the final-state particles, see Fig.3.9. The following variables describe the kinematics of the diffractive DIS process,

$$x = \frac{Q^2}{Q^2 + W^2} \ , \qquad \beta = \frac{Q^2}{Q^2 + M_X^2} \qquad x_{\mathbb{P}} = x/\beta \ , \tag{17}$$

where W^2 is the center-of-mass energy of the virtual photon-proton scattering and the Q^2 and M_X are the virtuality of the photon and the mass of the diffractive final state, respectively. The corresponding cross section for the single diffractive production is described by the following relation:

$$x_{\mathbb{P}}\sigma_r^{D,3} = x_{\mathbb{P}}F_T^{q\bar{q}} + x_{\mathbb{P}}F_T^{q\bar{q}g} + \frac{2-2y}{2-2y+y^2}\, x_{\mathbb{P}}F_L^{q\bar{q}} \tag{18}$$

[3]Note that our previous work [18] used Golec-Biernat, Wüsthoff (GBW) model which shows geometric scaling, $T(r,x) = T(r^2Q_s^2(x))$, and IIM model (which contains geometric violation) with and without fluctuations to fit inclusive DIS data. The outcomes seem to tell us that violations of geometric scaling are required for an accurate description of the HERA data.

with $y = Q^2/(sx)$ where $\sqrt{s} = 318$ GeV is the total energy in the $e - p$ scattering; $x_{\mathbb{P}}F_T^{q\bar{q}}$, $x_{\mathbb{P}}F_L^{q\bar{q}}$ are the transverse and longitudinal diffractive structure function contributing from the $q\bar{q}$ final state and $F_T^{q\bar{q}g}$ is the transverse diffractive structure function resulting from the $q\bar{q}g$ final state. Note that in Eq. (18) we don't include $F_L^{q\bar{q}g}$ which is the longitudinal diffractive structure function resulting from the $q\bar{q}g$ final state, since its contribution to $x_{\mathbb{P}}\sigma_r^{D,3}$ is negligible. Even though for small values of β it could be sizeable, as the kinematical reason for small β is associated with y close to 1, $(2-2y)/(2-2y+y^2) \sim 0$, in which case $F_L^{q\bar{q}g}$ doesn't contribution to $x_{\mathbb{P}}\sigma_r^{D,3}$. In what follows, we will extensively discuss the ingredients [4] of the r.h.s of Eq. (18).

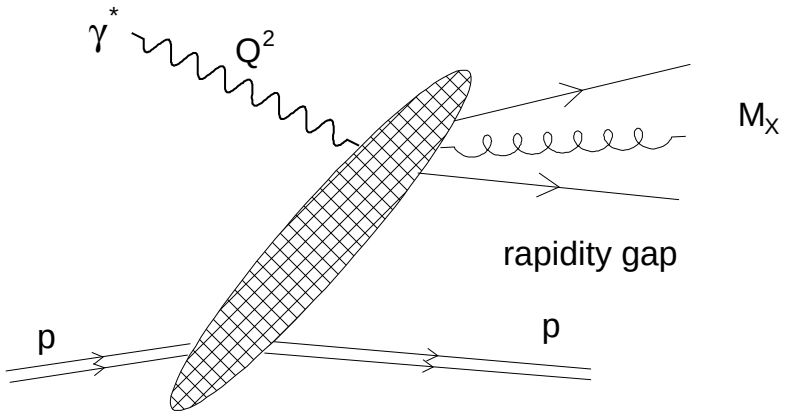

Figure 3.9: The diagram of inclusive diffractive DIS.

1. The $q\bar{q}$ components contribution to the diffractive final state

The incoming virtual photon γ^* (transversely or longitudinally polarized) splits into a dipole of size $\mathbf{r}$ which scatters diffractively off the proton at a given impact parameter $\mathbf{b}$ and dissociates into a final state of invariant mass M_X. The transverse and longitudinal $q\bar{q}$ components are the dominant contribution to the diffractive final state, because the possible final states containing gluons are suppressed by extra powers of α_s. However, the $q\bar{q}g$ component is most important at small β or large Q^2 limit,

[4] As one can see, within this approach, two distinct processes ($q\bar{q}$ and $q\bar{q}g$) contributing to the diffractive final state.

since the dipole will emit soft or collinear gluons which bring a large logarithm $\ln(1/\beta)$ or $\ln(Q^2)$ contributions to the diffractive final states and compensate the factors of α_s. In this subsection, we only take into account the $q\bar{q}$ components contribution to the diffractive structure functions, the $q\bar{q}g$ components will be discussed in the next subsection. For a virtual photon diffractive scattering off the proton, the diffractive cross-section is given by :

$$\begin{aligned}\frac{d\sigma_{L,T}^{\gamma^* p\to Xp}}{d\beta dt}(\beta, x_{\mathbb{P}}, Q^2, t) &= \frac{Q^2}{4\beta^2}\sum_f \int \frac{d^2r}{2\pi}\int \frac{d^2r'}{2\pi}\int_0^1 dz z(1-z)\Theta(\boldsymbol{\kappa}_f^2)e^{i\boldsymbol{\kappa}_f\cdot(\mathbf{r}'-\mathbf{r})} \\ &\times|\Psi_{L,T}^{(f)}(z,\mathbf{r},\mathbf{r}';Q^2)|^2\int d^2bd^2b'e^{i\boldsymbol{\Delta}\cdot(\mathbf{b}'-\mathbf{b})} \\ &\times T_{q\bar{q}}(\mathbf{r},\mathbf{b};x_{\mathbb{P}})T_{q\bar{q}}(\mathbf{r}',\mathbf{b}';x_{\mathbb{P}}) \qquad (19)\end{aligned}$$

with $\boldsymbol{\kappa}_f^2 = z(1-z)Q^2(1-\beta)/\beta - m_f^2$ and $\boldsymbol{\Delta}^2 = -t$. The impact parameter behavior of the scattering amplitude is a long standing problem, it cannot be calculated by perturbative QCD and it is usually modeled as:

$$T_{q\bar{q}}(\mathbf{r},\mathbf{b};x) = S(\mathbf{b})\ T(|\mathbf{r}|Q_s(x),x), \qquad (20)$$

where we introduce a Gaussian profile $S(\mathbf{b}) = e^{-\mathbf{b}^2/R_p}$ which is extracted from the experimental measurement of the impact parameter behavior in DIS [63, 64], here R_p is the transverse radius of the proton.

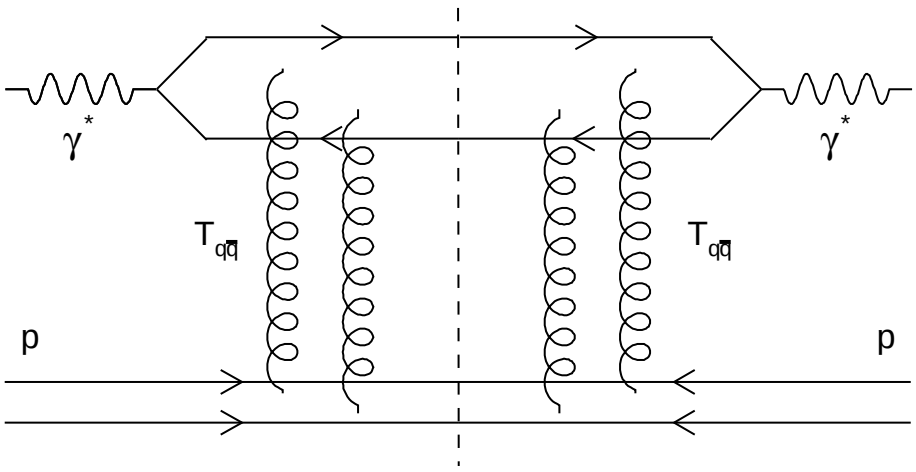

Figure 3.10: The QCD dipole picture of diffractive deep inelastic scattering. It corresponds to formula (19).

The transversely and longitudinally polarized photon wave functions can be computed in QED and are found to be

$$|\Psi_T^{(f)}(z,\mathbf{r},\mathbf{r}';Q^2)|^2 = \frac{\alpha_{em}N_c}{2\pi^2}e_f^2\Big((z^2+(1-z)^2)\varepsilon_f^2\frac{\mathbf{r}.\mathbf{r}'}{|\mathbf{r}||\mathbf{r}'|}K_1(\varepsilon_f|\mathbf{r}|)K_1(\varepsilon_f|\mathbf{r}'|) + m_f^2K_0(\varepsilon_f|\mathbf{r}|)K_0(\varepsilon_f|\mathbf{r}'|)\Big) , \tag{21}$$

$$|\Psi_L^{(f)}(z,\mathbf{r},\mathbf{r}';Q^2)|^2 = \frac{\alpha_{em}N_c}{2\pi^2}e_f^2 4Q^2z^2(1-z)^2K_0(\varepsilon_f|\mathbf{r}|)K_0(\varepsilon_f|\mathbf{r}'|) , \tag{22}$$

where the e_f and m_f are the charge and mass of the quark with flavor f and

$$\varepsilon_f^2 = z(1-z)Q^2+m_f^2 . \tag{23}$$

As in the case of inclusive DIS, where the F_2 structure function can be expressed by inclusive cross-sections

$$F_2(x,Q^2) = \frac{Q^2}{4\pi^2\alpha_{em}}(\sigma_T(x,Q^2)+\sigma_L(x,Q^2)), \tag{24}$$

we can study the diffractive structure function. Similarly, we obtain the diffractive structure function

$$x_{\mathbb{P}}F_\lambda^{D,3} = \frac{Q^2\beta}{4\pi^2\alpha_{em}}\frac{d\sigma_\lambda^{\gamma^*p\to Xp}}{d\beta} , \quad \frac{d\sigma_\lambda^{\gamma^*p\to Xp}}{d\beta} = \int_{t_{min}}^0 dt\frac{d\sigma_\lambda^{\gamma^*p\to Xp}}{d\beta dt} \simeq \frac{2}{R_p^2}\left.\frac{d\sigma_\lambda^{\gamma^*p\to Xp}}{d\beta dt}\right|_{t=0} , \tag{25}$$

with $e^{R_p^2t_{min}/2}\ll 1$. Note that we have used a trick to replace the integration of t in (19) by using the fact that the diffractive cross-section decreases exponentially with $|t|$ like $e^{R_p^2t/2}$ [62].

After some algebraic computation, we get the transverse diffractive structure function contributed from $q\bar{q}$ components

$$x_{\mathbb{P}}F_T^{q\bar{q}}(\beta,x_{\mathbb{P}},Q^2) = \frac{R_p^2N_c}{16\pi^2}\frac{Q^4}{\beta}\sum_f e_f^2\int_0^1 dz\ \Theta(\kappa_f^2)z(1-z)\left[(z^2+(1-z)^2)\times(z(1-z)Q^2+m_f^2)I_1^2(\kappa_f,\epsilon_f,Q_s)+m_f^2I_0^2(\kappa_f,\epsilon_f,Q_s)\right] . \tag{26}$$

By substituting the longitudinal overlap function (22) into (19), we get the $q\bar{q}$ components contribution to the longitudinal diffractive structure function:

$$x_{\mathbb{P}}F_L^{q\bar{q}}(\beta,x_{\mathbb{P}},Q^2) = \frac{R_p^2N_c}{16\pi^2}\frac{Q^4}{\beta}\sum_f e_f^2\int_0^1 dz\Theta(\kappa_f^2)4Q^2z^3(1-z)^3I_0^2(\kappa_f,\epsilon_f,Q_s) . \tag{27}$$

In the above two equations, the functions I_λ are given by

$$I_\lambda(\kappa, \epsilon, Q_s) = \int_0^\infty r dr J_\lambda(\kappa r) K_\lambda(\epsilon r) T(rQ_s, x_{\mathbb{P}}) \tag{28}$$

in terms of the Bessel functions J_λ and K_λ and the dipole scattering amplitude $T(rQ_s, x_{\mathbb{P}})$. In the mean field approximation, we will use the IIM model for the event-by-event scattering amplitude, $T(rQ_s, x_{\mathbb{P}})$, to do numerical simulation.

When taking into account the gluon number fluctuations (beyond mean field approximation), the scattering amplitude in Eq.(28) will be replaced by the averaged (physical) amplitude [5], $\langle T(rQ_s, x_{\mathbb{P}})\rangle$, which is given by averaging over all possible gluon realizations/events, corresponding to different events in an experiment.

In the following numerical simulation, we shall only focus on using the physical amplitude to describe the HERA data and compute the χ^2. However, to compare and demonstrate that the physical amplitude does improve the description of HERA data, we also compute the χ^2 by using the scattering amplitude derived in the mean field approximation.

2. The $q\bar{q}g$ components contribution to the diffractive final state

At large Q^2 and small β limits, the emission of soft or collinear gluons become important for getting a good description of HERA diffractive data. Because at large Q^2 and small β the dipole will emit soft or collinear gluons which bring a large logarithm $\ln(Q^2)$ or $\ln(1/\beta)$ contribution to the production of diffractive final state. Relative to the suppression of diffractive structure function by an extra power of α_s in the process of $\gamma^* p \longrightarrow Xp$ (where X standing for configuration $q\bar{q}g$), the large logarithm $\ln(Q^2)$ or $\ln(1/\beta)$ will compensate the factor of α_s. This subsection is devoted to discuss the $q\bar{q}g$ components contribution to the diffractive final state in the mean field approximation and beyond the mean field approximation at large Q^2 and small β limits.

- **The large$-Q^2$ limit**

  At large Q^2, there is a large $\ln(Q^2)$ contribution to the transverse diffractive structure function, which was computed in [65, 66]. In the coordinate space,

[5] For the more detail discussion of how to get physical amplitude, please see Section 3.1.2

the transverse distance between the quark and gluon is much larger than the transverse distance between the quark and antiquark(see Fig. 3.11). The gluon and the $q\bar{q}$ pair(it is equivalent to a gluon in the large N_c limit) form an effective gluonic color dipole which scatters off the proton. At leading $\ln(Q^2)$, the diffractive structure function can be written as

$$x_{\mathbb{P}} F_T^{q\bar{q}g}|_{LL(Q^2)}(\beta, x_{\mathbb{P}}, Q^2) = \frac{R_p^2 \alpha_s C_F N_c \beta}{16\pi^3} \sum_f e_f^2 \int_0^{Q^2} dk^2 \ln\left(\frac{Q^2}{k^2}\right) \int_\beta^1 dz \times \left[\left(1-\frac{\beta}{z}\right)^2 + \left(\frac{\beta}{z}\right)^2\right] \times I^2(\sqrt{1-z}, \sqrt{z}, Q_s/k) \quad (29)$$

with

$$I_g(a,b,c) = \int_0^\infty r dr J_2(ar) K_2(br) \tilde{T}(cr, x_{\mathbb{P}}) \quad (30)$$

where $\tilde{T}$ is equivalent to the $q\bar{q}$ dipole scattering amplitude T but for a gg dipole. In the mean field approximation case, we shall use the parametrization like $\tilde{T} = 2T - T^2$ which is in terms of large N_c limit and goes well with our model for the $q\bar{q}$ dipole scattering amplitude [62], to compute the diffractive structure function. In this work in addition to the light quark, we also take into account the heavy quark contribution to the diffractive structure function. To get a better description of HERA data, we shall replace the β variable in (29) by $\beta(1 + 4m_f^2/Q^2)$.

To go beyond the mean field approximation one has to include the effect of discreteness and fluctuations of gluon numbers. We use the relation between high-energy QCD evolution and reaction-diffusion process in statistical physics to perform gluon number fluctuations in scattering amplitude. The fluctuations in gluon numbers are taken into account by averaging over all the event-by-event amplitude, $\langle\tilde{T}\rangle = 2\langle T\rangle - \langle T^2\rangle$, see Eq.(8) in Section 3.1.2.

- **The small$-\beta$ limit**

At small β, we use a similar approach as in Ref. [62] to compute the diffractive structure function (for the details see for example Ref. [62]). At the leading $\ln(1/\beta)$, the transverse diffractive structure function, which contributes from the $q\bar{q}g$ final state, is given by

$$x_{\mathbb{P}}\ F_T^{q\bar{q}g}|_{LL(1/\beta)}(x_{\mathbb{P}}, Q^2) = \frac{C_F \alpha_s Q^2 R_p^2}{4\pi^2 \alpha_{em}} \int_0^\infty r dr \int_0^1 dz\ |\Psi_T(z, r; Q^2)|^2 A(r, x_{\mathbb{P}}) \quad (31)$$

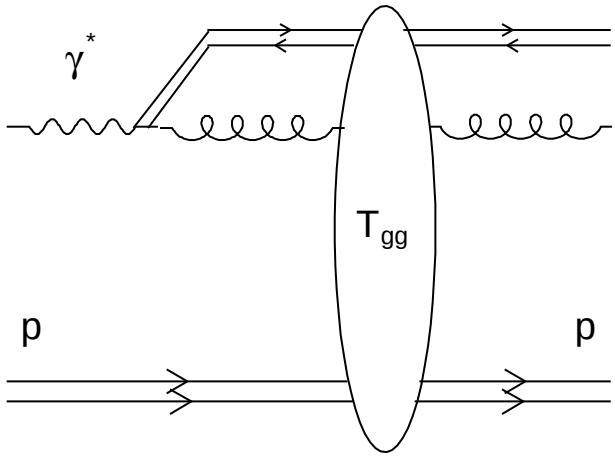

Figure 3.11: Large Q^2 limit, the $q\bar{q}g$ components contribution to the diffractive final state. The transverse distance of q-$\bar{q}$ is much larger than transverse distance of q-g, an effective gg dipole scatters off the proton.

with

$$A(|\mathbf{r}|, x_{\mathbb{P}}) = \int d^2r' \frac{\mathbf{r}^2}{\mathbf{r}'^2(\mathbf{r}-\mathbf{r}')^2} \left[T^{(2)}(|\mathbf{r}'|Q_s, |\mathbf{r}-\mathbf{r}'|Q_s, x_{\mathbb{P}}) - T(|\mathbf{r}|Q_s, x_{\mathbb{P}})\right]^2 . \tag{32}$$

The $T^{(2)}$ (resp.T) term represents the case where the interaction with the target takes place after (resp. before) the emission of the gluon (see Fig. 3.12). Since emitting a soft gluon is equivalent to a dipole splitting into two dipoles, the scattering of the $q\bar{q}g$ triple off the proton is equivalent to the scattering of two dipoles with size $\mathbf{r}'$ and $\mathbf{r}-\mathbf{r}'$ off the proton, and one has

$$\begin{aligned} T^{(2)}(|\mathbf{r}'|Q_s, |\mathbf{r}-\mathbf{r}'|Q_s, x_{\mathbb{P}}) &= T(|\mathbf{r}'|Q_s, x_{\mathbb{P}}) + T(|\mathbf{r}-\mathbf{r}'|Q_s, x_{\mathbb{P}}) \\ &\quad - T(|\mathbf{r}'|Q_s, x_{\mathbb{P}})T(|\mathbf{r}-\mathbf{r}'|Q_s, x_{\mathbb{P}}) . \end{aligned} \tag{33}$$

In the context of the BK evolution, substituting (33) into (32) the various terms in (32) can be interpreted as: The two linear terms with positive sign, $T(|\mathbf{r}'|Q_s, x_{\mathbb{P}})$ and $T(|\mathbf{r}-\mathbf{r}'|Q_s, x_{\mathbb{P}})$, describe the independent scattering of the daughter dipoles with the target, the quadratic term with a negative sign corrects for an overcounting of their simultaneous scattering, and the linear term with a negative sign is the "virtual term" which expresses the possibility that the parent dipole $\mathbf{r}$ survives without splitting.

To go beyond the mean field approximation, one has to include the gluon number fluctuations by carrying out the average of the event-by-event scattering amplitude over all events in Eqs. (33) and (32). Note that for the last term in r.h.s of Eq.(33) we cannot get an analytic expression for averaging of $T(|\mathbf{r}'|Q_s, x_{\mathbb{P}})T(|\mathbf{r}-\mathbf{r}'|Q_s, x_{\mathbb{P}})$, because this term refers to two dipoles with different size $\mathbf{r}'$ and $\mathbf{r}-\mathbf{r}'$ scattering off the proton and the integration over the saturation momentum is complicated. Fortunately, a numerical calculation provides the solution to this problem. The integration over ρ_s in Eq.(8) in Section 3.1.2 can be replaced by integration over the saturation momentum Q_s using the relation $\rho_s(Y) = \ln(Q_s^2(Y)/Q_0^2)$. After transforming the integration over ρ_s into Q_s in Eq.(8) in Section 3.1.2, one has

$$\begin{aligned}\langle T(|\mathbf{r}'|Q_s, x_{\mathbb{P}})T(|\mathbf{r}-\mathbf{r}'|Q_s, x_{\mathbb{P}})\rangle &= \int T(|\mathbf{r}'|Q_s, x_{\mathbb{P}})T(|\mathbf{r}-\mathbf{r}'|Q_s, x_{\mathbb{P}}) \\ &\times \frac{1}{\sqrt{\pi\sigma^2}}\frac{1}{Q_s^2}\exp\left(-\frac{\ln^2\left(\frac{\bar{Q}_s^2}{Q_s^2}\right)}{\sigma^2}\right) dQ_s^2,\end{aligned} \tag{34}$$

where $\bar{Q}_s^2$ denotes the averaged saturation momentum.

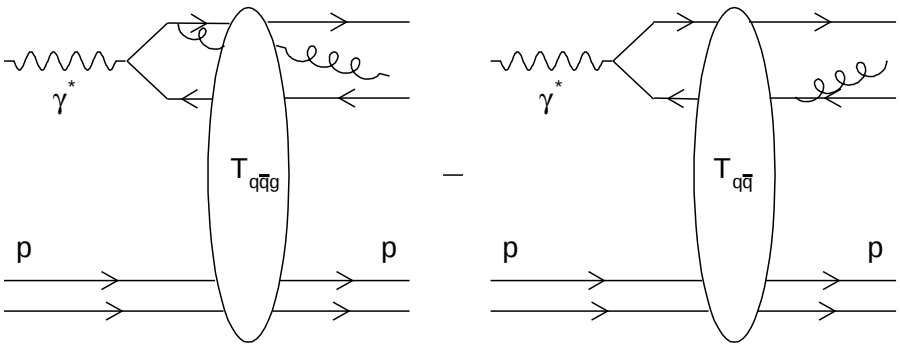

Figure 3.12: Small β limit, the $q\bar{q}g$ components contribution to diffractive final state. The $q\bar{q}g$ triplet scatters off the proton after the gluon emission, and the $q\bar{q}$ pair scatters off the proton before the gluon emission.

- **The model for $x_{\mathbb{P}}F_T^{q\bar{q}g}$**

  In order to obtain a correct $q\bar{q}g$ contribution to diffractive structure function at both large Q^2 and small β limits, we use the following way to reconstruct

$x_{\mathbb{P}}F_T^{q\bar{q}g}$ [62]

$$x_{\mathbb{P}}F_T^{q\bar{q}g}(\beta, x_{\mathbb{P}}, Q^2) = x_{\mathbb{P}}F_T^{q\bar{q}g}|_{LL(Q^2)}(\beta, x_{\mathbb{P}}, Q^2)\ \frac{x_{\mathbb{P}}F_T^{q\bar{q}g}|_{LL(1/\beta)}(x_{\mathbb{P}}, Q^2)}{x_{\mathbb{P}}F_T^{q\bar{q}g}|_{LL(Q^2)}(\beta=0, x_{\mathbb{P}}, Q^2)}, \quad (35)$$

where $x_{\mathbb{P}}F_T^{q\bar{q}g}|_{LL(Q^2)}(\beta=0, x_{\mathbb{P}}, Q^2)$ is the diffractive structure function of the $q\bar{q}g$ contribution at the small β limit in the leading $\ln(Q^2)$ approximation. Using the approximation $K_2(x) \sim 2/x^2$ for $x \to 0$, at $\beta = 0$ the Eq.(29) is reduced to

$$\begin{aligned} x_{\mathbb{P}}F_T^{q\bar{q}g}|_{LL(Q^2)}(\beta=0, x_{\mathbb{P}}, Q^2) &= \frac{C_F N_c \alpha_s R_p^2}{6\pi^3} \sum_f e_f^2 \int_0^{Q^2} dk^2 \left[\ln\left(\frac{Q^2}{k^2}\right)\right] \\ &\times \left| \int_0^\infty \frac{dr}{r} J_2(kr) \left(2T(rQ_s, x_{\mathbb{P}}) - T^2(rQ_s, x_{\mathbb{P}})\right)\right|^2 . \end{aligned} \quad (36)$$

For $Q^2 \gg Q_s^2$, Eqs.(36) and (31) are reduced to the same quantity, which has the form as

$$\begin{aligned} x_{\mathbb{P}}\ F_T^{q\bar{q}g}(\beta=0, x_{\mathbb{P}}, Q^2 \gg Q_s^2) &= \frac{C_F N_c \alpha_s Q_s^2 R_p^2}{3\pi^3} \sum_f e_f^2 \ln\left(\frac{Q^2}{Q_s^2}\right) \int_0^\infty \frac{d\bar{r}}{\bar{r}^3} \\ &\times \left[2T(\bar{r}, x_{\mathbb{P}}) - T^2(\bar{r}, x_{\mathbb{P}})\right]^2 . \end{aligned} \quad (37)$$

One can see that Eq.(35) is a reasonable expression for the $q\bar{q}g$ components contribution to diffractive structure function at large Q^2 and small β limits. This is because at the large Q^2 limit the ratio of $x_{\mathbb{P}}F_T^{q\bar{q}g}|_{LL(1/\beta)}(x_{\mathbb{P}}, Q^2)/x_{\mathbb{P}}F_T^{q\bar{q}g}|_{LL(Q^2)}(\beta=0, x_{\mathbb{P}}, Q^2) \sim 1$, the dominant contribution of the $q\bar{q}g$ components to the diffractive structure function comes from $x_{\mathbb{P}}F_T^{q\bar{q}g}|_{LL(Q^2)}(\beta, x_{\mathbb{P}}, Q^2)$, and at the small β limit the ratio of $x_{\mathbb{P}}F_T^{q\bar{q}g}(\beta, x_{\mathbb{P}}, Q^2)/x_{\mathbb{P}}F_T^{q\bar{q}g}|_{LL(Q^2)}(\beta=0, x_{\mathbb{P}}, Q^2) \sim 1$, the dominant contribution of the $q\bar{q}g$ components to the diffractive structure function comes from $x_{\mathbb{P}}F_T^{q\bar{q}g}|_{LL(1/\beta)}(\beta, x_{\mathbb{P}}, Q^2)$. The advantage of Eq.(35) is that it bridges the two limits.

To go beyond the mean field approximation, one has to perform the average of the event-by-event scattering amplitude over all events in Eqs. (36) and (37) which will be used to compute the diffractive structure function $x_{\mathbb{P}}F_T^{q\bar{q}g}(\beta, x_{\mathbb{P}}, Q^2)$ beyond the mean field approximation. We wish to note that for the average of $\langle T^2 \rangle$ we use the same way as in Eq. (34) to perform the integration over the saturation momentum. Note that the $q\bar{q}g$ contribution is only important at large Q^2 and small β regime. For the small Q^2 and large β regime, the $q\bar{q}g$

contribution cannot be correctly described, because in these regions the $q\bar{q}g$ contribution is overwhelmed by the $q\bar{q}$ components and is not relevant.

3.2.2 Numerical results

1. Fixing the model parameters by the HERA F2 data

We will use the averaged IIM model to compute the χ^2 which reflects the quality of our description of diffractive HERA data. The parameters have already been obtained in Sec. 3.1.3 (for details see Table. 3.3), in which both heavy quarks and gluon number fluctuations are included in the fit of the proton structure function. We will use the value of parameters in the third line at Table. 3.3 to estimate the χ^2.

2. Unified description of HERA diffractive data (beyond the mean field approximation)

The model which was proposed by Iancu, Itakura and Munier (IIM) was formulated in the color dipole picture. In this formalism both the inclusive and diffractive cross sections can be calculated. The inclusive cross section of IIM model in ep collision was extended to include gluon number fluctuations in our previous study [18]. In this work, we use the IIM model to further study the gluon number fluctuations in the diffractive ep scattering. In this case, the diffractive cross section and structure function can be expressed as:

$$\frac{d^3\sigma^{\gamma^* p\to Xp}}{dx_{\mathbb{P}}\ d\beta\ dQ^2} = \frac{4\pi\alpha_{em}^2}{\beta Q^4}\left(1-y+\frac{y^2}{2}\right)\sigma_r^{D,3}(\beta, x_{\mathbb{P}}, Q^2)\,, \qquad \sigma_r^{D,3} = F_T^{D,3} + \frac{2-2y}{2-2y+y^2}\,F_L^{D,3} \tag{38}$$

with $y = Q^2/(s\cdot x)$, where $\sqrt{s} = 318$ GeV is the center-of-mass energy in the $e-p$ collision.

To compare our model with HERA data, we use following formula to implement the computation of χ^2

$$x_{\mathbb{P}}\sigma_r^{D,3} = x_{\mathbb{P}}F_T^{q\bar{q}} + x_{\mathbb{P}}F_T^{q\bar{q}g} + \frac{2-2y}{2-2y+y^2}\ x_{\mathbb{P}}F_L^{q\bar{q}} \tag{39}$$

which is given in terms of the diffractive structure function. The $x_{\mathbb{P}}F_T^{q\bar{q}}$ and $x_{\mathbb{P}}F_L^{q\bar{q}}$ components dominate in the regime of large or intermediate values of β respectively, while the term $x_{\mathbb{P}}F_T^{q\bar{q}g}$ plays a important role at small β. The longitudinal component $x_{\mathbb{P}}F_L^{q\bar{q}g}$ does not contribute to longitudinal structure function, since for kinematical reasons small β is associated with y close to 1, $(2-2y)/(2-2y+y^2) \longrightarrow 0$.

Using formulae(26), (27), (35), and the dipole scattering amplitude (4), we compute the χ^2 with free parameters which we have extracted by fitting the ZEUS data with heavy quarks and gluon number fluctuations in the previous section. We compare our result of $\chi^2/d.o.f$ with the outcome in [62], in which the gluon number fluctuations are not taken into account. In this section, we only considered the $x_{\mathbb{P}} < 10^{-2}$ experimental data and used only the H1 [57] data to compute the χ^2, because there is a mismatch between the H1 and ZEUS [58] data with regard to the data normalization.

To estimate the quality of our description, we perform the following χ^2 computations. We use 343 H1 data points, with $x_{\mathbb{P}} < 10^{-2}$, to compute χ^2 and multiply the factor 1.23 to our results in order to account for the mismatch between the H1 and ZEUS data [57]. We obtain:

- **In the mean field approximation**
  $\chi^2/\text{d.o.f} = 1.282$ (see Table 3.4) which is consistent with the result in [62].

- **Beyond the mean field approximation**
  $\chi^2/\text{d.o.f} = 1.031$ (see Table 3.4). Comparing the $\chi^2/\text{d.o.f}$ in the mean field approximation with $\chi^2/\text{d.o.f}$ beyond the mean field approximation, one can see that the description of the diffractive DIS data is improved once gluon number fluctuations are included. This improvement after including fluctuations seems to support our previous results, namely the violations of geometric scaling or probably effects of gluon number fluctuations in the HERA data.

However, since in the case of the IIM model the fluctuations do not improve much the description of the HERA data, this is due to the fact that the IIM model does already contain some kind of the geometric scaling violations via the BK-diffusion term, $\ln(4/r^2Q_s^2)/\sqrt{2\kappa\lambda Y}$, and describes well the HERA data, even before including fluctuations. One may think that the BK-equation alone can describe the HERA data and that fluctuations may be negligible in the energy range of the HERA data. The intention of this work is to illustrate that even taking such a successful model as basis one can get improvement in description of the HERA data once gluon number fluctuations are taken into account.

3.2.3 Conclusions

Let us summarize the main results of this work. We have shown that the description of the diffractive DIS is improved once gluon number fluctuations are included. This

model/parameters	χ^2	χ^2/d.o.f	x_0 ($\times 10^{-4}$)	λ	γ_c	R_p(fm)	D
T^{IIM}	433.92	1.282	0.126	0.217	0.731	0.661	0
$\langle T^{\mathrm{IIM}} \rangle$	348.51	1.031	0.0017	0.162	0.689	0.836	0.1105

Table 3.4: IIM model: The parameters of diffractive structure function with (3 line) and without (2 line) gluon number fluctuations.

improvement after including the fluctuations supports our previous study [18], namely the violations of geometrical scaling or probably the effect of even gluon number fluctuations in the HERA data. However, the improvement is not much, this can be seen from the comparable $\chi^2/d.o.f$ values in Table 3.4, because the IIM model does already contain the geometrical scaling violations via the BK-diffusion term. The aim of this work is to illustrate the possibility that the gluon number fluctuations may be also present in the diffractive DIS data at HERA and to give further support to our previous results [18].

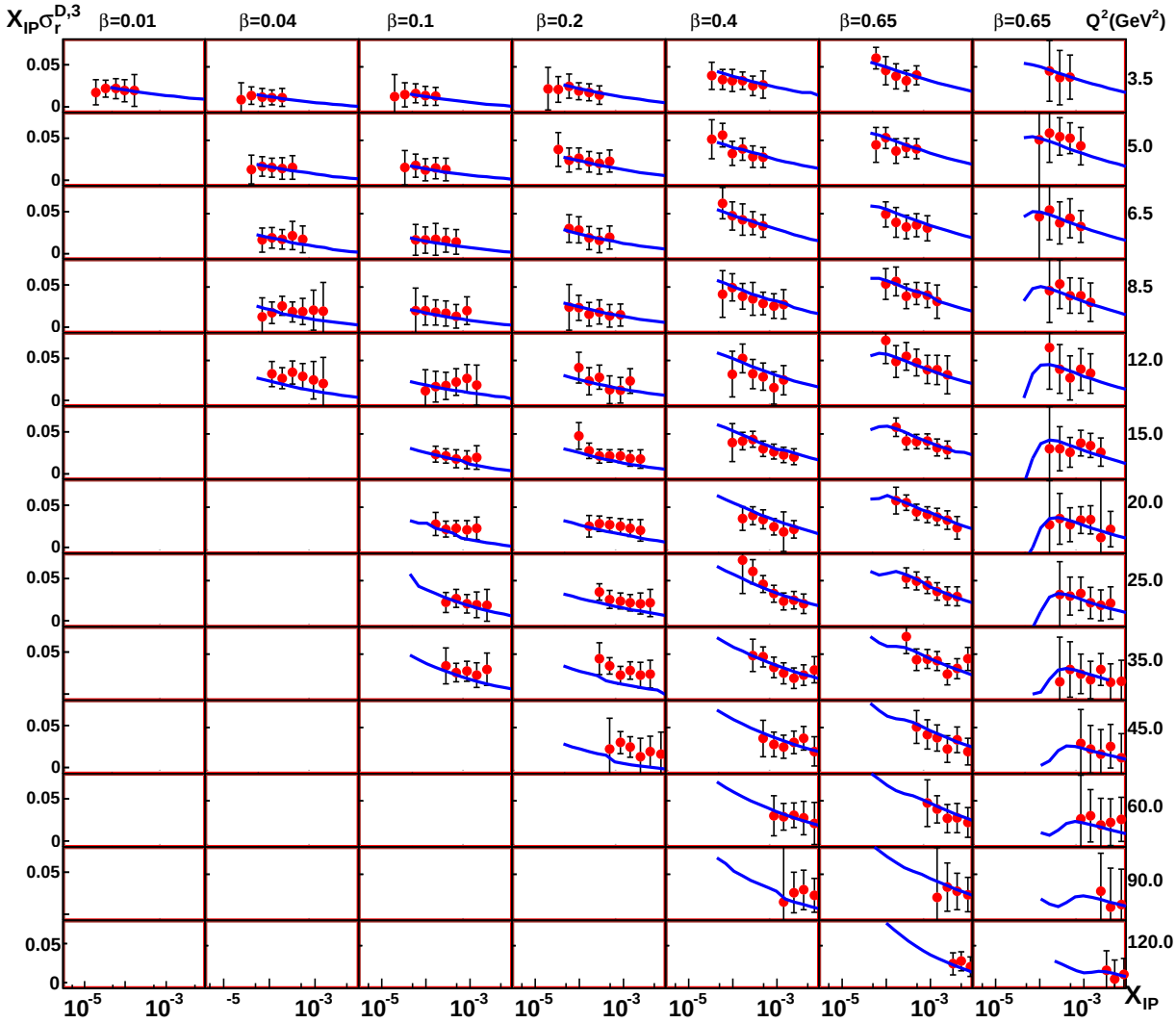

Figure 3.13: The diffractive structure function versus X_{IP} at different values of Q^2 and β. The experimental data comes from the latest H1 collaboration. The solid lines represent the results of averaged IIM model including gluon number fluctuations.

Chapter 4

Froissart bound and gluon number fluctuations

The consistent description of the impact parameter behavior of the scattering amplitude is a long standing problem. In this work we are going to discuss the influence of gluon number fluctuation on this behavior.

In fact, some activities toward understanding how fluctuations change the impact parameter dependence of the scattering amplitude have already started (see for example Refs. [67, 68, 69]). Nevertheless, it is necessary to admit that we are still far away from the complete and consistent theory related to this subject. The most crucial difficulty related to the impact parameter dependence is the *non-perturbative* (soft) contribution, which should be taken into account at large values of the impact parameter (for reviews see [21, 70, 71] and references therein). In our approach we use a quite different technique with comparison to Refs. [67, 68, 69]. Namely, we calculate the rapidity dependence of the radius of the black disk in the fluctuation-dominated (diffusive scaling) region at high energy and using the result we make our main conclusions.

The gluon number fluctuations become important at very high energy. Therefore, when considering the way how the Froissart bound may emerge based on the knowledge gathered in the small-x physics, the effects of the most recent elements in the evolution, the effects of Pomeron loop, have to be taken into account.

In this work we focus on the consequences of fluctuations on the impact parameter dependence of the scattering amplitude. In Section 4.1 and 4.2, we will briefly review the Froissart bound and the non-perturbative input of the scattering amplitude. The

Froissart bound including gluon saturation effects will be studied in Section 4.3. It turns out that the total cross section saturates the Froissart bound in the case of gluon saturation. In Section 4.4, we will compute the impact parameter dependence of the physical amplitude including gluon number fluctuations. We find that the physical amplitude has a Gaussian dependence on the impact parameter, which is in agreement with experimental measurements. We also calculate the radius of the black disk including gluon number fluctuations and find a unique rapidity dependence coming from fluctuations. Further, in Section 4.5 we calculate the slope parameter B and find that it agrees with experimental results. The discussion and conclusion are given in Section 4.6.

4.1 Unitarity and Froissart bound

In high energy scattering processes, the total cross section for the reaction $12 \longrightarrow n$ particles is

$$\sigma_{12\longrightarrow n} = \frac{1}{4|\mathbf{p_1}|\sqrt{\mathbf{s}}} \sum (2\pi)^4 \delta^4(P^f - P^i) |\langle f_n|T|i\rangle|^2. \tag{1}$$

Here $|\mathbf{p_1}|$ is the magnitude of the initial center-of-mass frame three momentum. It is well known that the probability conservation in the scattering processes requires the scattering S matrix to be a unitary matrix $SS^\dagger = 1$. Unitarity of S matrix provides a simple way to derive total cross sections from the forward($\theta_s = 0$) elastic scattering amplitude, which is known as the optical theorem. For any orthonormal states $|i\rangle$ and $\langle j|$, one has

$$\delta_{ji} = \langle j|SS^\dagger|i\rangle = \sum_f \langle j|S|f\rangle\langle f|S^\dagger|i\rangle \tag{2}$$

where we have used the completeness relation

$$\sum_f |f\rangle\langle f| = 1. \tag{3}$$

We define the T matrix as $S = 1 - iT$, then the unitarity condition requires that

$$\langle j|T|i\rangle - \langle j|T^\dagger|i\rangle = (2\pi)^4 i \sum_f \delta^4(P^f - P^i)\langle j|T^\dagger|f\rangle\langle f|T|i\rangle. \tag{4}$$

In the case of $j = i$, where the final state is the same as the initial state, we obtain the optical theorem

$$\sigma_{12}^{tot} = \frac{1}{2|\mathbf{p_1}|\sqrt{\mathbf{s}}} \mathtt{Im}\langle i|T|i\rangle \tag{5}$$

with

$$2\mathtt{Im}\langle i|T|i\rangle = \mathtt{Im}A(s,t=0) = \sum_f (2\pi)^4 i\delta^4(P^f - P^i)|\langle f|T|i\rangle|^2, \tag{6}$$

where $A(s,t)$ is the elastic scattering amplitude, s and t are the center-of-mass energy squared and a momentum transfer squared, respectively.

In high energy physics, the two particles scattering amplitude $A(s,\cos\theta_s)$ can be expanded in the partial-wave series,

$$A(s,\cos\theta_s) = 16\pi \sum_{l=0}^{\infty}(2l+1)A_l(s)P_l(\cos\theta_s), \tag{7}$$

where $P_l(\cos\theta_s)$ is the Legendre polynomial of the first kind, and θ_s is the s channel scattering angle in the center-of-mass frame. The partial-wave amplitude $A_l(s)$ can be written in terms of a real phase shift δ_s and an inelastic threshold η_l

$$A_l(s) = \frac{\eta_l(s)e^{2i\delta_l(s)} - 1}{2i\rho(s)}, \tag{8}$$

where $\rho(s) = 2|\mathbf{p_1}|/\sqrt{\mathbf{s}}$ with our choice of normalization, and unitarity requires that $0 < \eta_l < 1$. $A_l(s)$ will be exponentially small for

$$l \geq \alpha M^{-1}\sqrt{s}\ln(s) \tag{9}$$

and the scattering amplitude (7) may be truncated at this value [72]. With the unitarity constrain $0 < \eta_l < 1$ and (8), we can get

$$|A_l(s)| = \left|\frac{\eta_l(s)e^{2i\delta_l(s)} - 1}{2i\rho(s)}\right| \leq \frac{1}{\rho(s)}, \tag{10}$$

where $\rho(s) \longrightarrow 1$ as $s \longrightarrow \infty$. We know that the Legendre polynomial of the first kind $|P_l(\cos\theta_s = 1)| \leq 1$. So, for large s

$$|A(s,\cos\theta_s = 1)| \leq \sum_{l=0}^{l_m}(2l+1) \tag{11}$$

with [73]

$$l_m = \alpha M^{-1}\sqrt{s}\ln(s). \tag{12}$$

Performing the summation over l in (11), it gives

$$|A(s,\cos\theta_s = 1)| \leq \mathtt{constat} \times s\ln^2(s). \tag{13}$$

Substituting it in (5), the Froissart bound is [2]

$$\sigma^{tot} \leq \texttt{constant} \times \ln^2(s) \tag{14}$$

where we have used

$$|\mathbf{p_1}|^2 s = (P_1 \cdot P_2)^2 - m_1^2 m_2^2 = \frac{1}{4}[s - (m_1 + m_2)^2][s - (m_1 - m_2)^2]. \tag{15}$$

Here, P_1 and P_2 are the magnitude of the initial center-of-mass frame four momentum in the two-body scattering process $1 + 2 \longrightarrow 3 + 4$, the m_1 and m_2 are the mass of particle 1 and particle 2. The Froissart bound is one of the outstanding results of the analytic S matrix theory. This bound has been derived 1961 by Froissart[2] assuming that the two particles scattering amplitude has uniformly bounded partial wave amplitudes and satisfies the Mandelstam representation with a finite number of subtractions. The Froissart bound expresses that the hadronic total cross section can not rise faster than $\texttt{constant} \times \ln^2 s$.

4.2 The non-perturbative input

In many practical applications, it is too complicated to perform calculations of the scattering amplitude keeping precisely the information about the impact parameter dependence, since it is related to the *non-perturbative* physics. In order to simplify the situation, one considers the scattering at fixed impact parameter and then introduces the knowledge about the impact parameter dependence through some profile function, which we will denote by $S(b)$. Usually, the following two ansätze are used as a *non-perturbative* input:

1. The scattering amplitude expressed as the product of the scattering amplitude at fixed impact parameter times the profile function $S(b)$

$$T(Y, r, b) = T(Y, r) \cdot S(b). \tag{16}$$

   Such factorization form is usually used in the region of large values of the impact parameter b.

2. The second one is mostly inspired by the numerical study of BK equation with a modified BK kernel in which the kernel of the BK integral equation is regulated

to cut off infrared singularities [74]. The impact parameter dependence is introduced through the saturation scale, $Q_s(Y,b) = Q_s(Y) \cdot S(b)$, and consequently for the scattering amplitude we have:

$$T(Y,\, Q,\, b) \;=\; T(Q,\, Q_s(Y,b)) \;=\; T(Q,\, Q_s(Y,b=0) \cdot S(b))\,. \tag{17}$$

In both cases, the impact parameter profile function typically has the exponential behavior $S(b) = e^{-2m_\pi b}$ at large distances $b \gg R_0$, where R_0 is the typical radial size of the hadron under consideration and R_0 increases as $A^{1/3}$ for a nucleus with atomic number A. We use such an exponential fall-off at large impact parameter as a *non-perturbative* initial condition at low energy.

4.3 Single event amplitude

In the geometric scaling region and in the fixed coupling case, the scattering amplitude reads

$$T(Y,r,b) \simeq \left(r^2 Q_s^2(Y)\right)^{\gamma_s} \cdot S(b), \tag{18}$$

where the saturation momentum is

$$Q_s^2(Y) = Q_0^2 e^{\omega \bar{\alpha}_s Y} \tag{19}$$

with the arbitrary reference scale Q_0 ($Q_0 \sim \mathcal{O}(\Lambda_{QCD})$) and the $S(b)$ gives the impact parameter dependence. Note that here factorization is assumed, which is the case as in Refs.[75, 74]. Eq. (18) shows geometric scaling with the anomalous dimension

$$\gamma = 1 - \gamma_s \simeq 0.37. \tag{20}$$

Now, with the *non-perturbative* input

$$S(b) \simeq e^{-2m_\pi b} \tag{21}$$

at large b, one obtains from the condition

$$T(Y,r,R) = \kappa \simeq \mathcal{O}(1) \tag{22}$$

the "black disc radius"

$$R \simeq \frac{\gamma_s}{2m_\pi}\left(\omega \bar{\alpha}_s Y - \ln\left(\frac{Q^2}{Q_0^2}\right)\right). \tag{23}$$

Eq. (23) gives the standard result given in the literature [75]. We have gone through such a detailed derivation of (23) since one of the main purposes of the present work is to show how Eq. (23) is modified once gluon number fluctuation effects are included.

The resulting cross section saturates the Froissart bound

$$\begin{aligned}\sigma^{tot} &= 2\int d^2b T(Y,r,b) \\ &= 2\pi R^2 \\ &\simeq \frac{2\pi\gamma_s^2}{4m_\pi^2}\left(\omega\bar{\alpha}_s Y - \ln\left(\frac{Q^2}{Q_0^2}\right)\right)^2 \\ &\sim \frac{\pi\gamma_s}{2}\left(\frac{\omega\bar{\alpha}_s}{m_\pi}\right)^2 \ln^2 s \end{aligned} \tag{24}$$

with $Y = \ln(s/Q^2)$.

It is easy to check that both ansätze in Eq. (16) and Eq. (17) for the single event amplitude lead to the result in Eq. (23).

4.4 Including gluon number fluctuations

Based on the high energy QCD/statistical physics correspondence, we can write

$$\langle T(\rho,\rho_s(Y,b))\rangle = \int d\rho_s(Y,b) T(\rho-\rho_s(Y,b)) P(\rho-\langle\rho_s(Y,b)\rangle) \tag{25}$$

where we have used $\rho = \ln(Q^2/Q_0^2)$ and $\rho_s(Y,b) = \ln(Q_s^2(Y,b)/Q_0^2)$. The probability distribution of $\rho_s(Y,b)$ is argued to have Gaussian form,

$$P(\rho_s(Y,b)) \simeq \frac{1}{\sqrt{\pi DY}} \exp\left[-\frac{(\rho_s(Y,b)-\langle\rho_s(Y,b)\rangle)^2}{DY}\right] \tag{26}$$

and the single scattering amplitude $T(\rho-\rho_s(Y,b))$ is

$$T(\rho,\rho_s(Y,b)) = \begin{cases} 1 & \text{for } \rho \le \rho_s(Y,b) \\ \exp\left[-\gamma_s(\rho-\rho_s(Y,b))\right] & \text{for } \rho \ge \rho_s(Y,b). \end{cases} \tag{27}$$

It is easy to show that in the diffusive scaling region, $\sigma \ll \rho - \langle\rho_s(Y,b)\rangle \ll \gamma_s\sigma^2$,

$$\langle T(Y,r,b)\rangle \simeq e^{-(\rho-\langle\rho_s(Y,b)\rangle)^2/DY} \cdot \frac{\sqrt{DY}}{\rho-\langle\rho_s(Y,b)\rangle} \tag{28}$$

where we have used $\sigma^2 = DY$ with D the diffusion coefficient. Now, with the *non-perturbative* input

$$\langle\rho_s(Y,b)\rangle \simeq \rho_s(Y,b) \simeq \omega\bar{\alpha}_s Y - 2m_\pi b, \tag{29}$$

one can easy see that the exponential decrease with b in the single event case is turned into a Gaussian b dependence

$$\begin{aligned}\langle T(Y,r,b)\rangle &\simeq \frac{\sqrt{DY}}{\rho-\langle\rho_s(Y,b)\rangle}\cdot e^{-(\rho-\omega\bar{\alpha}_s Y+2m_\pi b)^2/DY}\\ &\propto \frac{1}{2\sqrt{\pi}}e^{-\frac{4m_\pi^2 b^2}{DY}}.\end{aligned} \tag{30}$$

This consequence of fluctuations seems to be supported by the experimental observations since, say for pp collision,

$$\frac{d\sigma_{el}}{dt}\sim e^{-B|t|} \tag{31}$$

which after a Fourier transform gives

$$S(b)\sim e^{-\frac{b^2}{2B}}. \tag{32}$$

Second consequence of fluctuations is that the factorization is broken, see Eq. (28),

$$\langle T(Y,r,b)\rangle \neq f(Y,r)\cdot S(b) \tag{33}$$

as compared to the single event amplitude in Eq. (18) where

$$\langle T(Y,r,b)\rangle = f(Y,r)\cdot S(b). \tag{34}$$

Third consequence of fluctuations is that also the averaged amplitude in Eq. (30) satisfies the Froissart bound. Namely, from the condition $\langle T\rangle = \kappa \simeq \mathcal{O}(1)$ (but $\kappa \leq 1$),

$$\kappa \simeq \frac{\sqrt{DY}}{\rho-\langle\rho_s(Y,R)\rangle}\cdot e^{-(\rho-\omega\bar{\alpha}_s Y+2m_\pi R)^2/DY} \tag{35}$$

which after taking the logarithm on both sides reads (κ' close to one)

$$-\kappa' = -\frac{(\rho-\langle\rho_s(Y,R)\rangle)}{DY}+\ln\left(\frac{\sqrt{DY}}{\rho-\langle\rho_s(Y,R)\rangle}\right) \tag{36}$$

and is fullfilled if

$$\rho-\langle\rho_s(Y,R)\rangle \simeq \sqrt{DY}. \tag{37}$$

Now, with $\langle\rho_s(Y,R)\rangle \simeq \omega\bar{\alpha}_s Y - 2m_\pi R$, one obtains

$$\begin{aligned}\rho-\omega\bar{\alpha}_s Y+2m_\pi R &= \sqrt{DY}\\ \Longrightarrow R &= \frac{1}{2m_\pi}\left(\omega\bar{\alpha}_s Y+\sqrt{DY}-\ln\left(\frac{Q^2}{Q_0^2}\right)\right).\end{aligned} \tag{38}$$

As compared to Eq. (23), this equation taking fluctuations into account contains a new term $\sqrt{DY}$.

So, including fluctuations and the impact parameter dependence in the way presented here seems to lead to reasonable results. However, the whole discussion is valid only in the fixed coupling case.

4.5 Phenomenological applications and estimation of the slope parameter B

It is well known from numerous hadronic scattering experiments

$$\frac{d\sigma_{exp}}{dt} \propto e^{-B|t|}. \tag{39}$$

where t is the squared four momentum transfer between the projectile and target. The $t-$slope B tends to a universal value determined by the proton shape alone [76]. From the experimental measurement of the $t-$distribution of the vector mesons, the effective slope B is found to be $B = 4GeV^{-2}$ [64, 77, 78].

In order to study the $t-$slope B, we take the Fourier transform of Eq.(39):

$$S_{exp}(b) \propto \frac{1}{2\,\pi\,B}\, e^{-\frac{b^2}{2B}}\,. \tag{40}$$

Now from comparison of factors in the exponent of Eq.(30) with Eq.(40), we can immediately see that

$$\begin{aligned} B &= \frac{\sigma^2}{8m_\pi^2} \\ &= \frac{D\bar{\alpha}_s Y}{8m_\pi^2} \\ &= \frac{D}{8m_\pi^2}\frac{\alpha_s N_c}{\pi}\ln\left(\frac{s}{Q^2}\right) \end{aligned} \tag{41}$$

where D is the diffusion coefficient. The value of $D = 0.325$ is determined by fitting the HERA data with color glass condensate model plus gluon number fluctuations [18]. Note that the B increases logarithmically with the center of mass energy s, which is in agreement with the Regge theory. This is the phenomenon known as the *shrinkage* of the diffraction peek in Regge theory, which can be interpreted as an increase of the interaction radius $R_{int} \sim \sqrt{\ln s}$. With the reasonable values $\alpha_s = 0.3$, $N_c = 3.0$,$m_\pi =$

$0.14GeV$, $\sqrt{s} = 90GeV$ and $Q^2 = 10GeV^2$, one obtains roughly the experimental values [64, 77, 78]

$$\begin{aligned} B &= \frac{D}{8m_\pi^2}\frac{\alpha_s N_c}{\pi}\ln\left(\frac{s}{Q^2}\right) \\ &\simeq 4.0GeV^{-2}. \end{aligned} \tag{42}$$

4.6 Discussion and conclusion

The main results of this chapter can be summarized as follows: We have argued that the impact parameter behavior of the scattering amplitude in the presence of fluctuations has Gaussian-like behavior. Such behavior is in agreement with various phenomenological models. This indicated that fluctuations may be the microscopic origin for the Gaussian behavior.

Further we have shown that the factorization of the impact parameter and the energy dependence of the scattering amplitude are lost once the gluon number fluctuations are included.

We calculated the rapidity dependence of radius of black disk in the fluctuation-dominated (diffusive scaling) region at high energy. We found that, due to fluctuations, the growth of the radius of black disk is enhanced by an additional (proportional to square root of rapidity) term.

Chapter 5

High-energy scattering in the saturation regime including running coupling and rare fluctuation effects

The Balitsky-Kovchegov (BK) equation [7, 5] is a non-linear evolution equation which describes the high energy scattering of a $q\bar{q}$ dipole on a target in the case of fixed coupling. An analytic solution to the BK equation in the saturation region has been found by Levin and Tuchin [20]. The BK equation can be viewed as a mean field version of more complete equation [7] where the higher correlations are neglected: The S-matrix of the scattering of two QCD dipoles on a target is replaced in the BK equation by the product of the S-matrices of the individual dipoles. Such a replacement is legitimate only in the absence of fluctuations in the light cone wave function of the target [13]. However, in Ref. [9] was shown that rare fluctuations do change the result for the S-matrix in the saturation region.

Recently, the evolution equations which include running coupling effects have been derived by Balitsky and Kovchegov-Weigert [15, 16]. They found that the running coupling corrections are included in the BK kernel by replacing the fixed coupling α_s in it with a "triumvirate" of the running couplings. A more complete evolution equation has been studied by Albacete and Kovchegov [17], they have calculated in addition to the Balitsky and Kovchegov-Weigert equations also the so-called subtraction contributions. A numerical solution of the more complete evolution equations

were given in [17].

In this work, we will analytically solve these equations in the saturation region and obtain an analytic result for the S-matrix. We find that the running coupling corrections modify the S-matrix a lot as compared to the fixed coupling case. Moreover, we study the effect of the rare fluctuations on top of the running coupling in the way as it was done in Ref. [9] for the fixed coupling case. We find that the rare fluctuations are less important in the running coupling case as compared to the fixed coupling case.

5.1 Fixed coupling case

The detailed study of the non-linear BK evolution equation in the fixed coupling case is introduced in 2.1. Here we only introduce the parts which will be used in this chapter. The BK equation is

$$\begin{aligned}\frac{\partial}{\partial Y}S(x_\perp - y_\perp, Y) &= \frac{\alpha N_c}{2\pi^2}\int d^2 z_\perp \frac{(x_\perp - y_\perp)^2}{(x_\perp - z_\perp)^2(z_\perp - y_\perp)^2} \\ &\quad \times \left[S(x_\perp - z_\perp, Y)S(z_\perp - y_\perp, Y) - S(x_\perp - y_\perp, Y)\right] . \quad (1)\end{aligned}$$

which gives the evolution with rapidity $Y = \ln(1/x)$ of the scattering amplitude $S(x_\perp, y_\perp, Y)$ of a $q\bar{q}$ dipole with a target that may be another dipole, a hadron or a nucleus. The BK equation is a simple equation to deal with the onset of unitarity and to study parton saturation phenomena at high energies. At high energies an analytic solution to the fixed coupling BK equation for the S-matrix deep in the saturation regime has been derived by Levin and Tuchin[20]. This solution agrees with the one derived by solving the BK equation in the small S limit [21].

The solution to the Eq. (1) is

$$S(x_\perp - y_\perp, Y) = \exp\left[-\frac{c}{2}\left(\frac{\alpha N_c}{\pi}\right)^2 (Y - Y_0)^2\right] S(x_\perp - y_\perp, Y_0), \quad (2)$$

where we have used [10, 24, 18]

$$Q_S^2(Y) = \exp\left[c\frac{\alpha N_c}{\pi}(Y - Y_0)\right] Q_S^2(Y_0) \quad (3)$$

and

$$Q_S^2(Y_0)(x_\perp - y_\perp)^2 = 1. \quad (4)$$

Eq. (2) gives the standard result given in the literature [21].

5.2 Running coupling case

The detailed study of the non-linear BK evolution equation in the running coupling case is introduced in 2.3. Here we only introduce the parts that will be used in the following study.

5.2.1 Balitsky and Kovchegov-Weigert equations

The evolution equation including higher order corrections reads [17]

$$\frac{\partial S(x_\perp - y_\perp, Y)}{\partial Y} = \mathcal{R}[S] - \mathcal{S}[S] \ . \tag{5}$$

The first term in r.h.s of (5), $\mathcal{R}$, which is referred to as the 'running coupling' contribution and resums all power of $\alpha_s N_f$ corrections to the evolution. The $\mathcal{R}$ has a form as the leading order one but with modified kernel which includes all effects of the running coupling

$$\begin{aligned} \mathcal{R}\left[S(x_\perp - y_\perp, Y)\right] &= \int d^2 z_\perp \, \tilde{K}(x_\perp, y_\perp, z_\perp) \left[S(x_\perp - z_\perp, Y)\, S(z_\perp - y_\perp, Y)\right. \\ &\quad \left. - S(x_\perp - y_\perp, Y)\right] \ . \end{aligned} \tag{6}$$

The second term in r.h.s of (5), $\mathcal{S}$, which is referred to as 'subtraction' contribution, is given by

$$\begin{aligned} \mathcal{S}[S] &= \alpha_\mu^2 \int d^2 z_{\perp 1}\, d^2 z_{\perp 2}\, K_{①}(x_\perp, y_\perp; z_{\perp 1}, z_{\perp 2}) \, \left[S(x_\perp - w_\perp, Y)\, S(w_\perp - y_\perp, Y)\right. \\ &\quad \left. - S(x_\perp - z_{\perp 1}, Y)\, S(z_{\perp 2} - y_\perp, Y)\right] \end{aligned} \tag{7}$$

with α_μ the bare coupling.

Eq. (7) shows that the $\mathcal{S}[S]$ is of order α_μ^2 while $\mathcal{R}[S]$ is of order α_s and all terms of $\mathcal{S}[S]$ are quadratic in S, $S(x_\perp - w_\perp, Y)\, S(w_\perp - y_\perp, Y)$, $S(x_\perp - z_{\perp 1}, Y)\, S(z_{\perp 2} - y_\perp, Y)$. Thus, for high rapidity and small S, the subtraction term is small as compared to the running coupling term, which also showed numerically in [17]. Since this is the kinematic region in which we are interested in this work, we will neglect the subtraction term hereafter. In this work we study the evolution equation in the saturation regime where the evolution equation including running coupling corrections can be solved analytically.

5.2.2 Solution to Balitsky and Kovchegov-Weigert equations in the saturation regime

In the saturation regime in which the interaction between partons is very strong, $S(x_\perp - y_\perp, Y) \to 0$, and unitarity corrections become important, the quadratic terms in (5) can be neglected in which case one only needs to keep the second term on the r.h.s of (6). The evolution equation including running coupling is given by

$$\frac{\partial S(x_\perp - y_\perp, Y)}{\partial Y} = -\int d^2 z_\perp \, \tilde{K}(\mathbf{r}, \mathbf{r}_1, \mathbf{r}_2) S(x_\perp - y_\perp, Y) \tag{8}$$

with modified kernel $\tilde{K}(\mathbf{r}, \mathbf{r}_1, \mathbf{r}_2)$. In the saturation region, $rQ_S(Y) \gg 1$, the main contribution to the integration on the r.h.s of (8) comes from either

$$1/Q_S \ll r_1 \ll r; \qquad r_2 \sim r \tag{9}$$

or

$$1/Q_S \ll r_2 \ll r; \qquad r_1 \sim r. \tag{10}$$

Let us look at one of them, i.e., when $1/Q_S \ll r_1 \ll r$, the r_2 is approximately equal to r, $r_2 \sim r$, the $\tilde{K}^{\rm Bal}(\mathbf{r}, \mathbf{r}_1, \mathbf{r}_2)$ becomes

$$\begin{aligned} \tilde{K}^{\rm Bal}(\mathbf{r}, \mathbf{r}_1, \mathbf{r}_2) &= \frac{N_c \alpha_s(r^2)}{2\pi^2} \left[\frac{1}{r_1^2} + \frac{1}{r_1^2} \left(\frac{\alpha_s(r_1^2)}{\alpha_s(r_2^2)} - 1 \right) \right] \\ &\approx \frac{N_c}{2\pi^2} \frac{\alpha_s(r_1^2)}{r_1^2} \end{aligned} \tag{11}$$

and the $\tilde{K}^{\rm KW}(\mathbf{r}, \mathbf{r}_1, \mathbf{r}_2)$ has the form as

$$\tilde{K}^{\rm KW}(\mathbf{r}, \mathbf{r}_1, \mathbf{r}_2) = \frac{N_c}{2\pi^2} \left[\alpha_s(r_1^2) \frac{1}{r_1^2} - 2 \, \frac{\alpha_s(r_1^2) \, \alpha_s(r_2^2)}{\alpha_s(r_1^2)} \, \frac{\mathbf{r}_1 \cdot \mathbf{r}_2}{r_1^2 \, r_2^2} + \alpha_s(r_2^2) \frac{1}{r_2^2} \right] , \tag{12}$$

here we use $R^2(\mathbf{r}, \mathbf{r}_1, \mathbf{r}_2) \approx r_1^2$ which can be obtained via simple calculation in (30) in Section 2.3 with condition of $1/Q_S \ll r_1 \ll r$ and $r_2 \sim r$. In the $r_1 \ll r_2$ limit, it is the first term which dominates Eq. (12) and has the running coupling scale given by the size of the smaller dipole

$$\tilde{K}^{\rm KW}(\mathbf{r}, \mathbf{r}_1, \mathbf{r}_2) \approx \frac{N_c}{2\pi^2} \alpha_s(r_1^2) \frac{1}{r_1^2} \, . \tag{13}$$

We wish to note that the modified Balitsky and Kovchegov-Weigert kernels including running coupling have the same form in the saturation regime. It is an interesting outcome which means that the evolution equation with running coupling corrections

is independent of the choice of transverse coordinate of subtraction point in the saturation regime. And the modified Balitsky and Kovchegov-Weigert equations with running coupling corrections are equivalent to each other in the saturation region. That means the S-matrix of the Balitsky and Kovchegov-Weigert equations are exactly the same in the saturation region.

Now let us put the modified kernel (11) or (13) into (8), we can get a simplified evolution equation as:

$$\frac{\partial S(r,Y)}{\partial Y} = -\frac{N_c}{2\pi^2}\int_{1/Q_S^2}^{r^2} d^2r_1\,\alpha_s(r_1^2)\frac{1}{r_1^2}S(r,Y), \tag{14}$$

with the running coupling at one loop accuracy

$$\alpha_s(r_1^2) = \frac{\mu}{1+\mu_1\ln\left(\frac{1}{r_1^2\Lambda^2}\right)}, \tag{15}$$

the Λ is an energy scale where the interactions become strong, $\mu = \alpha_s(\Lambda^2)$ and $\mu_1 = (33-2N_f)\alpha_s(\Lambda^2)/12\pi$ [79]. Eq.(14) gives

$$\frac{\partial S(r,Y)}{\partial Y} = -\frac{N_c\mu}{\pi\mu_1}\left[\ln\left(1+\mu_1\ln\left(\frac{Q_S^2(Y)}{\Lambda^2}\right)\right) - \ln\left(1+\mu_1\ln\left(\frac{1}{r^2\Lambda^2}\right)\right)\right]S(r,Y) \tag{16}$$

whose solution (see also [80]) is

$$S(r,Y) = e^{-\frac{N_c\mu}{c\pi\mu_1}\left[\ln^2\left(\frac{Q_S^2(Y)}{\Lambda^2}\right)\ln\left(\frac{1+\mu_1\ln\frac{Q_S^2}{\Lambda^2}}{1+\mu_1\ln\frac{1}{r^2\Lambda^2}}-\frac{1}{2}\right)+\frac{\ln\left(\frac{Q_S^2(Y)}{\Lambda^2}\right)}{\mu_1}-\frac{1}{\mu_1^2}\ln\left(1+\mu_1\ln\frac{Q_S^2}{\Lambda^2}\right)\right]}S(r,Y_0) \tag{17}$$

with the saturation momentum [24, 31]

$$\ln\left(\frac{Q_S^2(Y)}{\Lambda^2}\right) = \sqrt{c(Y-Y_0)} + O(Y^{1/6}). \tag{18}$$

We wish to note that the analytic form for the S-matrix at high energies including the running coupling corrections is different as compared to the fixed coupling case. The exponent in Eq. (17) is decreasing linearly with rapidity while the exponent in Eq. (2) is decreasing quadratically with rapidity, which indicates that the running coupling slows down the evolution of the scattering amplitude with rapidity.

5.3 Effects of rare fluctuations

5.3.1 Fixed coupling case

At very high energy the typical configuration of a dipole's light-cone wave function is a Color Glass Condensate which is a state having high occupancy for all gluonic levels of momentum less than or equal to saturation momentum Q_S. In the fixed coupling case, the authors of Ref. [9] computed the S-matrix of two typical configurations (of condensate type) and of dipole-typical configuration scattering, they found that the typical configurations lead to too small results for the S-matrix, being proportional to $\exp\{-c_1 Q_S^2 r^2/\alpha_s^2\}$ and $\exp\{-\frac{1}{2c}\ln^2(Q_S^2 r^2)\}$, respectively. c_1 and c are constant which are not important for our purpose. Thus they tried to search for configurations which are more rare in the wave function but which dominate very high energy dipole-dipole scattering and lead to a larger S-matrix. They found the reason why the typical configurations have given a small S-matrix is that the typical configurations contain too many gluons at the time of collision, therefore leading to the S-matrix is extremely small. This suggests that the strategy for finding the rare configuration is to minimize the number of gluons by suppressing the evolution (see next section for the details of how to obtain the rare configuration). The rare configuration is a state which has no more than one dipole of size κr or larger (with κ a constant of order 1 and r a size of parent dipole) when the system undertakes BK evolution. In the center of mass frame, the S-matrix is then given by the probability of the rare configurations for each of the parent dipoles partaking in the collision, times the S-matrix for the scattering of two dipoles separated by a rapidity gap Y_0,

$$S_Y(r) \approx e^{-\frac{1}{4c}\ln^2(Q_S^2 r^2)} S_{Y_0}(r) \tag{19}$$

which is significantly larger than the results coming from the condensate-condensate and dipole-condensate scattering.

5.3.2 Running coupling case

- Rare fluctuations in center of mass frame

  Following the framework of Ref. [9], consider the high-energy scattering of dipoles at zero impact parameter in the center of mass frame where one of dipoles is left-moving and the other is right-moving. In order to obtain rare configuration, we suppose that the wave function of the right-moving dipole only

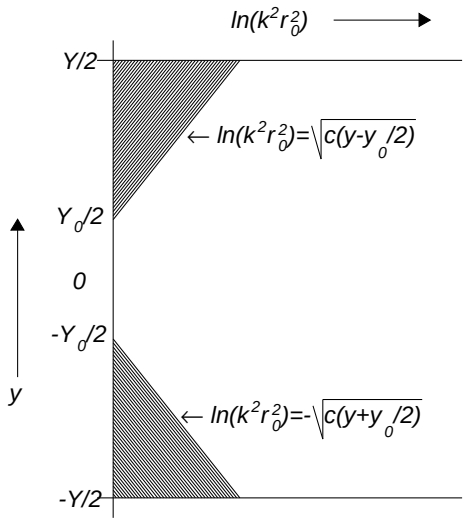

Figure 5.1: The configuration in center of mass frame.

consists of the parent dipole with size r in the rapidity interval $Y_0/2 < y < Y/2$, where Y_0 is the critical value of rapidity for the onset of unitarity corrections, with the similar requirement on the left-moving dipole in the rapidity interval $-Y/2 < y < -Y_0/2$. In the rapidity interval $0 < y < Y_0/2$ and $-Y_0/2 < y < 0$ the right-moving and left-moving dipoles have normal BFKL evolution, respectively.

However, we can not require that all evolution of right-moving dipoles are absent in the rapidity interval $Y_0/2 < y < Y$. The only thing that we can do is to allow the evolution which produces very small dipoles, in order to guarantee that the system has no more than one dipole of size κr or larger, with κ a constant of order one. And we setup constraints to suppress the creation of dipoles much smaller than r at rapidities $y > Y_0/2$ to avoid dipoles emitted at intermediate rapidities evolving into dipoles of size r or larger at rapidity $Y/2$. We require that the gluon emission from the parent dipoles is forbidden if the gluon has $k_\perp$

and y in the shaded triangles of Fig.5.1. The line

$$\ln(k_\perp^2 r^2) = \sqrt{c(y - \frac{Y_0}{2})} \tag{20}$$

and a similar line for the lower triangle, is determined by the requirement that gluons in the right hand side of that line can not evolve by normal BFKL evolution into shaded triangles.

Now we compute the probability of rare configurations $\mathbb{S}(x_\perp - y_\perp, Y - Y_0)$ which has the same meaning as the survival probability of the parent dipoles after a BFKL evolution over a rapidities interval $Y - Y_0$ [9]. This probability decreases with increasing Y due to gluon emission and the corresponding rate is the same as the virtual term in eq. (27) in Section 2.3:

$$\frac{\partial}{\partial Y}\mathbb{S}(x_\perp - y_\perp, Y - Y_0) = -\int d^2 z_\perp \, \tilde{K}(x_\perp, y_\perp, z_\perp)\mathbb{S}(x_\perp - y_\perp, Y - Y_0) \tag{21}$$

where $\tilde{K}(x_\perp, y_\perp, z_\perp)$ is the modified kernel with the form as (11) or (13). Substituting (11) into Eq. (21), one gets

$$\begin{aligned}\frac{\partial}{\partial Y}\mathbb{S}(x_\perp - y_\perp, Y - Y_0) &= -\frac{N_c \pi}{2\pi^2}\int_{1/Q_S^2}^{(x_\perp - y_\perp)^2} d(x_\perp - z_\perp)^2 \, \frac{\alpha_s((x_\perp - z_\perp)^2)}{(x_\perp - z_\perp)^2} \\ &\quad \times \mathbb{S}(x_\perp - y_\perp, Y - Y_0)\end{aligned} \tag{22}$$

whose solution is:

$$\begin{aligned}\mathbb{S}(r, Y - Y_0) &= \exp\left\{-\frac{N_c \mu}{c\pi\mu_1}\left[\ln^2\left(\frac{Q_S^2(Y)}{\Lambda^2}\right)\ln\left(\frac{1 + \mu_1 \ln\left(\frac{Q_S^2(Y)}{\Lambda^2}\right)}{1 + \mu_1 \ln\left(\frac{1}{r^2\Lambda^2}\right)} - \frac{1}{2}\right)\right.\right. \\ &\quad \left.\left. + \frac{\ln\left(\frac{Q_S^2(Y)}{\Lambda^2}\right)}{\mu_1} - \frac{1}{\mu_1^2}\ln\left(1 + \mu_1 \ln\left(\frac{Q_S^2(Y)}{\Lambda^2}\right)\right)\right]\right\},\end{aligned} \tag{23}$$

here $r = |x_\perp - y_\perp|$ is the size of parent dipole.

Let $\mathbb{S}(r, (Y - Y_0)/2)$ denote the probability of a parent dipole not given rise to any emission of gluon in the upper triangle of Fig.5.1. The S-matrix can be obtained by the product of $\mathbb{S}(r, (Y - Y_0)/2)$ for each of the parent dipoles participating in the scattering, times $S(r, Y_0)$ which is a S-matrix for the scattering of two

elementary dipoles. By using (23), one gets:

$$\begin{aligned} S(r,Y) &= \mathbb{S}(r,(Y-Y_0)/2)\mathbb{S}(r,(Y-Y_0)/2)S(r,Y_0) \\ &= \exp\left\{-\frac{N_c\mu}{c\pi\mu_1}\left[\ln^2\left(\frac{Q_S^2(Y)}{\Lambda^2}\right)\ln\left(\frac{1+\frac{\mu_1}{\sqrt{2}}\ln\left(\frac{Q_S^2(Y)}{\Lambda^2}\right)}{1+\mu_1\ln\left(\frac{1}{r^2\Lambda^2}\right)}-\frac{1}{2}\right)\right.\right. \\ &\quad \left.\left.+\frac{\sqrt{2}\ln\left(\frac{Q_S^2(Y)}{\Lambda^2}\right)}{\mu_1}-\frac{2}{\mu_1^2}\ln\left(1+\frac{\mu_1}{\sqrt{2}}\ln\left(\frac{Q_S^2(Y)}{\Lambda^2}\right)\right)\right]\right\} \\ &\quad \times S(r,Y_0) \end{aligned} \tag{24}$$

which only brings in very small corrections to (17) and indicates that the rare fluctuations are less important in the running coupling case as compared to the fixed coupling case [9], where the rare fluctuations are important and the exponential factor of S-matrix in the saturation regime has twice as large as the result which emerges when fluctuations are taken into account. We also consider the rare fluctuations on top of the running coupling effects in a general frame, we find the same result as (24).

- Rare fluctuations in a general frame

  Consider a high energy scattering of a right-moving dipole of size r_0 and rapidity $Y-Y_2$ on a left-moving dipole of size r_1 and rapidity $-Y_2$ in an arbitrary frame. The frame and scattering picture are illustrated in Fig. 5.2, where Y_0 is a rapidity gap between two dipoles. For later convenience, we require that $Y_2 \leq \frac{1}{2}(Y-Y_0)$. We require that no additional dipoles can be created from the gluon emission of left-moving dipole r_1 which would have a strong interaction with the right-moving dipoles. The dipoles which would have such strong interactions would be of size $r \geq 1/Q_S$ at the scattering time. So we should suppress the emission of those dipoles which could become of size $1/Q_S$ or larger after a normal evolution over the rapidity interval $-Y_2 < y < 0$. For the right-moving dipole r_0, we suppress evolution over its $Y - Y_2 - (Y_1 + Y_0)$ with the region of suppression given by the upper shaded triangle of Fig. 5.2. The line

$$\ln(k^2 r_0^2) = \sqrt{c(y - Y_1 - Y_0)} \tag{25}$$

  and a similar line for the lower triangle, is determined by the requirement that gluons locating in the right hand side of that line can not evolve by normal BFKL evolution into shaded triangles. We will determine Y_1 by maximizing

the S-matrix later. The unshaded triangle, whose rapidity values go from 0 to Y_1, is a saturation region where the dipole r_0 has evolved into a Color Glass Condensate.

After we have a clear scattering picture of dipoles, the S-matrix can be evaluated at hand

$$S(r_0, r_1, Y) = \mathbb{S}_R(r_0, Y - Y_0 - Y_1 - Y_2)\mathcal{S}(r_0, r_1, Y_0 + Y_1)\mathbb{S}_L(r_1, Y_2) \tag{26}$$

with $\mathcal{S}(r_0, r_1, Y_0+Y_1)$ is the S-matrix for scattering of a elementary dipole r_1 on a Color Glass Condensate state which is evolved from dipole r_0 and $\mathbb{S}_R(r_0, Y - Y_0 - Y_1 - Y_2)$ and $\mathbb{S}_L(r_1, Y_2)$ are the suppression factor from the no emission requirement for two dipoles, which are given in terms of the area of the upper and lower shaded regions of Fig. 5.2. After using (23), one obtains

$$\begin{aligned}\mathbb{S}_R(r_0, Y - Y_0 - Y_1 - Y_2) &= \exp\left\{-\frac{N_c\mu}{c\pi\mu_1}\left[c\ln\left(\frac{1+\mu_1\sqrt{c(Y-Y_2-Y_1-Y_0)}}{1+\mu_1\ln\left(\frac{1}{r^2\Lambda^2}\right)}\right.\right.\right. \\ &\quad \left.\left.\left. - \frac{1}{2}\right)(Y - Y_2 - Y_1 - Y_0) + \frac{\sqrt{c(Y-Y_2-Y_1-Y_0)}}{\mu_1}\right.\right. \\ &\quad \left.\left. - \frac{1}{\mu_1^2}\ln\left(1+\mu_1\sqrt{c(Y-Y_2-Y_1-Y_0)}\right)\right]\right\} \end{aligned} \tag{27}$$

and

$$\begin{aligned}\mathbb{S}_L(r_1, Y_2) &= \exp\left\{-\frac{N_c\mu}{c\pi\mu_1}\left[c\ln\left(\frac{1+\mu_1\sqrt{c(Y_1+Y_2)}}{1+\mu_1\ln\left(\frac{1}{r^2\Lambda^2}\right)} - \frac{1}{2}\right)(Y_1 + Y_2)\right.\right. \\ &\quad + \frac{\sqrt{c(Y_1+Y_2)}}{\mu_1} - \frac{1}{\mu_1^2}\ln\left(1+\mu_1\sqrt{c(Y_1+Y_2)}\right) \\ &\quad - c\ln\left(\frac{1+\mu_1\sqrt{cY_1}}{1+\mu_1\ln\left(\frac{1}{r^2\Lambda^2}\right)} - \frac{1}{2}\right)Y_1 - \frac{\sqrt{cY_1}}{\mu_1} \\ &\quad \left.\left. + \frac{1}{\mu_1^2}\ln\left(1+\mu_1\sqrt{cY_1}\right)\right]\right\}. \end{aligned} \tag{28}$$

The $\mathcal{S}$ can be computed by using the BK equation with running coupling corrections since the BK equation with running coupling corrections describes correctly the scattering of an elementary dipole on a Color Glass Condensate. By using (17), one gets

$$\mathcal{S}(r_0, r_1, Y_0 + Y_1) = e^{-\frac{N_c\mu}{c\pi\mu_1}\left[c\ln\left(\frac{1+\mu_1\sqrt{cY_1}}{1+\mu_1\ln\left(\frac{1}{r^2\Lambda^2}\right)} - \frac{1}{2}\right)Y_1 + \frac{\sqrt{cY_1}}{\mu_1} - \frac{1}{\mu_1^2}\ln\left(1+\mu_1\sqrt{cY_1}\right)\right]} S(r_0, Y_0). \tag{29}$$

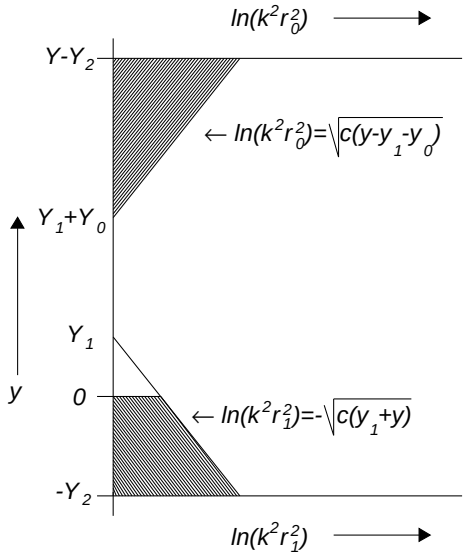

Figure 5.2: The configuration in a general frame.

Substituting (27), (28) and (29) into (26), one obtains:

$$\begin{aligned} S(r_0, r_1, Y) &= \exp\left\{ -\frac{N_c \mu}{c\pi\mu_1} \left[c \ln\left(\frac{1+\mu_1\sqrt{c(Y-Y_2-Y_1-Y_0)}}{1+\mu_1 \ln\left(\frac{1}{r^2\Lambda^2}\right)} - \frac{1}{2} \right) \right.\right. \\ &\quad \times (Y-Y_2-Y_1-Y_0) + \frac{\sqrt{c(Y-Y_2-Y_1-Y_0)}}{\mu_1} \\ &\quad - \frac{1}{\mu_1^2} \ln\left(1+\mu_1\sqrt{c(Y-Y_2-Y_1-Y_0)}\right) \\ &\quad + c \ln\left(\frac{1+\mu_1\sqrt{c(Y_1+Y_2)}}{1+\mu_1 \ln\left(\frac{1}{r^2\Lambda^2}\right)} - \frac{1}{2} \right) (Y_1+Y_2) + \frac{\sqrt{c(Y_1+Y_2)}}{\mu_1} \\ &\quad \left.\left. - \frac{1}{\mu_1^2} \ln\left(1+\mu_1\sqrt{c(Y_1+Y_2)}\right) \right] \right\} S(r_0, Y_0). \end{aligned} \tag{30}$$

which connects to a set of configurations of the wave function described by rapidity Y_1. The S-matrix is determined by the values of Y_1 which maximizes the r.h.s of Eq. (30) or equivalently minimizes the exponent of the r.h.s of Eq. (30). We obtain

$$Y_1 = \frac{1}{2}(Y - Y_0) - Y_2. \tag{31}$$

Taking this Y_1 into (30), finally the S-matrix is

$$S(r,Y) = \exp\left\{-\frac{N_c\mu}{c\pi\mu_1}\left[\ln^2\left(\frac{Q_S^2(Y)}{\Lambda^2}\right)\ln\left(\frac{1+\frac{\mu_1}{\sqrt{2}}\ln\left(\frac{Q_S^2(Y)}{\Lambda^2}\right)}{1+\mu_1\ln\left(\frac{1}{r^2\Lambda^2}\right)}-\frac{1}{2}\right)\right.\right.$$
$$\left.\left.+\frac{\sqrt{2}\ln\left(\frac{Q_S^2(Y)}{\Lambda^2}\right)}{\mu_1}-\frac{2}{\mu_1^2}\ln\left(1+\frac{\mu_1}{\sqrt{2}}\ln\left(\frac{Q_S^2(Y)}{\Lambda^2}\right)\right)\right]\right\} \qquad (32)$$

which is exactly the same as the corresponding result (24) in the center of mass frame.

5.4 The shape of dipole cross section including running coupling

The authors of Ref. [24] computed the scattering amplitude for $rQ_S \ll 1$ using BFKL evolution and running coupling. Combining the outcome of Ref. [24] and our result (17) which is valid for $rQ_S \gg 1$, the shape of dipole cross section with running coupling reads:

$$T(r,Y) = \begin{cases} \left(\frac{Q^2}{Q_S^2}\right)^{-(1-\lambda_0)}\left[\ln\left(\frac{Q^2}{Q_S^2}\right)+\frac{1}{1+\lambda_0}\right]T_0 & rQ_S \le 1\ , \\ 1-\exp\left\{-\frac{N_c\mu}{c\pi\mu_1}\left[\ln^2\left(\frac{Q_S^2(Y)}{\Lambda^2}\right)\ln\left(\frac{1+\mu_1\ln\left(\frac{Q_S^2(Y)}{\Lambda^2}\right)}{1+\mu_1\ln\left(\frac{1}{r^2\Lambda^2}\right)}-\frac{1}{2}\right)\right.\right. & \\ \left.\left.+\frac{\ln\left(\frac{Q_S^2(Y)}{\Lambda^2}\right)}{\mu_1}-\frac{1}{\mu_1^2}\ln\left(1+\mu_1\ln\left(\frac{Q_S^2(Y)}{\Lambda^2}\right)\right)\right]\right\}S_0 & rQ_S > 1\ , \end{cases}$$

where λ_0 is the solution to $\chi'(\lambda_0)(1-\lambda_0) = -\chi(\lambda_0)$ with χ the usual BFKL eigenvalue function, T_0 is a constant but with no control at this moment and Q_S is the saturation momentum including running coupling corrections.

Bibliography

[1] E.A. Kuraev, L.N. Lipatov and V.S. Fadin, *Sov. Phys. JETP* **45** (1977) 199; Ya.Ya. Balitsky and L.N. Lipatov,*Sov. J. Nucl. Phys.* **28**(1978) 822;

[2] M. Froissart, *Phys. Rev.* **123** (1961) 1053;

[3] A. H. Mueller, *Nucl. Phys.* **B415** (1994) 373; *Nucl. Phys.* **B437** (1995) 107;

[4] A. H. Mueller and B. Patel, *Nucl. Phys.* **B425** (1994) 471;

[5] Yu.V. Kovchegov, *Phys. Rev.* **D60** (1999) 034008, *ibid.* **D61** (1999) 074018;

[6] J. Jalilian-Marian, A. Kovner, A. Leonidov and H. Weigert, *Nucl. Phys.* **B504** (1997) 415; *Phys. Rev.* **D59** (1999) 014014;
J. Jalilian-Marian, A. Kovner and H. Weigert, *Phys. Rev.* **D59**, (1999) 014015;
E. Iancu, A. Leonidov and L. D. McLerran, *Phys. Lett.* **B510** (2001) 133; *Nucl. Phys.* **A692** (2001) 583;
Nucl. Phys. **A703** (2002) 823;

[7] I. Balitsky, *Nucl. Phys.* **B463** (1996) 99; *Phys. Lett.* **B518** (2001) 235; *"High-energy QCD and Wilson lines"*, hep-ph/0101042;

[8] G. P. Salam, *Nucl. Phys.* **B449** (1995) 589; *Nucl. Phys.* **B461** (1996) 512; A. H. Mueller and G. P. Salam, *Nucl. Phys.* **B475** (1996) 293;

[9] E. Iancu and A.H. Mueller, *Nucl. Phys.* **A730** (2004) 494;

[10] A.H. Mueller and A. Shoshi, *Nucl. Phys.* **B692** (2004) 175;

[11] E. Iancu, A.H. Mueller and S. Munier, *Phys. Lett.* **B606** (2005) 342;

[12] E. Iancu and D.N. Triantafyllopoulos, *Nucl. Phys.* **A756** (2005) 419;

[13] A.H. Mueller, A.I. Shoshi and S.M.H. Wong, *Nucl. Phys.* **B715** (2005) 440;

[14] E. Iancu and D.N. Triantafyllopoulos, *Phys. Lett.* **B610** (2005) 253;

[15] I.I. Balitsky, *Phys. Rev.* **D75** (2007) 014001;

[16] Yu.V. Kovchegov and H. Weigert, *Nucl. Phys.* **A784** (2007) 188;

[17] J.L. Albacete and Yu.V. Kovchegov, *Phys. Rev.* **D75** (2007) 125021;

[18] M. Kozlov, A. Shoshi and W.C. Xiang *JHEP* **10** (2007) 020;

[19] W.C. Xiang, *Phys. Rev.* **D79** (2004) 014012;

[20] E. Levin and K. Tuchin, *Nucl. Phys.* **B573** (2000) 83;

[21] A.H. Mueller, hep-ph/0111244;

[22] A. Shoshi, Habilitation 2007;

[23] A.H. Mueller, *Nucl. Phys.* **B415** (1994) 373;

[24] A.H. Mueller and D.N. Triantafyllopoulos, *Nucl. Phys.* **B640** (2002) 331;

[25] E. Iancu, K. Itakura and L. Mclerran, *Nucl. Phys.* **A708** (2002) 327;

[26] S. Munier and R. Peschanski, *Phys. Rev. Lett* **91** (2003) 232001;
S. Munier and R. Peschanski, *Phys. Rev.* **D69** (2004) 034008;

[27] A.M. Stasto, K.J. Golec-Biernat and J. Kwiecinski, *Phys. Rev. Lett* **86** (2001) 596;

[28] C. Marquet, G. Soyez and B. W. Xiao, *Phys. Lett.* **B639** (2006) 635;

[29] A. H. Mueller and D. N. Triantafyllopoulos, *Nucl. Phys.* **B640** (2002) 331;

[30] E. Iancu, K. Itakura and S. Munier, *Phys. Lett.* **B590** (2004) 199;

[31] D.N. Triantafyllopoulos, *Nucl. Phys.* **B648** (2003) 293;

[32] A. Kovner and M. Lublinsky, *Phys. Rev.* **D71**, 085004 (2005);

[33] M. Kozlov, A. I. Shoshi and B. W. Xiao, *Nucl. Phys.* **A792** (2007) 170; M. Kozlov, A. I. Shoshi and B. W. Xiao, "Fluctuation Effects on R_{pA} at High Energy," arXiv:0706.3998 [hep-ph];

[34] E. Iancu, C. Marquet and G. Soyez, *Nucl. Phys.* **A780** (2006) 52;

[35] A. H. Mueller, "Saturation and high density QCD," arXiv:hep-ph/0501012;
E. Iancu, *Eur. Phys. J.* **C43** (2005) 345;
S. Munier, *Acta Phys. Polon.* **B37** (2006) 3451;
D. N. Triantafyllopoulos, *Acta Phys. Polon.* **B36** (2005) 3593;
A. I. Shoshi, "High energy QCD beyond the mean field approximation," arXiv:0708.4316 [hep-ph];

[36] A. I. Shoshi and B. W. Xiao, *Phys. Rev.* **D73** (2006) 094014; *Phys. Rev.* **D75** (2007) 054002;

[37] S. Bondarenko, L. Motyka, A. H. Mueller, A. I. Shoshi and B. W. Xiao, *Eur. Phys. J.* **C50** (2007) 593;

[38] J. P. Blaizot, E. Iancu and D. N. Triantafyllopoulos, *Nucl. Phys.* **A784** (2007) 227;

[39] E. Iancu, J. T. de Santana Amaral, G. Soyez and D. N. Triantafyllopoulos, *Nucl. Phys.* **A786** (2007) 131;

[40] A. Dumitru, E. Iancu, L. Portugal, G. Soyez and D. N. Triantafyllopoulos,*JHEP* **08** (2007) 062;

[41] S. Munier, *Phys. Rev.* **D75** (2007) 034009;

[42] Y. Hatta, E. Iancu, K. Itakura and L. McLerran, arXiv:hep-ph/0501171;

[43] M. Kozlov and E. Levin, *Nucl. Phys.* **A779** (2006) 142;

[44] M. Kozlov, E. Levin, V. Khachatryan and J. Miller, *Nucl. Phys.* **A791** (2007) 382;

[45] E. Levin and A. Prygarin, "The BFKL Pomeron Calculus in zero transverse dimensions: summation of Pomeron loops and generating functional for the multiparticle production processes," arXiv:hep-ph/0701178;

[46] J. Breitweg *et al.* [ZEUS Collaboration], Phys. Lett. **B487** (2000) 53;
S. Chekanov *et al.* [ZEUS Collaboration], *Eur. Phys. J.* **C21** (2001) 443;
C. Adloff *et al.* [H1 Collaboration], *Eur. Phys. J.* **C21** (2001) 33;

[47] K. Golec-Biernat and M. Wusthoff, *Phys. Rev.* **D59** (1999) 014017;

[48] F. Gelis, R. Peschanski, G. Soyez and L. Schoeffel, *Phys. Lett.* **B647** (2007) 376;

[49] G. Soyez, *Phys. Rev.* **D72** (2005) 016007;

[50] E. Brunet, B. Derrida, A. H. Mueller and S. Munier, *Phys. Rev.* **E73** (2006) 056126;

[51] C. Ewerz and O. Nachtmann, *Annals Phys.* **322** (2007) 1670;

[52] Y. Hatta, E. Iancu, C. Marquet, G. Soyez and D. N. Triantafyllopoulos, *Nucl. Phys.* **A773** (2006) 95;

[53] G. P. Salam, *JHEP* **07** (1998) 019; M. Ciafaloni, D. Colferai, and G. P. Salam, *Phys. Rev.* **D60** (1999) 114036;

[54] C. Adloff*et al.* [H1 Collaboration],*Phys. Lett.* **B528** (2002) 199; A. Aktas*et al.* [H1 Collaboration] *Eur. Phys. J.* **C45** (2006) 23;

[55] S. Chekanov*et al.* [ZEUS Collaboration]*Phys. Rev.* **D69** (2004) 012004;

[56] G. Soyez, *Phys. Lett.* **B655** (2007) 32;

[57] A. Aktas *et al.* [H1 Collaboration], *Eur. Phys. J.* **C48** (2006) 715;

[58] S. Chekanov *et al.* [ZEUS Collaboration], *Nucl. Phys.* **B713** (2005) 3;

[59] L. V. Gribov, E. M. Levin and M. G. Ryskin, *Phys. Rept.* **100** (1983) 1;

[60] A. H. Mueller and J. W. Qiu, *Nucl. Phys.* **B268** (1986) 427;

[61] K. Golec-Bierna, M. Wusthoff, *Phys. Rev.* **D60**,(1999) 114023;

[62] C. Marquet, *Phys. Rev.* **D76** (2007) 094017;

[63] C. Adloff *et al.* [H1 Collaboration], *Eur. Phys. J.* **C10** (1999) 373;

[64] S. Chekanov *et al.* [ZEUS Collaboration], *Eur. Phys. J.* **C24** (2002) 345;

[65] M. Wuesthoff, *Phys. Rev.* **D56** (1997) 4311;

[66] E. Levin and M. Wuesthoff, *Phys. Rev.* **D50** (1994) 4306;

[67] E. Iancu, L. McLerran, *Nucl. Phys.* **A793**, (2007) 96;

[68] Y. Hatta, A. H. Mueller, *Nucl. Phys.* **A789**, (2006) 285;

[69] E. Avsar, Y. Hatta, *JHEP* **09** (2008) 102;

[70] A. H. Mueller,arXiv:hep-ph/9911289;

[71] E. Levin, arXiv:hep-ph/9710546;

[72] V. Barone and E. Predazzi, "High-Energy Particle Diffraction", Springer Press 2002;

[73] S. Donnachie, G. dosch, P. Landshoff and O. Nachtmann, "Pomeron Physics and QCD", Cambridge University Press 2005;

[74] T. Ikeda and L. McLerra, *Nucl. Phys.* **A756** (2005) 385;

[75] E. Ferreiro, E. Iancu, K. Itakura and L. McLerran, *Nucl. Phys.* **A710** (2002) 373;

[76] H. Kowalski, L. Motyka, and G. Watt,*Phys. Rev.* **D74** (2006)074016;

[77] S. Chekanov *et al.* [ZEUS Collaboration], *Nucl. Phys.* **B695** (2004) 3;

[78] A. Aktas *et al.* [H1 Collaboration], arXiv:hep-ex/0510016;

[79] N. Stephan, "QCD as a theory of hadrons," Cambridge University Press (2004);

[80] A.H. Mueller, *Nucl. Phys.* **B643** (2002) 501.

List of Figures

List of Tables

Acknowledgements

First, I would like to thank my advisor PD Dr. Arif. Shoshi. He has introduced me into the subject of this thesis and given me inestimable suggestions and numerous stimulating discussions. Without his patient guidance this thesis would not be possible. He also gave me many opportunities for participating at schools, workshops and conferences. His help is invaluable for me.

In addition, I would like to thank especially Prof. Dr. Edwin Laermann and Prof. Dr. Helmut Satz, who provided a good research environment for me. I also would like to thank Prof. Dr. Daicui Zhou and Dr. Misha Kozlov for their discussions and help.

I would like to thank all the members of the particle physics group at the department of physics of University of Bielefeld, especially thank Gudrun Eickmeyer and Susi von Reder, for creating a good and relaxing atmosphere.

Finally, I would like to thank my parents and my wife Jing Yang for their constant love and support. I would like to thank Chuan Miao, Nan Li, Wei Liu, Shunxiang Ouyang, Yongsheng Song, Hengtong Ding, Xianghui Zhang, Xuping Huang, Feng Ji, Xiaoliang Song, Qiulin Cao, Dai Wu, Zheng Yan for their friendly help during the last three years.